Glide to efficiency

Thermodynamic and techno-economic evaluation of high-temperature heat pumps for industrial sensible heat upgrading with temperature glides

MSc Thesis

Septemer 4th, 2026

J.C. Stok

Delft University of Technology

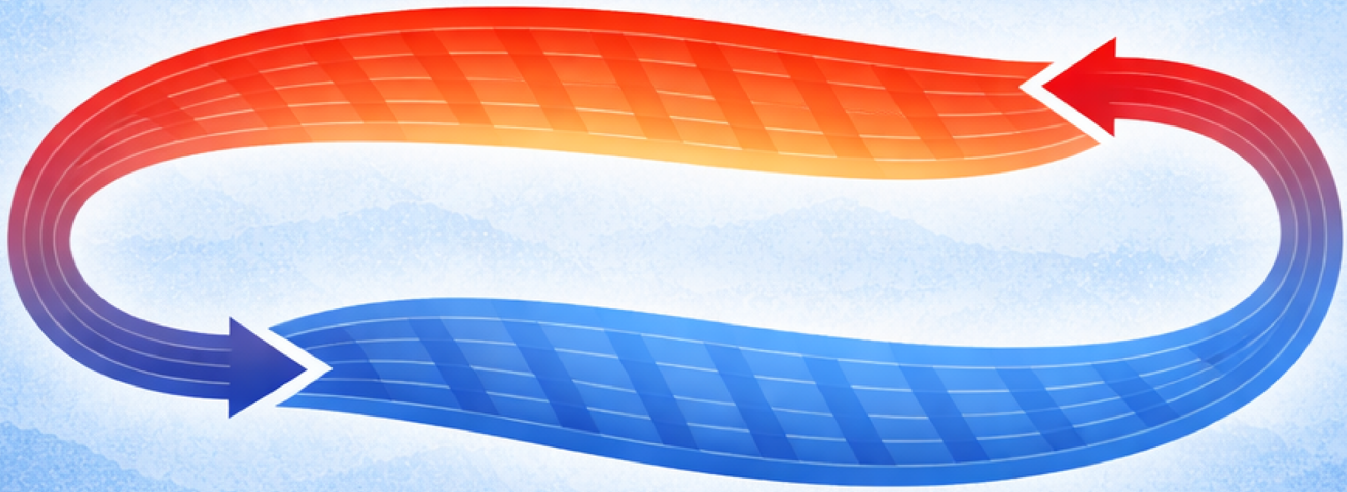

TU Delft

Glide to efficiency

Thermodynamic and techno-economic evaluation of high-temperature heat pumps for industrial sensible heat upgrading with temperature glides

by

J.C. Stok

to obtain the degree of Master of Science
at the Delft University of Technology,
to be defended publicly on Friday, September 11th, 2026, at 13:30.

Student number:	5125669	
Project duration:	November 26, 2025 – September 4, 2026	
Thesis committee:	Prof. dr. ir. S.A. Klein,	TU Delft, supervisor
	Prof. Dr. R. Pecnik,	TU Delft
	Dr. Ir. J.L.B. van Reisen,	McDermott Netherlands

Cover: Generated using ChatGPT (GPT-5.3, OpenAI), March 2026.
Style: TU Delft Report Style, with modifications by Daan Zwaneveld

TU Delft

Summary

Industrial process heat remains strongly dependent on fossil fuels. High-temperature heat pumps can reduce electricity demand and direct emissions by upgrading available waste heat, but their performance depends strongly on the temperature profiles of the heat source and heat sink. This study evaluates high-temperature heat pumps that absorb and reject heat over a temperature glide for industrial sensible-heat upgrading. Vapor-compression heat pumps (VCHPs), reversed-Brayton heat pumps (RBHPs), and an absorption-compression heat pump (ACHP) are compared for three heating scenarios with heat sink outlet temperatures of 150 or 200 °C using a 100 °C heat source.

Steady-state thermodynamic models were developed and validated for the VCHP and RBHP. Pure fluids and binary mixtures were optimized and evaluated through Pareto-based multi-objective screening and working-fluid family analysis. Thermodynamic performance was subsequently combined with environmental, safety, and practical criteria to select favorable working fluids. Preliminary compressor and heat-exchanger sizing, equipment-cost correlations, and levelized-cost-of-heat calculations were used to evaluate technical and economic performance at heating duties of 1 MW and 10 MW. Vendor data were used for the ACHP.

The VCHP achieved the highest and most consistent thermodynamic performance. Subcritical operation with a zeotropic mixture provided the largest benefit when the heat sink outlet temperature was 150 °C and both the heat source and heat sink had a 50 K temperature glide. The zeotropic mixture advantage decreased at higher heat sink temperatures, where transcritical operation made pure fluids and low-glide mixtures more competitive. The RBHP performed most favorably when the heat-source-to-heat-sink temperature glide ratio matched its sensible heat-transfer profile, but generally had a lower COP and required larger high-pressure heat exchangers. Its internal heat exchanger provided a significant benefit mainly for the scenario with the largest heat-source-to-heat-sink temperature gap.

Equipment feasibility and economics improved substantially with scale. At 1 MW, several compressor and RBHP turbomachinery configurations required small, high-speed, or high-temperature designs with uncertain practical feasibility. At 10 MW, larger dimensions and estimated compressor efficiencies near or above 80% made centrifugal turbomachinery more credible and reduced specific investment costs. The VCHP generally achieved the lowest levelized cost of heat, while all evaluated heat pumps remained less expensive than direct electric heating under the assumed conditions. At 10 MW, the heat pumps were also competitive with gas-fired heating in most scenarios. Overall, temperature-glide heat pumps are most effective when the cycle, working fluid, process-temperature profiles, and heating duty are selected together.

Contents

Summary **i**

Declaration of AI **viii**

Nomenclature **ix**

1 Introduction **1**

2 Background **3**
2.1 Sensible heat upgrading and temperature glide-matching . . . 3
2.1.1 Sensible heat sources and sinks . . . 3
2.1.2 Thermodynamic benefit of glide matching . . . 3
2.2 Heat pump cycles with a temperature glide . . . 4
2.2.1 Vapor-compression heat pump . . . 4
2.2.2 Reversed-Brayton heat pump . . . 5
2.2.3 Absorption-compression heat pump . . . 6
2.3 Working fluid effects and selection criteria . . . 6
2.3.1 Thermodynamic properties and cycle performance . . . 6
2.3.2 Pure fluids and mixtures . . . 7
2.3.3 Working-fluid families . . . 7
2.3.4 Environmental, safety, and practical criteria . . . 8
2.4 Equipment requirements and scale effects . . . 8
2.4.1 Compressor selection and limitations . . . 9
2.4.2 Turbine and expander selection . . . 10
2.4.3 Heat exchanger selection and heat-transfer requirements . . . 10
2.5 Reference heat supply . . . 12
2.6 Implications for the evaluation methodology . . . 12

3 Methodology **13**
3.1 Simulation and evaluation procedure . . . 13
3.2 Thermodynamic models . . . 14
3.2.1 Vapor-compression heat pump . . . 14
3.2.2 Reversed-Brayton heat pump . . . 15
3.2.3 Performance indicators . . . 18
3.3 Working-fluid screening and selection criteria . . . 19
3.3.1 Pareto-based multi-objective screening . . . 19
3.3.2 Working-fluid family mean performance analysis . . . 19
3.3.3 Environmental, safety and practical selection criteria . . . 19
3.3.4 Flammability classification of working-fluid mixtures . . . 20
3.4 Equipment sizing and economic evaluation . . . 20
3.4.1 Equipment selection . . . 21
3.4.2 Component dimensioning . . . 21
3.4.3 Equipment cost estimation . . . 24
3.4.4 LCOH . . . 25
3.4.5 Scale evaluation . . . 26
3.5 Reference heat supply . . . 26

4 Results **27**
4.1 Thermodynamic performance . . . 27
4.1.1 Fluid screening . . . 27
4.1.2 Cycle comparison . . . 30

4.1.3 Zeotropic mixtures . . . 32
4.1.4 Transcritical operation . . . 32
4.1.5 Natural working fluids . . . 33
4.1.6 Working-fluid family mean performance . . . 34
4.1.7 Thermodynamic screening synthesis . . . 34
4.2 Fluid selection . . . 35
4.3 Equipment sizing . . . 36
4.3.1 Centrifugal compressor . . . 36
4.3.2 Radial turbines . . . 38
4.3.3 Heat exchanger . . . 38
4.3.4 Equipment overview . . . 38
4.4 Economic performance . . . 38
4.4.1 Investment costs . . . 39
4.4.2 LCOH . . . 39
4.4.3 Effect of scale . . . 41

5 Conclusions, discussion, and recommendations 42
5.1 Conclusions . . . 42
5.2 Discussion and limitations . . . 43
5.3 Recommendations . . . 44
5.3.1 Industrial decision-makers . . . 44
5.3.2 Scientific research . . . 44

References 46

A Working fluids 54

B Equipment sizing 55

C Results 58

List of Figures

2.1 (a) Flow sheet of vapor-compression heat pump and (b) the corresponding pressure-enthalpy and (c) temperature-entropy diagrams [1]. 5
2.2 (a) Flow sheet of reversed-Brayton heat pump and (b) the corresponding pressure-volume and (c) temperature-entropy diagrams [74, 103]. 5
2.3 (a) Flow sheet of absorption-compression heat pump and (b) a diagram of the temperature profiles over the transferred heat [53]. 6

3.1 Overview of the simulation and evaluation procedure to identify, select and evaluate working-fluid cycle combinations for the vapor-compression and reversed-Brayton heat pump and compare them to the absorption-compression heat pump. 13
3.2 Overview of the simulation procedure for the vapor-compression heat pump consisting of a thermodynamic model and an optimization procedure that maximizes condenser and internal heat exchanger heat transfer. 14
3.3 Process flow diagram of a single-stage vapor-compression heat pump with an internal heat exchanger. 15
3.4 Overview of the simulation procedure for the reversed-Brayton heat pump consisting of a thermodynamic model and an optimization procedure. The optimization procedure consists of a grid search and a local optimization using a sequential least squares quadratic programming method. 16
3.5 Process flow diagram of a reversed-Brayton heat pump (a) without and (b) with an internal heat exchanger. 17

4.1 The coefficient of performance (COP) is compared against the volumetric heating capacity (VHC), along with the required heat transfer area derived from the simulation results of the vapor-compression heat pump for different heating scenarios: S1 (a), S2 (b), and S3 (c). Selected and Pareto-optimal mixtures, which maximize both COP and VHC while minimizing pressure ratio and required heat transfer area, are highlighted. 27
4.2 The relative occurrence of (a) individual fluids and (b) specific mixtures in the Pareto-optimal solutions of the vapor-compression heat pump simulation results is compared for different heating scenarios. The occurrence of an individual working fluid can be as a pure fluid or as part of a mixture, and the occurrence of a mixture can be any composition. 28
4.3 The coefficient of performance (COP) is compared against the volumetric heating capacity (VHC), along with the required heat transfer area derived from the simulation results of the reversed-Brayton heat pump without (a, b, c) and with an internal heat exchanger (d, e, f) for different heating scenarios: S1 (a & d), S2 (b & e), and S3 (c & f). Selected and Pareto-optimal mixtures, which maximize both COP and VHC while minimizing pressure ratio and required heat transfer area, are highlighted. 28
4.4 The relative occurrence of (a & c) individual fluids and (b & d) specific mixtures in the Pareto-optimal solutions of the reversed-Brayton heat pump simulation results (a & b) without and (c & d) with an internal heat exchanger is compared for different heating scenarios. The occurrence of an individual working fluid can be as a pure fluid or as part of a mixture, and the occurrence of a mixture can be any composition. 29
4.5 The coefficient of performance (COP), Lorenz efficiency, pressure ratio, volumetric heating capacity (VHC), and estimated heat-transfer area of selected high-COP working-fluid cycle combinations of the vapor-compression heat pump and the reversed-Brayton heat pump compared across the three heating scenarios to the obtained absorption-compression heat pump vendor performance data and the modeled conventional pure fluid subcritical vapor-compression heat pump. 30

4.6 Temperature-entropy and temperature-heat transfer diagrams of selected high-coefficient-of-performance working fluids of the vapor-compression heat pump simulation results for heating scenarios (a) S1, (b) S2, and (c) S3. 31
4.7 Temperature-entropy and temperature-heat transfer diagrams of selected high-coefficient-of-performance working fluids of the reversed-Brayton heat pump with an internal heat exchanger simulation results for heating scenarios (a) S1, (b) S2, and (c) S3. 31
4.8 The coefficient of performance (COP) is compared against the volumetric heating capacity (VHC) of the vapor-compression heat pump simulation results for heating scenarios (a) S1, (b) S2, and (c) S3, with mixtures and pure fluids highlighted. 32
4.9 The coefficient of performance (COP) is compared against the volumetric heating capacity (VHC) of the reversed-Brayton heat pump simulation results for heating scenarios (a) S1, (b) S2, and (c) S3, with mixtures and pure fluids highlighted. 32
4.10 The coefficient of performance (COP) is compared against the volumetric heating capacity (VHC) of the vapor-compression heat pump simulation results for heating scenarios (a) S1, (b) S2, and (c) S3, with subcritical and transcritical cycles highlighted. 33
4.11 The coefficient of performance (COP) is compared against the volumetric heating capacity (VHC) of the reversed-Brayton heat pump simulation results with an internal heat exchanger for heating scenarios (a) S1, (b) S2, and (c) S3, with subcritical, transcritical, and supercritical cycles highlighted. 33
4.12 The coefficient of performance (COP) is compared against the volumetric heating capacity (VHC) of the vapor-compression heat pump simulation results for heating scenarios (a) S1, (b) S2, and (c) S3, with synthetic and natural working fluids highlighted. A mixture is highlighted as a natural working fluid when it contains only natural fluids. 33
4.13 Specific levelized cost of heat (LCOH) for the vapor-compression heat pump and the reversed-Brayton heat pump for the three heating scenarios with a heating duty of 1 MW, compared to a conventional vapor-compression heat pump and an absorption-compression heat pump, as well as a gas-driven and electric boiler. 40
4.14 Specific levelized cost of heat (LCOH) for the vapor-compression heat pump and the reversed-Brayton heat pump for the three heating scenarios with a heating duty of 10 MW, compared to a conventional vapor-compression heat pump and a gas-driven and electric boiler. 40

List of Tables

1.1 Definition of the evaluated heating scenarios. 2

2.1 Main characteristics of the high-temperature heat pump cycles covered in this study. . . 4
2.2 Categorization of working-fluid components used for the vapor-compression heat pump evaluation into distinct working-fluid families. 7
2.3 Categorization of working-fluid components used for the reversed-Brayton heat pump evaluation into distinct working-fluid families. 7
2.4 Relevant working-fluid parameters for the environmental, safety, and practical selection criteria. 8
2.5 Summary of the operating range, pressure and temperature capabilities, advantages, and limitations of the most relevant compressors. 9
2.6 Summary of the operating range, pressure and temperature capabilities, advantages, and limitations of the most relevant expanders and turbines. 10
2.7 Summary of the pressure and temperature capabilities, advantages, and limitations of the most relevant heat exchangers. 11

3.1 Comparison of the vapor-compression heat pump model results to simulation results reported by Vieren et al. [95] for pure acetone with a heat source of sensible heat from 100 °C to 90 °C and a heat sink of sensible heat from 140 °C to 200 °C. 16
3.2 Comparison of the reversed-Brayton heat pump model results to simulation results reported by Zühlsdorf et al. [103] for pure CO_2 with a heat source of sensible heat from 110 °C to 60 °C and a heat sink of sensible heat from 140 °C to 280 °C. 18
3.3 Input parameters for the centrifugal compressor sizing and efficiency estimation. 22
3.4 Comparison of the one-dimensional loss-correlation model efficiency and geometrical parameters results to three literature design studies and the estimation by Uusitalo et al. [93]. 23
3.5 Equipment investment cost correlation parameters for 2011 [91]. 24
3.6 Bare module factors and calculation parameters for the equipment investment cost estimation [91]. 25
3.7 Operational parameters for the levelized cost of heat estimation [38, 103]. 26

4.1 Summary of the vapor-compression heat pump working-fluid family mean performance analysis. 34
4.2 Combined thermodynamic, environmental, safety, and practical assessment of the most favorable vapor-compression heat pump working-fluid families. 35
4.3 Performance data of the selected working fluids for further evaluation of the vapor-compression heat pump and the reversed-Brayton heat pump per heating scenario. . . . 36
4.4 The required stage count and rotational speed, as well as the resulting overall isentropic efficiency, of the centrifugal compressor sizing and efficiency estimation for the vapor-compression heat pump and reversed-Brayton heat pump for the three heating scenarios for a 1 MW and 10 MW heating duty. 37
4.5 Estimated most feasible compressor technologies for the vapor-compression heat pump and reversed-Brayton heat pump for the three heating scenarios and a 1 MW and 10 MW heating duty. 37
4.6 Total, specific, and per-component capital investment costs for the vapor-compression heat pump and reversed-Brayton heat pump as a result of the equipment sizing and cost estimation, compared to a conventional vapor-compression heat pump and an absorption-compression heat pump. 39

A.1 Selected high-temperature heat pump working fluids and their critical selection criteria [105][7][104][20]. . . . 54

B.1 Centrifugal compressor one-dimensional loss correlations. . . . 55
B.2 Input parameters for the centrifugal compressor one-dimensional loss-correlation model literature comparison. . . . 56
B.3 Heat-transfer coefficient correlations. . . . 56

C.1 Environmental, safety, and practical parameters for working-fluid selection of the individual working-fluid components of the vapor-compression heat pump and the reversed-Brayton heat pump [24, 86, 43, 42, 84, 85, 63, 3, 13]. . . . 58
C.2 Mean performance indicators of the best-performing vapor-compression heat pump working fluids of distinct working-fluid families. . . . 59
C.3 Mean performance indicators of the best-performing reversed-Brayton heat pump without internal heat exchanger working fluids of distinct working-fluid families. . . . 60
C.4 Mean performance indicators of the best-performing reversed-Brayton heat pump with internal heat exchanger working fluids of distinct working-fluid families. . . . 61
C.5 Centrifugal compressor dimensions and efficiency estimation results for the vapor-compression heat pump for the three heating scenarios for a heating duty of 1 MW and 10 MW. . . . 62
C.6 Centrifugal compressor dimensions and efficiency estimation results for the reversed-Brayton heat pump without and with internal heat exchanger for the three heating scenarios for a heating duty of 1 MW and 10 MW. . . . 62
C.7 The required type and resulting heat transfer area requirement of the heat exchanger sizing for the vapor-compression heat pump and reversed-Brayton heat pump for the three heating scenarios. . . . 63

Declaration of AI

The author declares that Grammarly AI was used for grammar and spelling checks as well as sentence improvement.

Nomenclature

Abbreviations

Abbreviation	Definition
ACHP	Absorption-compression heat pump
AIT	Autoignition temperature
CFD	Computational fluid dynamics
CO_2	Carbon dioxide
COP	Coefficient of performance
CRF	Capital recovery factor
EN	European Norm
EU	European Union
GWP	Global warming potential
HCFO	Hydrochlorofluoroolefin
HFC	Hydrofluorocarbon
HFO	Hydrofluoroolefin
IHX	Internal heat exchanger
ISO	International Organization for Standardization
LCOH	Levelized cost of heat
LFL	Lower flammability limit
LMTD	Logarithmic mean temperature difference
NIST	National Institute of Standards and Technology
NTU	Number of transfer units
ODP	Ozone depletion potential
OEL	Occupational exposure limit
OH	Annual operating hours
OPEX	Operational expenditure
PFAS	Per- and polyfluoroalkyl substances
RBHP	Reversed-Brayton heat pump
REFPROP	Reference fluid thermodynamic and transport properties database
SLSQP	Sequential least squares quadratic programming
TCI	Total capital investment
TFA	Trifluoroacetic acid
TU Delft	Delft University of Technology
VCHP	Vapor-compression heat pump
VHC	Volumetric heating capacity

Roman symbols

Symbol	Definition
A	Heat transfer area
B_1, B_2	Bare module cost coefficients
c_h	Levelized cost of heat
c_p	Specific heat capacity at constant pressure
CF	Annual cash flow
D	Diameter
F_{BM}	Bare module factor

Symbol	Definition
F_M	Material factor
F_P	Pressure factor
G	Mass flux
h	Specific enthalpy
i	Discount rate
K	Nitrogen equivalence value or supercritical heat-transfer parameter
K_1, K_2, K_3	Equipment cost correlation coefficients
LFL	Lower flammability limit
$LMTD$	Logarithmic mean temperature difference
$\dot{m}$	Mass flow rate
n	Project lifetime
N	Rotational speed
p	Pressure
$\dot{Q}$	Heat transfer rate
Re	Reynolds number
T	Temperature
U	Overall heat transfer coefficient
$\dot{V}$	Volumetric flow rate
$\dot{W}$	Power or work rate
x	Vapor quality
Z	Number of compressor blades

Greek symbols

Symbol	Definition
α	Heat transfer coefficient
β	Thermal expansion coefficient
Δh	Specific enthalpy difference
ΔT	Temperature difference
δ_b	Blade thickness
ϵ	Heat exchanger effectiveness
η	Efficiency
η_{is}	Isentropic efficiency
η_{Lorenz}	Lorenz efficiency
μ	Dynamic viscosity
ν	Kinematic viscosity
Π	Pressure ratio
ρ	Density
Ψ	Evaporation correction factor

1 Introduction

Over the last few years, residential and industrial heat combined accounted for roughly half of global final energy consumption, making it the largest energy end-use, followed by electricity and transport. Industrial process heat accounts for 26% of global energy consumption. With growing demand and heavy reliance on fossil fuels, decarbonizing process heat is one of the most critical and challenging requirements for meeting global net-zero emissions targets [45, 44, 46].

Replacing coal- or gas-fired boilers with electric boilers or high-temperature heat pumps can directly eliminate on-site fossil fuel combustion and cut emissions. Electric boilers are a mature and relatively simple technology and can supply high-temperature heat without a waste heat source; however, their heat ouput is approximately equal to their electricity input. High-temperature heat pumps can upgrade existing heat, delivering multiple times (3-5) more thermal energy than the electricity they consume, potentially reducing operational cost and electricity demand [54, 38, 46]. While thermodynamically advantageous, high-temperature heat pump operation requires high-temperature heat sources to minimize the temperature lift, which is crucial for a high coefficient of performance (COP) and minimal electricity consumption. Additionally, the industrial development and adoption of high-temperature heat pumps are limited by their economic competitiveness and low technology readiness levels at temperatures above 150 °C [6, 54].

A conventional subcritical vapor-compression heat pump (VCHP) using a pure working fluid exchanges most of its heat during isothermal evaporation and condensation. While this efficiently uses latent heat, industrial heat sources and heat sinks commonly exchange sensible heat, causing temperature changes. The resulting mismatch between the heat pump working fluid and process stream temperature profiles causes the heat pump to operate with a higher mean temperature lift than ideally required. Additionally, temperature differences in the heat exchangers caused by temperature-profile mismatch create irreversibilities and lower COP.

Heat pump cycles that absorb and reject heat with a temperature glide can potentially achieve a higher COP and be more attractive than a conventional VCHP. A heat pump that absorbs and rejects heat with the same temperature glide as the heat source and heat sink can theoretically minimize the mean temperature lift and reduce heat-transfer temperature differences with sensible industrial processes. Beyond minimizing mean temperature lift and reducing heat-transfer irreversibilities, integration with a sensible heat source allows further cooling of the source, increasing recovered heat and reducing the required source flow rate.

This study considers three heat pump cycles that absorb and reject heat with a temperature glide. The VCHP is included as it is the most mature technology and can achieve high COPs, while zeotropic mixtures and transcritical operation provide options for operation with a temperature glide. The reversed-Brayton heat pump (RBHP) is included because it uses a gaseous working fluid and inherently exchanges sensible heat. The absorption-compression heat pump (ACHP), while less flexible, is included because absorption and desorption inherently occur with a temperature glide.

The suitability of these heat pump cycles cannot be assessed independently of the working fluid. Thermophysical properties determine the achievable temperature glide, compression work, volumetric heating capacity (VHC), pressure levels, compressor discharge temperature, and heat-transfer behavior. Additionally, high-temperature heat pump working fluids can have environmental impacts, pose safety risks, and affect equipment requirements. A broad screening is therefore required to identify working-fluid cycle combinations that offer favorable thermodynamic performance and practical feasibility.

Previous studies have demonstrated the potential of zeotropic mixtures, transcritical VCHPs, RBHPs, and ACHPs for high-temperature process heating. However, these technologies are often evaluated separately or compared using limited working fluids and operating conditions. It remains unclear whether high-temperature heat pumps that absorb and reject heat with a temperature glide offer a significant advantage over established heating solutions. Comparisons may also overlook important trade-offs involving thermodynamic performance, equipment requirements, and environmental and safety impact. A comparison that combines broad working-fluid screening, cycle optimization, multi-objective analysis, preliminary equipment sizing, and economic evaluation across multiple operating conditions is therefore required.

The objective of this study is to thermodynamically and techno-economically evaluate high-temperature heat pumps and working fluids for industrial sensible heat upgrading with substantial temperature glides at both the heat source and heat sink. The VCHP and RBHP are modeled and optimized for a broad set of pure fluids and binary mixtures, while vendor data is used for the ACHP. The resulting working-fluid and cycle combinations are then screened using thermodynamical, environmental, safety, and practical criteria, and selected combinations are evaluated through preliminary equipment sizing, cost estimation, and comparison of the levelized cost of heat (LCOH).

Three heating scenarios are considered to assess the effects of the heat sink temperature, heat source-heat sink temperature glide ratio, and mean temperature lift. The heating scenarios are listed in Table 1.1. In all scenarios, the heat source and heat sink consist of water that remains fluid at all times.

Table 1.1: Definition of the evaluated heating scenarios.

ID	Heat source	Heat sink
	$T_{in} - T_{out}$ [°C]	$T_{in} - T_{out}$ [°C]
S1	100–50	100–150
S2	100–50	100–200
S3	100–50	150–200

This study is limited to simple VCHP and RBHP configurations with and without an internal heat exchanger (IHX). The VCHP and RBHP are modeled using simple steady-state thermodynamic models, while ACHP data is obtained from a technological vendor. Equipment sizing is preliminary and used to assess practical feasibility; it does not represent final component designs. The thermodynamic, equipment, and economic results are intended as comparative screening estimates.

The remainder of this study consists of the theoretical background for temperature-glide matching by introducing the investigated heat-pump cycles, working-fluid selection criteria, equipment limitations, and reference technologies (chapter 2), the thermodynamic models, optimization procedures, screening and selection, equipment sizing and economic evaluation methods (chapter 3), the thermodynamic screening, working-fluid selection, equipment sizing, and economic results (chapter 4), and the main findings, limitations, and the conclusions (chapter 5).

2

Background

This chapter introduces sensible heat sources and heat sinks, the investigated heat-pump cycles, working-fluid selection criteria, equipment requirements and limitations, and reference technologies. The findings are then synthesized into the evaluation methodology for the reviewed high-temperature heat pump cycles.

2.1. Sensible heat upgrading and temperature glide-matching

The thermodynamic performance and integration potential of a high-temperature heat pump depend strongly on the temperature glide match between the heat pump's working fluid and the industrial heat source and heat sink. A heat pump that matches the temperature glide of the industrial heat source and heat sink can potentially reduce the required mean temperature lift and heat-transfer irreversibilities, and allow for maximum heat recovery. This section discusses the role of sensible heat sources and sinks and the potential benefits of implementing high-temperature heat pumps into these processes.

2.1.1. Sensible heat sources and sinks

Industrial waste-heat sources such as cooling liquid, wastewater, warm compressed air, or flue gas release sensible heat as they cool down. Similarly, many industrial heat sinks, such as preheating combustion air or liquid feed, or drying moist air, involve sensible heating. Unlike latent heat, sensible heat transfer is accompanied by a temperature change. The resulting heat duty $\dot{Q}$ of sensible heat transfer is given by Equation 2.1 and is determined by the mass flow $\dot{m}$, the specific heat capacity at constant pressure c_p, and the temperature change $T_{in} - T_{out}$.

$$\dot{Q} = \dot{m} c_p (T_{in} - T_{out}) \tag{2.1}$$

The recoverable heat duty from a heat source with a given specific heat capacity is thus determined by the mass flow rate and the temperature change. A larger amount of heat can be recovered from a source by allowing for a larger temperature reduction. Similarly, for a given heat duty, increasing the allowable temperature change reduces the mass flow rate of a heat source or heat sink.

2.1.2. Thermodynamic benefit of glide matching

The COP of a high-temperature heat pump can be increased by matching the working-fluid temperature profile to the heat source and heat sink, reducing the required mean temperature lift and heat-transfer irreversibilities.

For an ideal heat pump cycle transferring heat between two isothermal reservoirs (the Carnot cycle), the required temperature lift equals the difference between the hot and cold reservoirs. When this cycle is coupled to sensible source and sink streams, the isothermal Carnot cycle must evaporate below the source-stream temperature and condense above the sink-stream temperature to allow heat to flow. Thus, the required Carnot temperature lift exceeds the mean temperature difference between the heat source and heat sink. In contrast, the Lorenz cycle absorbs and rejects heat exactly at the local temperatures of the source and sink streams. The Lorenz cycle effectively operates by transferring heat between the thermodynamic average of the heat source and heat sink. Because these mean temperatures are closer together than the evaporation and condensation temperatures of an isothermal cycle, the Lorenz cycle achieves a higher ideal COP. The COP of the Carnot cycle is given by Equation 2.2, where T_H and T_C are the temperatures of the hot and cold reservoirs, respectively. The COP of the Lorenz cycle is given by Equation 2.3, where $T_{H,M}$ and $T_{C,M}$ are the thermodynamic mean temperatures of the hot and cold reservoirs, respectively.

$$COP_{Carnot} = \frac{T_H}{T_H - T_C} \tag{2.2}$$

$$COP_{Lorenz} = \frac{T_{H,M}}{T_{H,M} - T_{C,M}} \tag{2.3}$$

Unlike ideal Carnot and Lorenz cycles, real heat transfer requires a finite temperature difference. In a heat exchanger, streams are routed to create local temperature differences and facilitate heat transfer; however, finite temperature differences also generate thermodynamic irreversibilities. Larger local temperature differences increase entropy production and reduce the maximum achievable performance by a heat pump cycle. Entropy production in the heat exchangers can therefore be minimized by matching the heat pump's working-fluid temperature profile to the heat source and heat sink.

2.2. Heat pump cycles with a temperature glide

Heat-pump cycles can produce temperature glides through zeotropic phase change, transcritical or supercritical sensible heat transfer, or absorption and desorption processes, with each approach introducing distinct thermodynamic and equipment trade-offs. This section discusses the working principles, advantages, and limitations of the high-temperature heat pump cycles covered in this study: the VCHP, RBHP, and the ACHP. Table 2.1 summarizes the main characteristics of each high-temperature heat pump cycle and its treatment in this study.

Table 2.1: Main characteristics of the high-temperature heat pump cycles covered in this study.

Characteristic	VCHP	RBHP	ACHP
Main heat-transfer mechanism	Latent and sensible	Sensible	Sorption and sensible
Heat source glide	Mixtures	Inherent	Inherent
Heat sink glide	Mixtures and transcritical operation	Inherent	Inherent
Main efficiency limitation	Compression and expansion losses	Compression losses and work extraction	Compression and solution-cycle losses
Main practical limitation	Compressor and fluid limitations	High-pressure turbomachinery and IHX effectiveness	Complexity and limited flexibility
Treatment in this study	Modeled	Modeled	Vendor data

2.2.1. Vapor-compression heat pump

The VCHP can absorb and reject heat over a temperature glide using zeotropic mixtures, transcritical operation, or a combination of both. VCHPs are included because they are the most mature and robust heat pump technology currently available; however, they are not yet established at high temperatures, and the use of zeotropic mixtures and transcritical cycles remains emerging [95, 1, 18]. The VCHP operates based on a Carnot cycle, as shown in Figure 2.1 with the corresponding pressure-enthalpy and temperature-entropy diagrams.

The evaporator absorbs heat from the heat source by evaporating the working fluid. A compressor then raises the working-fluid gas's temperature and pressure, after which it condenses back into a fluid, releasing heat to the heat sink in the condenser. Finally, an expansion valve expands the fluid and returns it to the evaporator. This cycle is called a single-stage vapor-compression heat pump. An IHX can improve performance by superheating the working-fluid gas exiting the evaporator before it enters the compressor and subcooling the liquid exiting the condenser before it enters the expansion valve. It allows more heat to be absorbed in the evaporator and additionally helps to prevent wet compression.

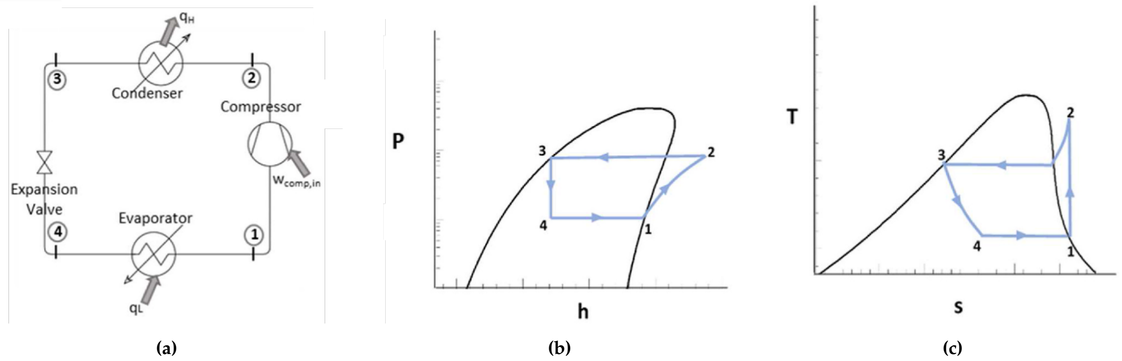

Figure 2.1: (a) Flow sheet of vapor-compression heat pump and (b) the corresponding pressure-enthalpy and (c) temperature-entropy diagrams [1].

VCHPs can absorb and reject heat via a temperature glide by using a mixture of two working fluids with a significant difference in boiling points, causing the mixture to undergo a phase change over a range of temperatures (a zeotropic mixture) and/or by compressing the working fluid(s) to a pressure above the critical pressure and releasing sensible heat at a supercritical pressure (transcritical cycle). Zeotropic mixtures allow customization of the temperature glide in the evaporator and condenser but also alter other fluid properties that affect the heat pump's performance, such as pressure ratio, critical point, latent heat, vapor density, and heat-transfer behavior [40, 104]. Transcritical cycles offer superior COPs to subcritical cycles for high-temperature and large-temperature-glide applications, as they better match the heat sink temperature profile [1, 95]. However, transcritical cycles require high transcritical pressures and can experience higher compression and expansion losses when operated with insufficient heat sink temperature glide [1].

2.2.2. Reversed-Brayton heat pump

The RBHP uses an always gaseous working fluid and therefore inherently absorbs and rejects sensible heat over a temperature glide. RBHPs are included as they are better established at absorbing and rejecting heat via a temperature glide than VCHPs, and they are less limited in heat sink temperature or temperature lift [56, 21, 71]. The RBHP is shown in Figure 2.2 with the corresponding pressure-volume and temperature-entropy diagrams.

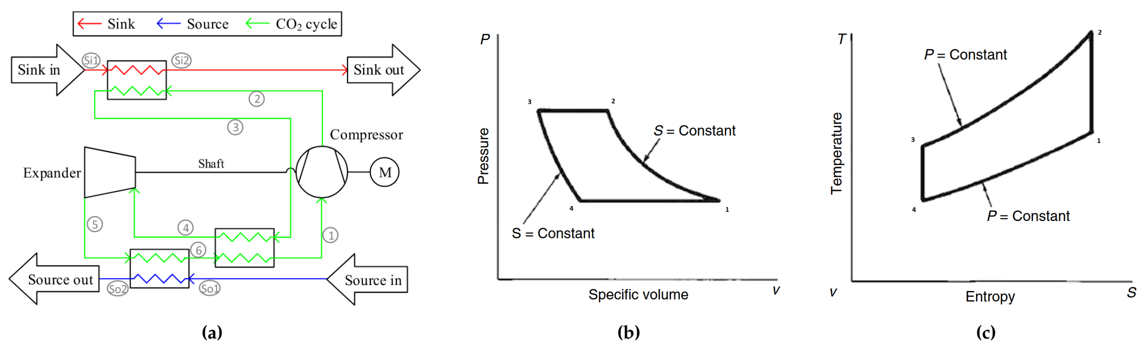

Figure 2.2: (a) Flow sheet of reversed-Brayton heat pump and (b) the corresponding pressure-volume and (c) temperature-entropy diagrams [74, 103].

The working fluid vapor first absorbs heat from the source. The working fluid vapor is then compressed to raise its temperature and pressure, after which it rejects heat to the heat sink. Finally, a portion of the compression work is extracted using a turbine or expander, thereby lowering the temperature and pressure of the working-fluid vapor. Its performance, especially for large temperature lifts, is often improved by using an IHX to preheat and precool the compressor and turbine/expander suction vapor, respectively [16, 56, 21]. At moderate temperatures and temperature lifts, the RBHP generally has a lower COP than the VCHP, but because it does not operate using phase change, it can operate at higher temperatures and temperature lifts where VCHP performance deteriorates. Additionally, the relative performance of the RBHP compared to the VCHP increases for very large temperature glides [21, 16, 71]. Although the RBHP can operate across a wider temperature range, it is restricted by its equipment as it requires high-pressure and high-efficiency turbomachinery and heat exchangers to remain feasible [4, 71, 103].

2.2.3. Absorption-compression heat pump

The ACHP non-isothermally absorbs and desorbs a working-fluid mixture to absorb and reject heat over a temperature glide, using sorption principles to minimize required compression work and pressure levels. Despite its higher complexity, the ACHP is included because its temperature levels and glides are not determined by saturation properties and it inherently absorbs and rejects heat via a temperature glide. Figure 2.3 shows the ACHP with a diagram of its temperature profiles.

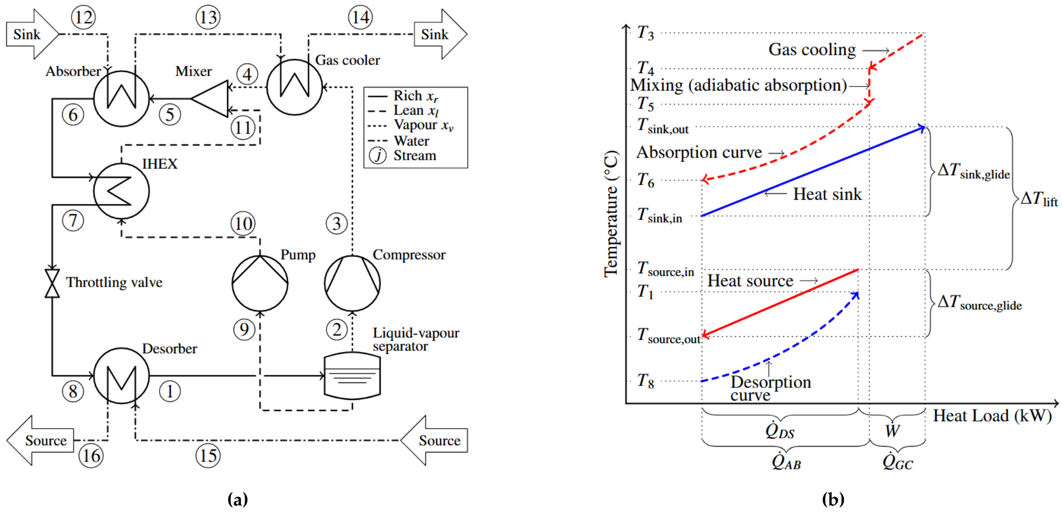

Figure 2.3: (a) Flow sheet of absorption-compression heat pump and (b) a diagram of the temperature profiles over the transferred heat [53].

A zeotropic mixture (typically ammonia-water) is partly evaporated in the desorber using heat from the heat source. The resulting weak ammonia-water solution and ammonia vapor are separated. The weak solution is preheated in the IHX and pumped to a higher pressure. The ammonia vapor is compressed, thereby raising its temperature and pressure. Both high-pressure streams are combined in the absorber, where the vapor is absorbed into the solution, rejecting heat to the heat sink. The resulting rich solution is cooled down in an IHX and expanded back to the desorber pressure. ACHPs are commercially available, but due to their higher complexity, only a limited number of vendors offer them [105, 10]. Additionally, they are less flexible than other high-temperature heat pumps in temperature range, cycle configurations, and working-fluid choice [10, 53].

2.3. Working fluid effects and selection criteria

A high-temperature heat pump working fluid affects not only thermodynamic performance but also operating conditions, equipment requirements, environmental impact, safety, and practical feasibility.

2.3.1. Thermodynamic properties and cycle performance

The thermophysical properties of a working fluid determine the achievable temperature glide during heat transfer, compression work, VHC, compressor discharge conditions, and the heat-transfer behavior.

A working fluid's critical temperature and pressure affect not only the operating boundaries of subcritical, transcritical, or supercritical operation, but also pressure levels, performance, and equipment requirements. Near the critical point, many properties, such as the latent heat, specific heat, density, and compressibility, fluctuate, which affects the heat transfer behavior and compression and expansion work [1, 100, 11, 4, 47, 52]. The working fluid's molecular mass and vapor density determine the compressor requirements such as rotational speed and physical size. Faster-rotating compressors are more complex, and physically larger compressors are associated with larger input power and heat losses [19, 27]. Furthermore, the working fluid's heat capacity and heat capacity ratio determine the compressor discharge temperature for a given increase in compression pressure, affecting the compressor and/or intercooling requirements [19, 83, 8]. The working fluid's latent heat and specific heat determine the balance between phase-change heat and sensible heat, as well as the temperature glide in a heat exchanger for a given mass flow rate [71]. Finally, the working fluid's thermal and momentum transport properties determine the heat transfer coefficients and required heat-transfer area as well as the resulting pressure drop in a heat exchanger [83, 90, 62].

Overall, these properties are represented in the screening by COP, VHC, pressure ratio, discharge pressure and temperature, and estimated heat-transfer area, which together characterize the thermodynamic performance, equipment requirements, and operating severity. These performance parameters are further described in subsection 3.2.3.

2.3.2. Pure fluids and mixtures

Pure fluids undergo phase change at an approximately constant temperature, whereas zeotropic mixtures evaporate and condense over a temperature range, allowing the temperature glide in a VCHP to be customized. Mixtures also alter the temperature glide in an RBHP; however, for both the VCHP and RBHP, mixtures also affect the heat pumps' compression work, equipment requirements, environmental impact, safety, and practical feasibility [100, 40]. Additionally, the best temperature-profile match does not automatically yield the maximum COP in a VCHP, as this depends on a combination of factors [104]. Mixtures also come with disadvantages and challenges such as the degradation of heat-transfer coefficients as a result of diffusion resistances, the risk of composition shift as a result of leakage, and overall more design and operational sensitivity as a result of more property fluctuations and uncertainty [104, 18, 95].

2.3.3. Working-fluid families

Chemically related working-fluid families each have their own performance trends and characteristic thermodynamic and practical trade-offs. Table 2.2 and Table 2.3 list the working-fluid components considered in this study for the VCHP and RBHP, respectively, divided among their distinct working-fluid families.

Table 2.2: Categorization of working-fluid components used for the vapor-compression heat pump evaluation into distinct working-fluid families.

Acetone	Alcohol	Ammonia	Ether	CO_2	HC1	HC2	HC3	HC4	HC5	HC6	HC7	Synthetic	Water
Acetone	Ethanol Methanol	Ammonia	Diethylether Dimethylether	CO_2	Methane	Ethane Ethylene	Propane Propylene Cyclopropane	Butane Isobutane Butene Isobutene	Pentane Isopentane Cyclopentane Neopentane	Hexane Isohexane Cyclohexane	Heptane	R1224yd(Z) R1233zd(E) R1234yf R1234ze(E) R1234ze(Z) R1336mzz(Z)	Water

Table 2.3: Categorization of working-fluid components used for the reversed-Brayton heat pump evaluation into distinct working-fluid families.

Ammonia	Ether	Gasses	HC1	HC2	HC3	HC4	HC5	Noble gasses	Water
Ammonia	Dimethylether	CO_2 Nitrogen Oxygen	Methane	Ethane Ethylene	Propane Propylene Cyclopropane	Butane Isobutane Butene Isobutene	Neopentane	Argon Helium Krypton	Water

Acetone is a flammable, strong organic solvent with a high critical temperature and latent heat of vaporization, potentially providing a high COP; however, its strong solvent capability requires careful evaluation of component and seal materials [37, 35]. Methanol and ethanol are flammable and toxic organic solvents with high critical temperatures that can achieve high COPs [37]. Ammonia is a well-established toxic natural refrigerant with lower flammability that requires high pressures and therefore reaches a high volumetric heating capacity [98]. Diethylether and dimethylether are natural ethers with a high critical temperature that have previously been used in mixtures with synthetic working fluids [31, 41]. CO_2 is a natural, non-toxic, and non-flammable working fluid with a low critical temperature, mostly used for transcritical and supercritical cycles [98, 16]. Hydrocarbons such as alkanes, alkenes, and cycloalkanes are natural flammable working fluids with a wide range of critical temperatures and heat pump applications and generally exhibit low compressor discharge temperatures [41]. Synthetic refrigerants are the historically dominant VCHP working fluids and are transitioning to low-environmental-impact versions; however, newer low-flammability, low-environmental-impact working fluids are classified as per- and polyfluoroalkyl substances (PFAS) [101].

2.3.4. Environmental, safety, and practical criteria

A thermodynamically favorable working fluid is feasible for industrial applications only if its environmental impact, toxicity, flammability, thermal stability, and compatibility with materials and lubricants are suitable. Table 2.4 summarizes the parameters considered to access these criteria.

Table 2.4: Relevant working-fluid parameters for the environmental, safety, and practical selection criteria.

Environmental	Flammability	Toxicity	Thermal stability
ODP	ISO classification	ISO classification	AIT
GWP	LFL	OEL	
PFAS	AIT		
TFA-formation			

The European Commission restricts the use of substances with high ozone depletion potential (ODP) and high global warming potential (GWP) in accordance with the Montreal Protocol of 1983 on substances that deplete the ozone layer and the Kyoto Protocol of 1997 on measures to reduce greenhouse gas emissions. The use of working fluids with an ODP not equal to zero is already forbidden, and by 2036 only working fluids with a GWP less than 150 will be allowed [73, 72, 88, 87]. The atmospheric breakdown of PFAS working fluids can produce trifluoroacetic acid (TFA), a highly mobile and persistent substance that can accumulate in the environment [5]. Although no long-term effects on humans and the environment have been proven yet, it can be harmful to aquatic organisms at concentrations above 0.1 mg/L, and there are emerging concerns regarding liver and reproductive health in mammals [3][105][5]. Furthermore, some degradation pathways may form HFC-23, a super pollutant with an extremely high GWP and a long atmospheric lifetime [75]. As future policies are expected to limit TFA emissions, a better understanding of TFA sources is required to assess their environmental impacts and their sustainability as industrial working fluids [5].

Human safety standards for heat pumps are set out in the European standard EN 378 (1-4), which will be revised in 2026 to include a new method for determining charge limits for flammable working fluids [28, 68]. The European standard uses the ISO 817 safety classification to classify working fluids based on their ability to propagate a flame in air, their burning velocities, and their potential to cause health hazards [48]. Flammability is classified as 1, 2L, 2, or 3, with group 1 having no flame propagation and group 3 being highly flammable, and toxicity is classified as low toxicity (A) or high toxicity (B). For example, ammonia has safety group B2L, CO_2 has safety group A1, and propane has safety group A3. For a working fluid to be classified as less flammable (2), the lower flammability limit (LFL) must be more than 10 kg/m^3 at 23 °C and 1 atm and the heat of combustion must be less than roughly 19000 kJ/kg [7]. The LFL of most working fluids is publicly available, and the LFL of a mixture can be estimated using an ISO calculation method [33]. Additionally, the autoignition temperature (AIT) is a relevant parameter for a safe compressor discharge temperature in a high-temperature heat pump and also indicates how prone a working fluid is to thermal degradation or thermolysis, which compromises performance and safety [95, 99]. For a working fluid to be classified as low toxicity (A), the occupational exposure limit can't be greater than 400 ppm. Regulatory agencies determine the OELs of working fluids, and they are mostly publicly available.

Depending on the working fluid or equipment, the corrosivity, compatibility with materials, miscibility with compressor lubricant, and the fouling potential of a working fluid can also affect the working fluid feasibility [41, 1, 39, 101].

2.4. Equipment requirements and scale effects

Beyond thermodynamic performance, the technical feasibility of a high-temperature heat pump also depends on equipment type, dimensions, efficiency, and cost, which depend on the heat pump's operating conditions and scale. This section covers the major components of a VCHP and an RBHP. It describes the most relevant types of compressors, heat exchangers, and turbines and expanders, along with their working principles, advantages, limitations, and applications.

2.4.1. Compressor selection and limitations

Compressor selection is governed by inlet volumetric flow, pressure ratio, and inlet and discharge conditions, and it greatly affects the cost and overall feasibility of a high-temperature heat pump. However, the relation to inlet volumetric flow, pressure ratio, and inlet and discharge conditions differs per compressor type. The compressor type can also have practical implications, such as the need for downstream oil separation or damping equipment. This section presents an overview of the operating range and capabilities, as well as the advantages and limitations of the most relevant compressors. Table 2.5 summarizes these findings.

Table 2.5: Summary of the operating range, pressure and temperature capabilities, advantages, and limitations of the most relevant compressors.

Type	Operating range	Pressure capability	Temperature capability	Main advantages	Main limitations
Reciprocating	Low to moderate volume flow	Very high discharge pressure; low to moderate pressure ratio	Constrained to 180-200 °C	Suitable for low volume flow; high-pressure capability	Not suited for high discharge temperatures; pulsating flow, maintenance, lubricant requirements
Flooded screw	Moderate volume flow	Moderate discharge pressures; high pressure ratios possible	Constrained to 120 °C	Oil provides sealing and cooling enabling high pressure ratios; broad operating range	Not suited for high discharge pressures and temperatures; oil separation and return are required;
Oil-free screw	Moderate volume flow	Low to moderate discharge pressures; moderate pressure ratios possible	Constrained to 200-220 °C	Oil-free working fluid	Not suited for high discharge pressures; higher complexity
Centrifugal	Moderate to high volume flow	High discharge pressure; low pressure ratio	High discharge temperatures	Suitable for high discharge pressures and temperatures; reliable	Low volume flows produce complex designs; performance is sensitive to fluid and off-design

Compressors fall into two distinct categories: positive displacement compressors and dynamic compressors. Positive displacement compressors increase a gas's pressure by trapping a volume of the gas and reducing that volume. Reciprocating and rotary screw compressors are examples of positive displacement compressors. Dynamic or turbo compressors increase a gas's pressure by continuously increasing its momentum and converting that kinetic energy into static pressure as the gas decelerates. Centrifugal or radial flow compressors are examples of a dynamic compressors [19, 83, 8].

Reciprocating compressor Reciprocating compressors can handle extremely high discharge pressures and are highly flexible in handling varying gas densities and flow rates; however, they have high maintenance costs and their discontinuous flow requires damping equipment [34, 19, 83]. Because the moving parts require oil for cooling, sealing, and lubrication, the discharge temperature is limited by oil degradation, and the oil must be soluble in the working fluid to prevent accumulation in the heat exchangers [27, 89]. Reciprocating compressors are generally not capable of handling low-VHC fluids, as the large volumetric flows require unfeasible cylinder and piston dimensions [27].

Rotary screw compressor Oil-flooded rotary screw compressors allow very high compression ratios as the lubrication and sealing oil absorbs part of the heat of compression; however, to prevent oil degradation, the maximum discharge temperature is limited, and oil solubility in the working fluid and downstream separation systems are required [19, 83, 89]. Oil-flooded rotary screw compressors are constrained in their use of low-VHC fluids, as the large volumetric flows require large rotor sizes and fast rotor tip speeds [27]. The oil-free rotary screw compressors produce oil-free gas, and the discharge temperature is not limited by oil degradation; however, they are more complex, expensive, and are limited in their pressure ratio by the thermal expansion of the rotors [83, 27]. Oil-free rotary screw compressors are also limited in their use of low-VHC fluids for the same reasons as oil-flooded designs, but they are also limited in their use of high-VHC fluids. The oil-free design utilizes internal clearances as sealing, which become proportionally larger at small scales, reducing efficiency [27]. Both designs are also limited in discharge pressure by mechanical limits of the rotors and casing [19].

Centrifugal compressor Centrifugal compressors are very reliable, with long continuous run times and minimal maintenance, and the moving parts don't require oil in the compression path. However, they have a limited operating range and are highly sensitive to operating conditions and changes in gas composition [19, 34, 83, 27]. Centrifugal compressors are the only compressors that can handle low-VHC fluids. Using high-VHC fluids can result in very small dimensions and fast rotational speeds, complicating the design. But as centrifugal compressors are widely developed and applied, this is less of a constraint than for other compressor types [93, 8].

2.4.2. Turbine and expander selection

Turbine and expander selection is governed by the outlet volume flow, pressure ratio, and inlet and discharge conditions, and the efficiency and cost greatly affect the overall feasibility of an RBHP. This section presents an overview of the operating range and capabilities, as well as the advantages and limitations of the most relevant expanders. Table 2.6 summarizes these findings.

Table 2.6: Summary of the operating range, pressure and temperature capabilities, advantages, and limitations of the most relevant expanders and turbines.

Type	Operating range	Pressure capability	Main advantages	Main limitations
Rotary screw	Low to moderate volume flow	Moderate pressure ratio; limited pressure	Suitable for lower rotational speeds; tolerant of two-phase conditions	Internal leakage; lubrication requirements
Radial-inflow	Moderate volume flow	High pressure ratio	High efficiency; compact and reliable	Low volume flows produce complex designs
Axial	High volume flow	Low pressure ratio per stage	High efficiency at large scale	Complex; less suitable for low volume flows

Turbines can also be divided into the same categories as compressors: volumetric expanders and dynamic or turbo-expanders [83, 2]. Volumetric expanders operate cyclically by trapping a volume of gas and expanding it; the gas exerts a net force on the movable component. Among volumetric expanders, rotary screw expanders are the only type reported to operate at outputs above 50 kW [2]. Dynamic expanders convert the high pressure to momentum by accelerating the fluid and transferring that momentum to blades on a rotating shaft. Radial and axial turbines are examples of dynamic expanders [83, 8, 2].

Rotary screw expander Rotary screw expanders can handle small volumetric and two-phase flows. They can achieve moderate expansion ratios, but they are more costly and do not achieve very high efficiencies. They operate exactly the same as rotary screw compressors and generally require oil for sealing and lubrication and can't handle high pressures [2, 8].

Radial turbine Radial inflow turbines are highly efficient, have a large operating range, and can handle large pressure ratios and high pressures and temperatures. Like centrifugal compressors, their performance is sensitive to off-design operation, and small volumetric flows can lead to very small dimensions and high rotational speeds, complicating design [2, 17].

Axial turbine Axial turbines are the dominant technology for large volumetric flows, achieving high efficiencies and capable of handling high pressures and temperatures. Their efficiency drops significantly at smaller volumetric flows, and their expansion ratio is limited per stage; they require complex design, leading to high cost [9, 2, 17].

2.4.3. Heat exchanger selection and heat-transfer requirements

Heat exchanger selection is governed by the heat-transfer behavior, minimum approach temperature, fluid properties, and operational conditions. This section discusses the basics of heat transfer and presents an overview of the operating range and capabilities, as well as the advantages and limitations of the most relevant heat exchangers. Table 2.7 summarizes these findings.

Heat transferred over a surface is described by Equation 2.4, where $\dot{Q}$ is the heat transferred in $Watt$, U is the overall heat transfer coefficient in W/m^2K, A is the heat transfer area in m^2, and ΔT_{LMTD} is the

Table 2.7: Summary of the pressure and temperature capabilities, advantages, and limitations of the most relevant heat exchangers.

Type	Pressure capability	Temperature capability	Main advantages	Main limitations
Gasketed plate	Low pressure	Moderate temperature	Close temperature approach; compact	Gasket constrains maximum pressure and temperature
Brazed or welded plate	Moderate pressure	High temperature	Close temperature approach; compact	Limited differential pressure
Multiple pipe	High pressure	High temperature	Close temperature approach; suitable for high differential pressures; simple construction	Large footprint and less feasible at large duties
Shell-and-tube	High pressure	High temperature	Suitable for high differential pressures; robust; scalable to large duties	Close temperature approach more complex; larger footprint; less feasible at small scale

logarithmic mean temperature difference between the two heat-exchanging media in K. The overall heat transfer coefficient U depends on the heat-transfer fluids and the heat exchanger.

$$\dot{Q} = UA\Delta T_{LMTD} \tag{2.4}$$

Overall, phase change and liquid-to-liquid duties result in higher heat transfer coefficients than liquid-to-gas and gas-to-gas duties. The logarithmic mean temperature difference ΔT_{LMTD} is the temperature driving force for heat transfer, and it depends on the flow configuration and the temperature profiles of the heat-transfer fluids. A countercurrent flow configuration is essential for non-isothermal temperature glide matching, as it allows a temperature cross and small temperature differences throughout the heat exchanger. Additionally, countercurrent flow results in a larger logarithmic mean temperature difference than cocurrent flow. Real heat exchangers can experience non-ideal countercurrent flow configurations, limiting the minimum temperature approach and requiring more heat transfer area [83, 90].

The most relevant heat exchangers are plate, multiple-pipe, and shell-and-tube heat exchangers. Plate heat exchangers consist of stacked, bonded corrugated plates that separate the heat-transfer fluids. Multiple-pipe heat exchangers consist of multiple concentric pipes through which the heat-transfer fluids run. Shell-and-tube heat exchangers consist of a bundle of tubes enclosed in a cylindrical shell, with a head at each end. As one fluid travels through the tubes, the other travels through the shell and is directed repeatedly across the tubes by baffles to exchange heat; many configurations are possible [83, 90].

Plate heat exchangers Plate heat exchangers can achieve very small approach temperatures, and the corrugated plates enhance turbulence and have a large surface area, resulting in high heat transfer. Additionally, increased turbulence reduces fouling and enables operation with viscous fluids.

Gasketed plate heat exchangers are limited in pressure and temperature by the gasket sealing capabilities [62, 90, 69, 83]. Brazed plate heat exchangers eliminate the need for a gasket by employing an all-metal core [62, 69]. As a result, the brazed plate heat exchanger is suitable for higher pressures and temperatures compared to the gasketed plate heat exchanger [69]. A drawback of the brazed plate heat exchanger is that the permanently sealed plates don't allow for easy dismantling or mechanical cleaning. Additionally, they are mainly manufactured for small-scale applications [69, 62]. Welded plate heat exchangers can handle even more extreme pressures and temperatures because of stronger seals [90, 83]. Just like brazed plate heat exchangers, their main drawback is that they are sealed; however, welded plate heat exchangers are often available for large-scale applications [69]. Both brazed and welded plate heat exchangers are limited in the differential pressure between the two fluids [69, 90].

Plate heat exchangers can also be constructed with fins, increasing heat-transfer area and effectiveness. Plate-fin heat exchangers are mainly used for gas-to-gas applications. They are highly customizable, enabling crosscurrent, countercurrent, cross-countercurrent, co-current flow, and multi-stream configurations [62, 83, 69].

Multiple-pipe heat exchanger Multiple-pipe heat exchangers can also achieve very small approach temperatures and they can easily be designed for high pressures and temperatures. They have a flexible design, but low area density makes them physically larger and heavier than plate heat exchangers. As a result, their use at large thermal duties is uneconomical and unfeasible [83, 69].

Shell-and-tube heat exchanger The shell-and-tube heat exchanger is the most robust and well-known heat exchanger and can be designed for almost any application. They can easily be designed for high (differential) pressures and temperatures; however, they are less capable of achieving a temperature cross and small temperature approaches than other heat exchangers, but they can be arranged in series to compensate. While this increases costs, their scalability advantage usually compensates at large thermal duties [90, 83].

2.5. Reference heat supply

Established heat-supply technologies provide industrial references for determining the feasibility of high-temperature heat pumps upgrading sensible heat over a temperature glide. The reference heat-supply technologies include a gas-driven boiler, an electric boiler, and a conventional VCHP. The investigated and reference technologies are compared on their thermodynamic performance, investment costs, and LCOH.

Gas-driven boiler Gas-driven boilers are a mature technology and represent the industry standard for supplying process heat. They can produce hot water while achieving high combustion efficiencies, can be scaled to very large sizes (250 MW), and have long technical lifetimes [38].

Electric boiler Electric boilers are a mature, simple technology that represents a direct-electrification reference. They can also produce hot water with high efficiency, but they are more costly and have a shorter technical lifetime than gas-driven boilers [38].

Conventional vapor-compression heat pump A conventional subcritical VCHP using a pure working fluid represents a potential future industrial reference using isothermal heat transfer. They are even more costly than electric boilers, but they achieve significantly better efficiencies by using a heat source [38].

2.6. Implications for the evaluation methodology

The reviewed high-temperature heat pump cycles, working-fluid criteria, equipment requirements, and reference technologies indicate that the thermodynamic performance and integration potential of high-temperature heat pumps into industrial sensible heat processes must be evaluated through a combined thermodynamic, practical, and techno-economic methodology. The reviewed high-temperature heat pump cycles offer different approaches to absorbing and rejecting heat with a temperature glide, each with its own working-fluid and equipment trade-offs.

Therefore, the screening must combine thermodynamic, environmental, safety, and practical criteria to evaluate working-fluid and cycle combinations. Additionally, a preliminary equipment design and economic evaluation are required to evaluate potential trade-offs with equipment limitations, feasibility risks, and investment costs. Finally, a comparison with reference technologies must show the overall potential of high-temperature heat pump absorbing and rejecting heat with a temperature glide for industrial sensible heat applications.

3
Methodology

This chapter describes the modeling, screening, selection, and evaluation methodology used to compare high-temperature heat pumps for a sensible heat source and heat sink. First, the overall simulation and evaluation procedure is introduced, followed by the thermodynamic models for the VCHP and RBHP. Next, the performance indicators, Pareto-based multi-objective screening, and working-fluid family analysis are introduced, along with selection criteria for selecting favorable working fluids from the thermodynamic screening. Finally, the equipment feasibility assessment, sizing relations, and cost estimations are presented.

3.1. Simulation and evaluation procedure

The simulation and evaluation procedure is structured to identify, select, and evaluate promising working-fluid cycle combinations for the VCHP and RBHP and compare them to the ACHP. **??** shows an overview of the simulation and evaluation procedure.

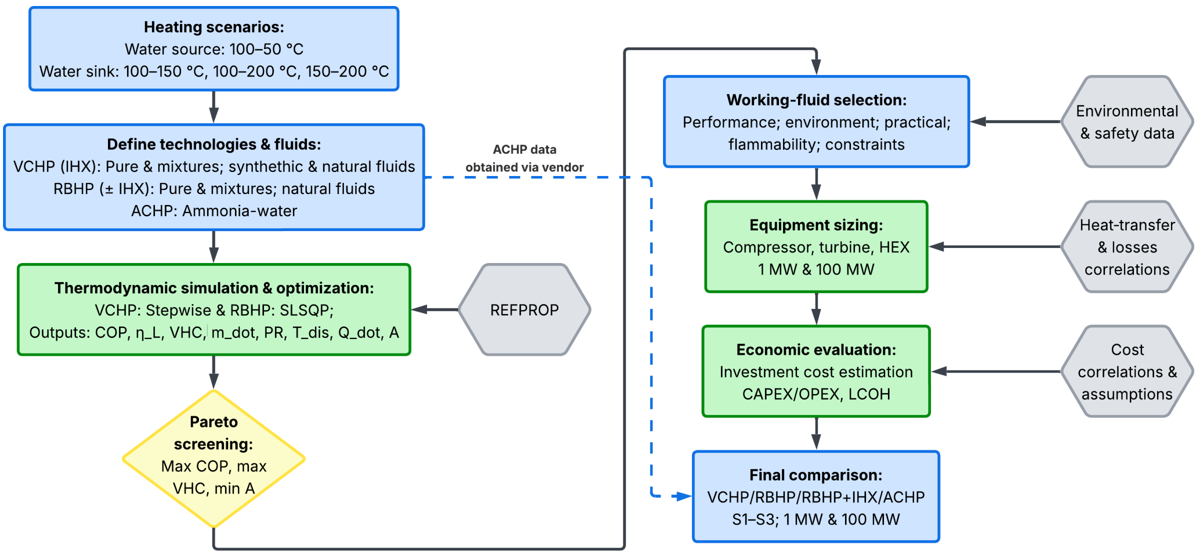

Figure 3.1: Overview of the simulation and evaluation procedure to identify, select and evaluate working-fluid cycle combinations for the vapor-compression and reversed-Brayton heat pump and compare them to the absorption-compression heat pump.

For the three heating scenarios, a thermodynamic screening of working fluids is performed for the VCHP and the RBHP. The VCHP and RBHP are simulated and thermodynamically optimized for every pure fluid and binary mixture with 10 $mol\%$ increments of the working fluids presented in subsection 2.3.3. Table A.1 lists the main thermodynamic, environmental, and safety characteristics of these working fluids. The ACHP is not simulated because of limited flexibility in working-fluid selection and the added complexity of modeling thermochemical reactions. Instead, performance data were obtained directly from a commercial technical vendor through McDermott.

The VCHP and RBHP simulation results are screened and analyzed using the performance indicators, a Pareto-based multi-objective screening, and a working-fluid family mean performance analysis. Working fluids for further evaluation are then selected based on the screening results and environmental, safety, and practical criteria. For the selected working-fluid cycle combinations, an equipment feasibility and economic evaluation is performed.

The thermodynamic simulations are performed for a heating duty of 1 MW, and the economic evaluation is performed for both a heating duty of 1 MW and 10 MW. For the ACHP, two suitable vendors were identified; however, only one met the minimum heat sink temperature requirement (150 °C). The ACHP is considered only for heating scenario S1, as the reported maximum heat sink temperature for this system was 160 °C. The performance data were obtained for a heating duty of 1 MW.

3.2. Thermodynamic models

Working-fluid cycle combinations for the VCHP and RBHP are modeled and optimized for the three heating scenarios to screen and select favorable combinations. This section presents the thermodynamic models and optimization methods, along with the performance indicators used to evaluate the simulation results.

Both the VCHP and RBHP models were developed in Python 3.13.3 [70] and use the NIST REFPROP V10 [60] database, accessed via the CoolProp Python interface, to calculate thermophysical properties [15, 14]. The NIST REFPROP database provides some of the most accurate thermophysical property models for a large variety of industrially relevant fluids and fluid mixtures [60]. However, thermophysical property calculations can fail to converge, especially near phase boundaries, critical regions, or for mixtures under conditions where the used property model is numerically sensitive. In this study, these cases are referred to as failed property calculations. Several procedures are implemented to prevent failed property calculations from causing unusable simulation results and are described throughout the following sections.

3.2.1. Vapor-compression heat pump

Figure 3.2 shows an overview of the VCHP simulation procedure, which consists of a thermodynamic model and an optimization procedure. This section outlines the model and optimization assumptions and constraints, along with validation against literature data.

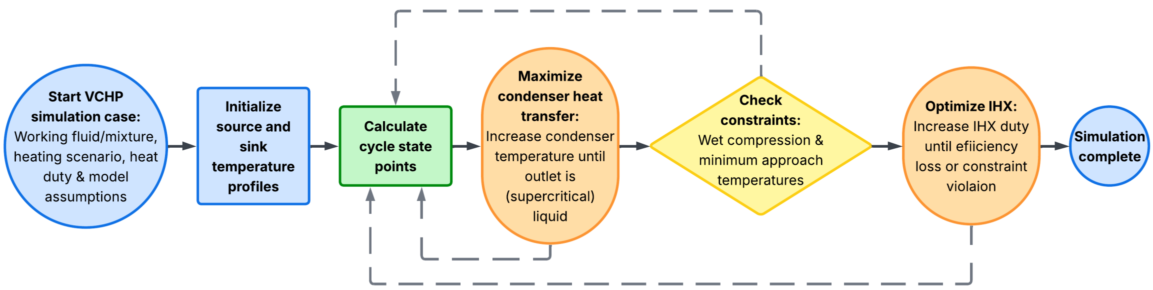

Figure 3.2: Overview of the simulation procedure for the vapor-compression heat pump consisting of a thermodynamic model and an optimization procedure that maximizes condenser and internal heat exchanger heat transfer.

Thermodynamic model The VCHP was modeled as a simple cycle with an IHX as shown in Figure 3.3. The model is based on the first and second laws of thermodynamics. For all components, the steady-state mass and energy balances are satisfied, and no mass or energy is lost to the environment. The compression is modeled using an isentropic efficiency, as given in Equation 3.1, where h_i and h_o denote the enthalpy values at the inlet and outlet of the compressor, and $h_{o,s}$ denotes the enthalpy value at the outlet of the compressor for an isentropic compression.

$$\eta_{is,comp} = \frac{h_{o,s} - h_i}{h_o - h_i} \tag{3.1}$$

The compression is also constrained to avoid liquid formation during compression (wet compression). The expansion valve is modeled as an isenthalpic process. The heat exchangers are constrained using a minimum approach temperature. The heat exchanger paths are discretized into 100 state points to validate the constraints. At least 90% of these property calculations of the heat exchanger state points must succeed. The compression path is also discretized into 100 state points to check the wet compression constraint, with the same minimum property-calculation success rate requirement. The constraints and assumptions of the VCHP model are:

1. The compression has an isentropic efficiency of 80%.
2. The minimum approach temperature for the evaporator, condenser, gas cooler, and IHX is 5 K.
3. No pressure losses occur in the system.
4. The condenser outlet is liquid.
5. The compression remains in a gaseous state at all times.

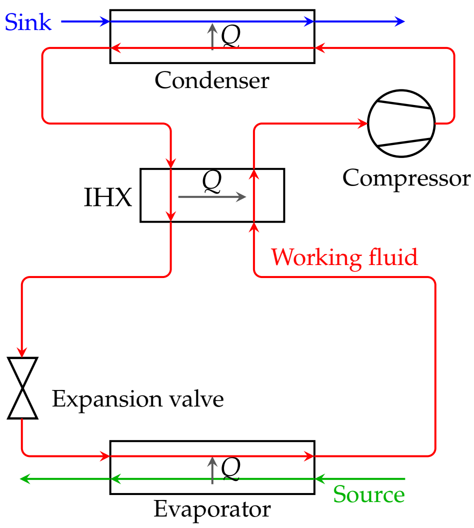

Figure 3.3: Process flow diagram of a single-stage vapor-compression heat pump with an internal heat exchanger.

Optimization The VCHP cycle is thermodynamically optimized based on the work of Lammers [59]. It entails a fast, stepwise, iterative, constraint-based approach that maximizes heat transfer in the condenser and evaporator, starting from the minimum approach temperatures of the heat source and heat sink. Additionally, the degree of superheating is optimized using the total entropy production, thereby maximizing heat transfer in the IHX. If the cycle cannot meet the IHX constraints, the optimization is performed for a simple cycle without an IHX.

Validation The resulting model was validated by reproducing the thermal oil heating operating case reported by Vieren et al. [95]. It operated with pure acetone and assumed an isentropic efficiency of 75 % for the compressor, a minimum approach temperature of 5 K in the evaporator and condenser, an IHX effectiveness of 75 %, and the pressure levels and amount of superheating and subcooling were optimized with respect to a maximum COP. Validation was performed with the same modeling assumptions, except for the IHX, which was modeled with a minimum approach temperature of 5 K. Table 3.1 compares the results and shows minimal deviations.

3.2.2. Reversed-Brayton heat pump

Figure 3.4 shows an overview of the RBHP simulation procedure, which uses the thermodynamic model in multiple optimization iterations to find the global optimum within its pressure operating domain. This section outlines the assumptions and constraints of the thermodynamic model and the optimization procedure and algorithm, along with a validation of the simulation against literature data.

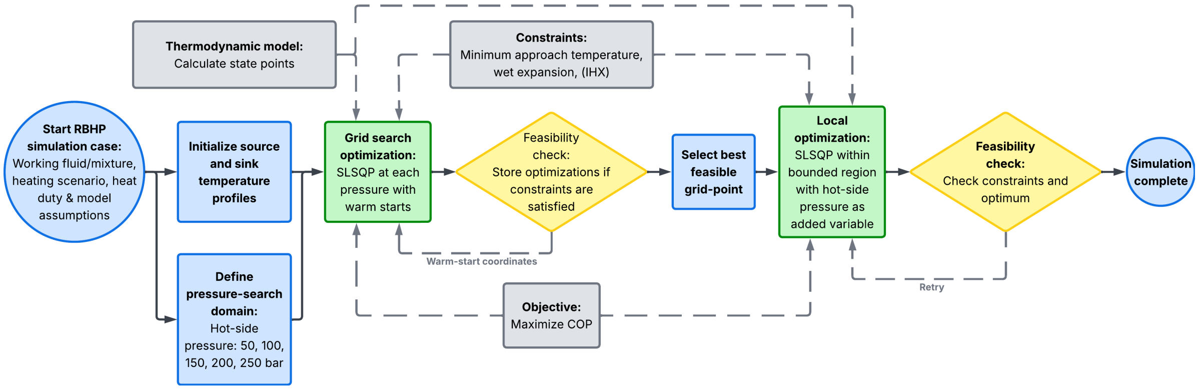

Figure 3.4: Overview of the simulation procedure for the reversed-Brayton heat pump consisting of a thermodynamic model and an optimization procedure. The optimization procedure consists of a grid search and a local optimization using a sequential least squares quadratic programming method.

Thermodynamic model The RBHP was modeled as a simple cycle without an IHX, as shown in Figure 3.5b, and as a simple cycle without an IHX, as shown in Figure 3.5a. The model satisfies the same mass and energy balances and assumptions as the VCHP model. The compression and expansion are modeled using an isentropic efficiency, as given in Equation 3.1 and Equation 3.2.

$$\eta_{is,turb} = \frac{h_o - h_i}{h_{o,s} - h_i} \tag{3.2}$$

The gas heater and gas cooler are constrained using a minimum approach temperature. The gas heater and gas cooler paths are discretized into 10 state points to validate the constraints. At least 90% of these property calculations of the heat exchanger state points must succeed. The expansion path is also discretized into 10 state points to check for liquid formation, with the same minimum property-calculation success rate requirement. As the RBHP model is computationally significantly less efficient than the VCHP model, the number of discretization points is also chosen to be significantly lower. The IHX is modeled using the effectiveness-NTU method, as shown in Equation 3.3, where $\dot{Q}$ is the heat flow in the IHX, $\dot{m}$ is the mass flow of the working fluid, $c_{p,min}$ is the minimum of the isobaric specific heats of the hot and cold stream in the IHX, and $T_{i,hot}$ and $T_{i,cold}$ are the inlet temperatures of the hot and cold streams in the IHX.The constraints and assumptions of the RBHP model are:

1. The compression has an isentropic efficiency of 75%.
2. The expansion has an isentropic efficiency of 75 %.
3. The minimum approach temperature for the gas heater and cooler is 7.5 K.
4. The IHX has an effectiveness of 85%.
5. The expansion remains in a gaseous state at all times
6. No pressure losses occur in the system.

Table 3.1: Comparison of the vapor-compression heat pump model results to simulation results reported by Vieren et al. [95] for pure acetone with a heat source of sensible heat from 100 °C to 90 °C and a heat sink of sensible heat from 140 °C to 200 °C.

Source	COP [-]	Pressure ratio [-]	Condenser pressure [bar]	Evaporator pressure [bar]
Vieren et al. [95]	3.34	9.24	23.14	2.46
Model	3.40	9.09	22.61	2.49
Relative difference [%]	1.9	1.6	2.3	1.1

$$\dot{Q}_{IHX} = \epsilon_{IHX}\dot{m}c_{p.min}(T_{i,hot} - T_{i,cold}) \tag{3.3}$$

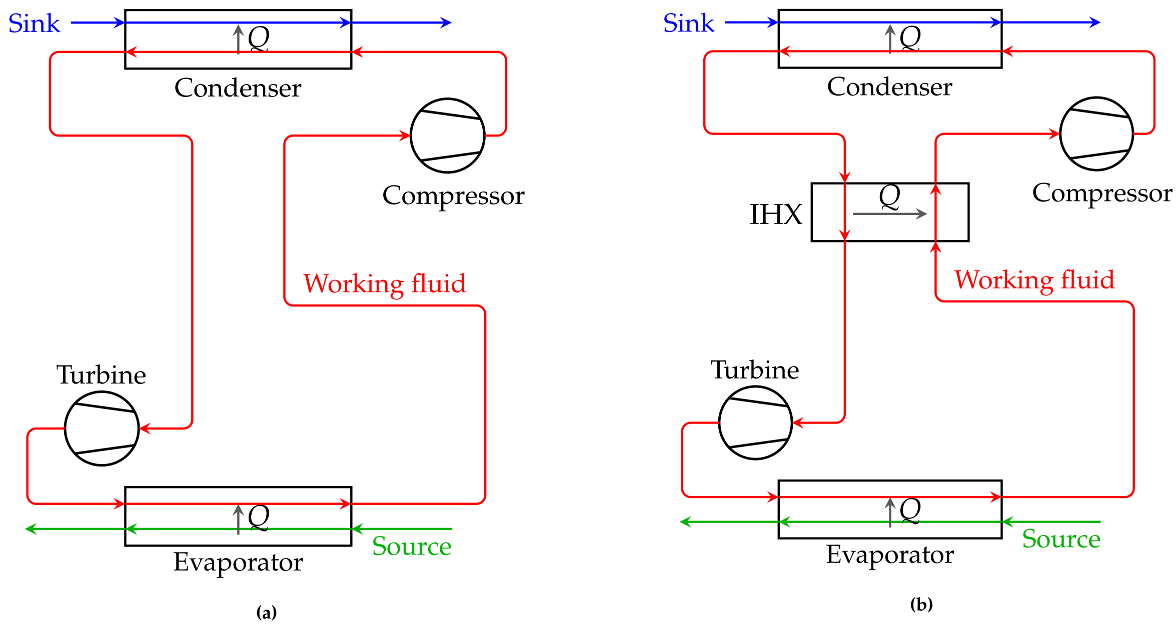

Figure 3.5: Process flow diagram of a reversed-Brayton heat pump (a) without and (b) with an internal heat exchanger.

Optimization The RBHP cycle is thermodynamically optimized using a gradient-based constrained optimization. Specifically, the sequential least squares quadratic programming (SLSQP) method implemented by SciPy for non-linear constrained optimization in Python [57, 96]. While a stepwise iterative model, as used for the VCHP, is computationally more efficient, it converges to the first point where all constraints are met. However, for some RBHP cycles, this is not a thermodynamic optimum. An SLSQP optimization allows for an optimum search across the full design space while rigorously enforcing all constraints. It approximates the objective function quadratically and combines it with linearized constraints to find an optimum. It requires careful tuning of the variable and constraint scaling, the constraint fault margins, and the precision target.

To balance computational effort and accuracy, a grid-search optimization strategy is implemented. The high-side pressure design space was evaluated sequentially at five grid points using a perturbed warm-start approach; subsequently, local optimization was performed in a bounded neighborhood of the best-performing grid point, with high-side pressure added as an additional variable. The warm-start approach uses the local optimum coordinates from the previous grid-point optimization as the starting coordinates for the current optimization.

As SLSQP is a local optimizer, it can converge to infeasible regions or fail near boundaries. To ensure robustness, a custom algorithm was developed by testing over a wide range of working fluids. If the optimization failed or converged to an infeasible region during the grid search, the results are not used for the final local optimization and the warm-start approach. If the final local optimization failed, converged to an infeasible region, or produced a result inferior to that identified in the grid search, additional optimization runs are initiated with other perturbations and with adaptively adjusted simulation bounds near infeasible regions. The constraints and assumptions of the RBHP optimization are:

1. The grid search is performed at 50, 100, 150, 200, and 250 bar.
2. The final optimization is performed within ±50 bar of the best-performing grid point, with a maximum of 250 bar.

Table 3.2: Comparison of the reversed-Brayton heat pump model results to simulation results reported by Zühlsdorf et al. [103] for pure CO_2 with a heat source of sensible heat from 110 °C to 60 °C and a heat sink of sensible heat from 140 °C to 280 °C.

Source	COP [-]	Mass flow rate [kg/s]	Pressure ratio [-]	Compressor discharge pressure [bar]	Compressor discharge temperature [°C]
Zühlsdorf et al. [103]	1.72	279	3.44	140	290
Model	1.70	287	3.32	140	293
Relative difference [%]	1.0	2.9	3.3	0.0	1.1

Validation The resulting model was validated by reproducing the alumina production operating case reported by Zühlsdorf et al. [103]. It operated with pure CO_2 and assumed an isentropic efficiency of 75% for both the compressor and turbine, a motor and gear efficiency of 95%, a minimum approach temperature of 7.5 K in all heat exchangers, and the pressure levels were optimized with respect to a maximum COP, with a maximum pressure of 140 bar. The validation used the same modeling assumptions, except for the IHX, which was modeled with an effectiveness of 85%. A comparison of the results is listed in Table 3.2 and shows minimal deviations.

3.2.3. Performance indicators

The simulation results are evaluated using indicators representing thermodynamic performance, compactness and equipment demand, and operating severity and feasibility. The COP and Lorenz efficiency characterize thermodynamic performance; VHC and heat-transfer area provide preliminary indications of compressor and heat-exchanger size and requirements; and pressure ratio as well as compressor discharge pressure and temperature indicate compressor and equipment feasibility.

The COP determines the heat pump's energy efficiency and strongly influences the electricity consumption, operational costs, and LCOH. The COP is defined in Equation 3.4, where $\dot{Q}_{out}$ is the heat rejected to the heat sink and $\dot{W}_{in}$ is the required work of the heat pump in $Watt$. The required work $\dot{W}_{in}$ equals the work of the compressor for the VCHP and the difference between the work of the compressor and the work extracted from the expander for the RBHP.

$$COP = \frac{\dot{Q}_{out}}{\dot{W}_{in}} \tag{3.4}$$

The work of the compressor W_{comp} is given by Equation 3.5, and the work of the turbine W_{turb} is given by Equation 3.6, where $\dot{m}_{wf}$ is the mass flow rate of the working fluid in kg/s.

$$\dot{W}_{comp} = \dot{m}_{wf}(h_{o,comp} - h_{i,comp}) \tag{3.5}$$

$$\dot{W}_{turb} = \dot{m}_{wf}(h_{o,turb} - h_{i,turb}) \tag{3.6}$$

The Lorenz efficiency compares cycle performance across heating scenarios by relating the COP to the ideal Lorenz COP, as given by Equation 3.7.

$$\eta_{Lorenz} = \frac{COP}{COP_{Lorenz}} \tag{3.7}$$

VHC relates the heat rejected to the heat sink to the compressor inlet volumetric flow and indicates the compressor's compactness. While a compact compressor is associated with smaller power input and heat losses, it can result in a small inlet volumetric flow, complicating design for certain compressor types at small scales. For larger heating duties, the absolute volumetric flow also increases, allowing high VHC while maintaining compressor feasibility. The volumetric heating capacity VHC is given by Equation 3.8, where $\dot{V}_{in,comp}$ is the volumetric flow rate at the compressor inlet in m^3/s.

$$VHC = \frac{\dot{Q}_{out}}{\dot{V}_{in,comp}} \tag{3.8}$$

The required heat-transfer area determines the size and cost of the heat exchangers [83, 90]. The required heat-transfer area for a pure counter-current flow heat exchanger is given by Equation 3.9, where the overall heat-transfer coefficient U is approximated using the fluid heat-transfer coefficients, and the wall and fouling-layer heat-transfer resistances are assumed negligible.

$$A = \frac{\dot{Q}}{U \Delta T_{LMTD}} \tag{3.9}$$

The fluid heat-transfer coefficients α_h and α_c are estimated using literature correlations and assumptions. As a result, the estimated heat-transfer area does not represent the final heat exchanger design, but it does compare working fluid properties and heat-transfer behavior, indicating size and capital costs. The heat-transfer coefficient correlations are discussed in detail in subsection 3.4.2.

The pressure ratio dictates compression staging and intercooling requirements, increasing complexity and costs as well as compromising efficiency [27, 8]. The pressure ratio Π is given by Equation 3.10, where p_{out} and p_{in} are the compressor outlet and inlet pressures. Furthermore, the compressor discharge pressure and temperature are thermodynamic simulation results and are key to compressor selection and design, as well as overall safety, complexity, and costs.

$$\Pi = \frac{p_{out}}{p_{in}} \tag{3.10}$$

3.3. Working-fluid screening and selection criteria

VCHP and RBHP working-fluid cycle combinations are screened and interpreted to select favorable candidates for further preliminary equipment and economic evaluation. This section presents a working-fluid screening method, a working-fluid family analysis method, and environmental, safety, and practical selection criteria for favorable working fluids. Additionally, it presents a method for assessing the flammability of a working-fluid mixture. The screening and family analysis also provide complementary checks on result consistency. Agreement across the two methods reduces the influence of isolated results that may result from numerical anomalies such as unstable optimizer convergence, REFPROP instabilities, or uncertainty in heat-transfer coefficient correlations.

3.3.1. Pareto-based multi-objective screening

Pareto-based multi-objective screening evaluates four primary objectives: maximizing COP, maximizing VHC, minimizing pressure ratio, and minimizing the total estimated heat-transfer area. These objectives represent electricity consumption and operational costs, compressor compactness and simplicity, and heat exchanger size and costs.

A working-fluid cycle combination is identified as Pareto-optimal when no other result simultaneously achieves a higher COP, higher VHC, lower pressure ratio, and a lower heat-transfer-area requirement. In addition to identifying working fluids with a favorable balance between the primary performance indicators, the Pareto-based screening is also used to analyze trends across the simulation results, such as performance trade-offs across the heating scenarios or frequently Pareto-optimal fluids and mixtures.

3.3.2. Working-fluid family mean performance analysis

The working-fluid family mean performance analysis complements the individual-fluid Pareto screening by identifying whether favorable performance is characteristic of a broader chemical family or limited to individual fluids or mixture compositions. Thermodynamic trends across distinct working-fluid families are identified by analyzing the mean performance indicators of the best-performing working fluids within a working-fluid family. An individual working fluid is assigned to a fluid family when the combined mole fraction of the components belonging to that family is at least 50 $mol\%$.

3.3.3. Environmental, safety and practical selection criteria

The non-thermodynamic feasibility of a working fluid is assessed by evaluating several environmental, safety, and practical selection criteria. In this section, the properties assessed and evaluations performed to select a favorable working fluid are listed:

- Only working fluids with minimal to zero ODP and GWP are selected.
- Non-PFAS working fluids are preferred. Minimal TFA formation potential is preferred for working fluids containing PFAS.
- Non-flammable working fluids are preferred. A high LFL and an AIT well above the compressor discharge temperature are preferred for flammable working fluids.
- Non-toxic working fluids are preferred. A high OEL is preferred for toxic working fluids.
- Working fluids that are known to be resistant to thermal decomposition and have a high OEL are preferred.
- Working fluids that are compatible with common materials and oils are preferred.
- Working fluids that have been studied for use as a high-temperature heat pump working fluid are preferred.

3.3.4. Flammability classification of working-fluid mixtures

The flammability of a working-fluid mixture is assessed by estimating the ISO 817 safety classification of the mixture via the LFL. This section presents a calculation method for the LFL of the working-fluid mixture.

The LFL is calculated using the ISO 10156:2017 calculation method for mixtures of flammable gases, mixtures of flammable gases with nitrogen and/or air, and mixtures of flammable gases with other inert gases [33, 78]. Equation 3.11 is used for mixtures of flammable gases, nitrogen, and air. LFL_M and LFL_i are the lower flammability limits of the mixture and the flammable gas in $mol\%$, respectively, and A_i is the molar fraction in $mol\%$ of the flammable gas i.

$$LFL_M = \frac{100}{\sum_i^n \frac{A_i}{LFL_i}} \tag{3.11}$$

Equation 3.12 is used in accordance with Equation 3.13 for mixtures of flammable gases with air and other inert gases other than nitrogen. LFL_i' is the corrected lower flammability limit of a flammable gas due to the change in molar heat capacity of the air-inert mixture, LFL_M' is the average lower flammability limit of the mixture of flammable gases weighted according to their molar fractions, calculated with Equation 3.11, $\overline{K}$ is the average nitrogen equivalence value of the inert gases weighted according to their molar fractions, and B_k is the molar fraction in $mol\%$ of inert gas k.

$$LFL_M = \frac{100}{\sum_i^n \frac{A_i}{LFL_i'}} \tag{3.12}$$

$$LFL_i' = \frac{100 - LFL_M' - (1-\overline{K})\frac{\sum_p^i B_k}{\sum_i^n A_i} LFL_M'}{100 - LFL_M'} LFL_i \tag{3.13}$$

The required lower flammability limit and nitrogen-equivalence data of working fluids were retrieved from the CHEMSAFE database for Safety Characteristics in Explosion Protection, maintained by the Bundesanstalt für Materialforschung und -prüfung [67].

3.4. Equipment sizing and economic evaluation

The thermodynamic simulation results provide the necessary information required for preliminary equipment design and economic evaluation of the VCHP and RBHP. This section defines the equipment types assessed and translates the simulation results into an equipment choice. The resulting equipment is dimensioned to assess feasibility and estimate the components' investment costs. Finally, the component costs are combined with the electricity consumption and operating assumptions to assess the financial feasibility in the form of the LCOH.

3.4.1. Equipment selection

Based on the findings from chapter 2 and the thermodynamic simulation results, preliminary equipment design starts with the choice of equipment type. In this section, the design choices for the compressor, heat exchanger, and turbine are defined to assess the feasibility of the VCHP and RBHP.

Compressor Centrifugal, reciprocating, and rotary screw compressors are all considered as possible solutions for VCHP and RBHP. Centrifugal compressors are generally preferred over screw and reciprocating compressors for higher discharge pressures and temperatures as well as higher volumetric flow rates. Additionally, they are reliable and common for industrial-scale operation. Reciprocating compressors are more common for smaller volumetric flow; however, their pulsating flow, maintenance, and lubricant requirements can drive up costs, and they are not suited for discharge temperatures above 200 °C. Oil-free rotary screw compressors are able to achieve slightly higher discharge temperatures, but are limited in their discharge pressure.

The feasibility of a centrifugal compressor for a high-temperature heat pump cycle is assessed by evaluating the optimal rotational speed, impeller diameter, and isentropic efficiency, using the one-dimensional loss model presented in subsection 3.4.2. Designs with rotational speeds above approximately 50 $krpm$ and impeller diameters below approximately 15 cm are assessed as less feasible, and the applicability of a reciprocating or oil-free rotary screw compressor is evaluated based on the volumetric flow and discharge conditions. No detailed dimensioning is performed for reciprocating and screw compressors, and their maximum pressure ratios are assumed to be 4 and 10, respectively.

Heat exchangers Multiple-pipe, welded plate, and shell-and-tube heat exchangers each have their own applicability range for the VCHP and RBHP. The feasibility of these heat exchangers was discussed with an expert from McDermott and was found to be sufficient; however, detailed design might reveal other trade-offs [12]. Multiple-pipe heat exchangers can handle high (differential) pressures and temperatures and achieve a close temperature approach; however, they are only feasible at small scales. Welded plate heat exchangers offer similar advantages and are feasible at larger scales; however, they can handle limited differential pressure. Shell-and-tube heat exchangers may require more complex configurations to achieve a close temperature approach, but they are largely unrestricted in pressure, temperature, and size applicability.

The applicability and feasibility of the multiple-pipe and welded plate heat exchangers are evaluated based on the required heat-transfer area and differential pressure. When neither heat exchangers are applicable or feasible, fixed tubesheet shell-and-tube heat exchangers are assumed. Based on the cost correlations and bare module factors in subsection 3.4.3 and the heat-transfer coefficient estimation in subsection 3.4.2, multiple-pipe heat exchangers are estimated to be economically feasible up to the estimated plate heat exchanger heat-transfer area of approximately 100 m^2, and shell-and-tube heat exchangers are estimated to be cheaper than welded plate heat exchangers for estimated plate heat exchanger heat-transfer areas approximately larger than 200 m^2. Based on the literature discussed in subsection 2.4.3 welded plate heat exchangers are assumed to be applicable up to a differential pressure of 50 bar.

Radial turbine Only radial turbines are considered as options for the RBHP. Radial turbines can achieve high efficiencies and are suitable for high pressures and temperatures; however, they are not feasible for small volumetric flows. Axial turbines can also achieve high efficiencies and are suitable for high pressures and temperatures, but they require very large volumetric flows.

The feasibility of radial turbines is evaluated based on the centrifugal compressor sizing results. Radial turbines are similar to centrifugal compressors and can be dimensioned using similar models [92]. Additionally, they operate with similar volumetric flows and the same pressure ratio. A radial turbine is assessed as less feasible if the centrifugal compressor design is below its feasibility limits.

3.4.2. Component dimensioning

Component dimensions are derived from the thermodynamic simulation results to assess equipment feasibility and estimate component investment costs. In this section, the size and efficiency of centrifugal compressors and the heat-transfer area required for the heat exchangers are estimated.

Centrifugal compressor sizing The total pressure ratio from the thermodynamic simulation results is divided by the number of compression stages, and each stage is evaluated using a one-dimensional, loss-correlation-based model. The number of compression stages is chosen to achieve a pressure ratio per stage of roughly 2 to 3.

Uusitalo et al. [94, 93] presents a one-dimensional, loss-correlation-based model for finding the optimal rotational speed iteratively using minimal inputs. The method involves solving velocity triangles and determining the compressor's main dimensions and losses per compression stage. The isentropic efficiency per compression stage $\eta_{is,st}$ is determined based on the losses using Equation 3.14, where Δh_{is} is the isentropic compression enthalpy difference and Δh_{loss} is the total enthalpy loss of the compression.

$$\eta_{is,st} = \frac{\Delta h_{is}}{\Delta h_{is} + \Delta h_{loss}} \tag{3.14}$$

The total enthalpy loss Δh_{loss} is calculated using Equation 3.15, where each term denotes a specific enthalpy term Δh that can be estimated using correlations from the literature.

$$\Delta h_{loss} = \Delta h_{df} + \Delta h_{tc} + \Delta h_{sf} + \Delta h_{bl} + \Delta h_{rec} + \Delta h_{mix} + \Delta h_{diff} \tag{3.15}$$

Specifically, these include disk friction, tip clearance, skin friction, blade loading, recirculation loss, mixing loss, and diffuser loss. The correlations for each term were selected from literature by Lammers [59] and are listed in Table B.1. They entail the same correlations used by Uusitalo et al. [93], only with slightly simpler geometrical assumptions.

To determine the compressor design resulting in the highest isentropic efficiency for a given number of compression stages, the specific speed is varied from 0.6 to 1.3. For each specific speed, the isentropic efficiency per stage is then determined iteratively based on an efficiency guess. For that initial guess, the preliminary outlet state, stage work, velocity triangles, and impeller geometry are determined. Next, the enthalpy losses and the resulting updated isentropic efficiency are determined. The updated efficiency is used as input for the next iteration, and the procedure is repeated until the calculated efficiency converges to the efficiency used to evaluate the losses. When multiple stages are used, the rotational speed determined for the first compression stage is used for the subsequent stages, allowing a shared driving axis. The overall isentropic efficiency is calculated as the inlet-to-outlet isentropic efficiency, obtained by sequentially calculating the outlet states. The assumed fixed dimensions, dimension ratios, and parameters for the centrifugal compressor sizing calculations were compiled by Uusitalo et al. [93] and are listed in Table 3.3.

Table 3.3: Input parameters for the centrifugal compressor sizing and efficiency estimation.

Parameter	Description	Value	Reference
Z	Number of blades	18	[94, 93]
δ_b	Blade thickness	2 mm	[94, 93]
t	Tip clearance height	0.5 mm	[94, 93]
$D_{1,tip}/D_2$	Impeller inlet tip to outlet diameter ratio	0.5	[64]
$D_{1,hub}/D_{1,tip}$	Impeller inlet hub-to-tip diameter ratio	0.3	[64]
C_{u2}/U_2	Peripheral absolute velocity to peripheral velocity ratio	0.65	[64]
C_{r2}/U_2	Radial absolute velocity to peripheral velocity ratio	0.3	[64]
D_3/D_2	Diffuser outlet to impeller outlet diameter ratio	1.6	[51]
$b*$	Diffuser pinch	0.95	[51]
e	Relative wake coverage of diffuser passage	0.25	[58]

The model is compared to three design studies of different compressor sizes and fluids. Additionally, the results are compared with estimates from Uusitalo et al. [93]. The inlet state, pressure ratio, impeller inlet hub-to-tip diameter ratio $D_{1,hub}/D_{1,tip}$, diffuser outlet-to-impeller outlet diameter ratio D_3/D_2, blade thickness x, tip clearance height t, peripheral absolute velocity-to-peripheral velocity ratio C_{u2}/U_2, and the rotational speed N are set to the same value as the original compressor design or a value evaluated as suitable by Uusitalo et al. [93] and the resulting isentropic efficiency η_{is} and geometrical parameters are compared in Table 3.4. The complete list of input parameters is listed in Table B.2.

Table 3.4: Comparison of the one-dimensional loss-correlation model efficiency and geometrical parameters results to three literature design studies and the estimation by Uusitalo et al. [93].

Compressor	Fluid	Source	η_{is} [%]	D_2 $[mm]$	$D_{1,tip}$ $[mm]$	$D_{1,hub}$ $[mm]$	b_2 $[mm]$
Compressor 1	Air	Dewar et al. [25] (experimental)	79.4	270.9	134.9	40.5	12.2
		Uusitalo et al. [93] (1D-model)	84.2	274.7	136.4	40.9	12.23
		Model	84.3	266.9	133.5	40.0	11.15
Compressor 2	CO_2	Kus and Nekså [58] (1D-model/CFD)	89/91	37.4	18.7	5.0	1.7
		Uusitalo et al. [93] (1D-model)	87.9	34.8	18.5	5.0	2.55
		Model	82.0	36.1	18.0	4.8	2.17
Compressor 3	R134a	Schiffmann and Favrat [77, 76] (experimental)	79	20.0	11.2	4.0	1.2
		Uusitalo et al. [93] (1D-model)	79.4	21.0	10.6	3.8	0.74
		Model	81.1	20.1	10.1	3.6	0.73

The comparison results generally show good agreement between the estimated isentropic efficiency and the geometrical parameters. The estimated isentropic efficiency shows some deviations but stays within an acceptable range. The estimated rotor outlet blade height b_2 of both the model and the estimations by Uusitalo et al. [93] for the CO_2 and R134a compressors show a similar deviation, which could be explained by the smaller scale, which results in a higher sensitivity to the predicted flow angle, slip model, and the used blade thickness [93]. Overall, the model can predict isentropic efficiency and geometrical parameters with acceptable accuracy, especially for larger impeller diameters.

Heat exchanger sizing The heat exchangers are sized by estimating the required heat-transfer area from the simulated heat duties, temperature profiles, and working-fluid properties. The LMTD is used as the mean driving force, as all heat exchangers are assumed to behave as (near) ideal counter-current. The overall heat-transfer coefficient is estimated using Equation 3.16, where the heat-transfer coefficients of the working fluids and the water in the heat source and heat sink are determined using heat-transfer coefficient correlations from literature. The heat transfer coefficient correlations and assumptions used represent a plate heat exchanger. The estimated heat-transfer area is scaled to represent the required heat-transfer area for heat exchangers with larger channels, such as the multiple-pipe or shell-and-tube heat exchanger

$$\frac{1}{U} = \frac{1}{\alpha_h} + \frac{1}{\alpha_c} \tag{3.16}$$

Similar to the models' minimum approach temperature constraints, the streams in the heat exchangers are discretized into 100 state points for the VCHP and 10 for the RBHP, with a minimum property calculation success rate requirement of 90%. At each state point, the heat-transfer coefficient is approximated using a correlation appropriate to the heat-transfer process. The overall heat-transfer coefficient of the fluid α is then calculated as the mean of the heat-transfer coefficients at each state point with successful property calculations.

Different heat-transfer coefficient correlations are used for single-phase heating and cooling, evaporation, condensation, supercritical heating, and supercritical cooling. For single-phase heating and cooling, a correlation by Gnielinski [36] is used with the friction factor by Petukhov [66], a widely used correlation based on the Reynolds and Prandtl numbers. For evaporation, the correlation by Shah [79] is used. It is one of the most widely known correlations for the evaporation heat-transfer coefficient and considers different boiling mechanisms to determine the most predominant one [32]. A different correlation by Shah [81, 82] is used for condensation. It considers forced convection, gravity-driven condensation, and a transition heat-transfer regime. It was evaluated using a large dataset and exhibited the fewest deviations [80]. For supercritical heating and cooling, the correlations by Zhu et al. [102] and Liao and Zhao [61] are used, respectively. Zhu et al. [102] uses a dimensionless supercritical number K with thermophysical properties at the inner wall, which represents the thickness of the wall-attached vapor-like fluid layer that dominates heat transfer, and showed superior accuracy [97]. Liao and Zhao [61] also considers the thermophysical properties at the inner wall, and the correlation was constructed based on experiments of supercritical CO_2 in horizontal mini/micro channels [97].

For all calculations, a mass flux G of 300 kg/s, hydraulic diameter D_h of 3 mm, and, if applicable, a wall heat flux q of 15 kW/m^2 and a temperature difference of 10 K between the wall and the bulk temperature are assumed. The mass flux G, hydraulic diameter D_h, and wall heat flux q were chosen based on examples from Towler and Sinnott [90]. The full heat-transfer coefficient correlations are listed in detail in Table B.3. To prevent property calculation failures from exceeding the maximum, small temperature and pressure perturbations were applied during specific heat calculations until a successful calculation was obtained or 100 iterations were reached.

It is assumed that the required heat-transfer area for multiple-pipe and shell-and-tube heat exchangers is 3 times larger than the estimated heat-transfer area for plate heat exchangers based on the comparison of heat-transfer coefficients of comparable fluids and heat exchangers listed in Compact heat exchangers: a training package for engineers [69].

3.4.3. Equipment cost estimation

Equipment investment costs are used to assess the financial feasibility of VCHPs and RBHPs. In this section, component dimensions and operating conditions from the thermodynamic simulation results are used to estimate equipment investment costs.

The purchased equipment cost is estimated using cost correlations, and the total capital cost is estimated using bare module factors to account for both direct costs and indirect costs for a process plant. Data for the purchased cost of equipment at ambient operating pressure and using carbon steel construction were fitted to Equation 3.17 by Turton et al. [91].

$$\log_{10}(C_p^0) = K_1 + K_2 \log_{10}(A) + K_3(\log_{10}(A))^2 \tag{3.17}$$

Table 3.5 lists the scaling parameter A, the minimum and maximum size of the scaling parameter, and the variables $K1$, $K2$, and $K3$ used in the equation for the equipment considered. The cost correlations are also used to scale sizes outside the indicated range when the equipment selection methodology (subsection 3.4.1) deems it most feasible, and no objections to normal operation are found in the literature assessed in this study. For example, it is assumed that reciprocating compressors are also available for sizes smaller than 450 kW at similar pricing. For these cases, the specific cost at the boundary of the scaling range is used to calculate the cost.

Table 3.5: Equipment investment cost correlation parameters for 2011 [91].

Equipment	Description	Scaling parameter A	Range	k_1	k_2	k_3
Centrifugal and reciprocating compressors	-	Fluid power [kW]	450-3000	2.2897	1.3604	-0.1027
Rotary compressor	-	Fluid power [kW]	18-950	5.0355	-1.8002	0.8253
Radial turbine	-	Fluid power [kW]	100-1500	2.2476	1.4965	-0.1618
Electric drive	Totally enclosed	Shaft power [kW]	75-2600	1.9560	1.7142	-0.2282
Shell-and-tube heat exchanger	Fixed tube sheet	Area [m^2]	10-1000	4.3247	-0.3030	0.1634
Multiple pipe heat exchanger	-	Area [m^2]	10-100	2.7652	0.7282	0.0783
Plate heat exchanger	-	Area [m^2]	10-1000	4.6656	-0.1557	0.1547

The bare module costs are calculated using Equation 3.18. The bare module factors F_{BM} are either calculated using constants $B1$ and $B2$, a pressure factor F_P, and a material factor F_M, or are given directly for a given construction material. Table 3.6 lists the constants and factors used for the equipment considered and was compiled from literature by Turton et al. [91].

$$C_{BM} = C_p^0 F_{BM} = C_p^0(B_1 + B_2 F_P F_M) \tag{3.18}$$

Carbon steel is chosen for the equipment in contact with the heat pumps' working fluids, and stainless steel is chosen for equipment in contact with the process water of the heat source and heat sink. Several average pressure factors are calculated or extrapolated from the data listed in Turton et al. [91]. Pressure factors for high pressure in both the shell and tubes were used for multiple-pipe and shell-and-tube heat exchangers, as this allows only the tubes to be constructed of stainless steel, resulting in a lower overall bare module factor. For high-pressure plate heat exchangers, a pressure factor is estimated.

Table 3.6: Bare module factors and calculation parameters for the equipment investment cost estimation [91].

Equipment	Description	$B1$	$B2$	f_P	f_M	f_{BM}
Centrifugal compressor	Carbon steel	-	-	-	-	2.7
Reciprocating compressor	Carbon steel	-	-	-	-	3.4
Rotary compressor	Carbon steel	-	-	-	-	2.4
Radial turbine	Carbon steel	-	-	-	-	3.5
Electric drive	Totally enclosed	-	-	-	-	1.5
Shell-and-tube heat exchanger		1.63	1.66			
	Carbon steel shell and tubes, <50 bar			1.1	1.0	3.5
	Carbon steel shell and tubes, 50-100 bar			1.4	1.0	4.0
	Carbon steel shell and tubes, >150 bar			1.6[1]	1.0	4.3
	Carbon steel shell, stainless steel tubes, <50 bar			1.1	1.8	4.9
	Carbon steel shell, stainless steel tubes, 50-100 bar			1.4	1.8	5.8
	Carbon steel shell, stainless steel tubes, >150 bar			1.6[1]	1.8	6.1
Multiple pipe heat exchanger		1.74	1.55			
	Carbon steel shell and tubes, <50 bar			1.0	1.0	3.3
	Carbon steel shell and tubes, 50-100 bar			1.2	1.0	3.6
	Carbon steel shell and tubes, 100-150 bar			1.5	1.0	4.1
	Carbon steel shell and tubes, >150 bar			1.8[1]	1.0	4.5
	Carbon steel shell, stainless steel tubes, <50 bar			1.0	1.8	4.5
	Carbon steel shell, stainless steel tubes, 50-100 bar			1.2	1.8	5.1
	Carbon steel shell, stainless steel tubes, 100-150 bar			1.5	1.8	5.9
	Carbon steel shell, stainless steel tubes, >150 bar			1.8[1]	1.8	6.8
Plate heat exchanger		0.96	1.21			
	Carbon steel, <50 bar			1.0	1.0	2.2
	Carbon steel, 50-100 bar			1.5[2]	1.0	2.8
	Stainless steel, <50 bar			1.0	2.4	3.8
	Stainless steel, 50-100 bar			1.5[2]	2.4	5.3

[1]Extrapolated
[2]Estimated

All final costs are escalated to 2026 using the Chemical Engineering Plant Cost Index (846.1) and converted to euros using a conversion rate of 0.87 EUR/USD.

3.4.4. LCOH

The thermodynamic performance and equipment investment costs are combined to assess the economic performance of the VCHP and RBHP. In this section, the LCOH is calculated using the component investment costs, the electricity consumption, and operating assumptions.

The LCOH relates total annualized investment and operating costs to the annually supplied heat and is given by Equation 3.19.

$$c_h = \frac{TCI \cdot CRF}{OH \cdot \dot{Q}_{sink}} + \frac{\sum CF}{OH \cdot \dot{Q}_{sink}} \tag{3.19}$$

The total annualized investment cost is given by the total capital investment TCI and the capital recovery factor CRF, which is given by Equation 3.20 and is determined by the interest rate i and the project lifetime n. The annualized operational costs are the sum of cash flows CF due to electricity consumption, maintenance, and other operational expenses. The annually supplied heat is given by the annual operational hours OH and the heat supplied to the heat sink $\dot{Q}_{sink}$.

$$CRF = \frac{i(1+i)^n}{(1+i)^n - 1} \tag{3.20}$$

The assumptions and parameters used in the LCOH calculation are listed in Table 3.7. Zühlsdorf et al. [103] selected the specific capital investment for the gas-driven boiler and electric boiler for comparison using the same cost estimation methods applied in this study. The operational expenditures (OPEX), along with the electricity consumption, efficiency, and project lifetime, are compiled from Grosse et al.

[38]. Finally, the electricity and gas prices were selected based on European averages for industrial consumers [29, 30].

Table 3.7: Operational parameters for the levelized cost of heat estimation [38, 103].

Parameter	Unit	VCHP	RBHP	ACHP	Gas boiler	Electric boiler
Capital investment	[$€/kW$]	-	-	-	103	210
Fixed OPEX	[$k€/MW_{th}/a$]	2.7	2.7	2.7	1.9	0.5
Variable OPEX	[$€/MWh$]	1.7	1.7	1.7	0.2	0.2
Electricity consumption	[$\%/MW_{th}$]	7.0	7.0	7.0	0.4	101.0
Efficiency	[%]	-	-	-	95	-
Lifetime	[a]	25	25	25	35	20
Electricity price	[$€/MWh_e$]	100 ± 20				
Natural gas price	[$€/MWh_e$]	50 ± 10				
Operating hours	[h]	8000				
Discount rate	[%]	5				

3.4.5. Scale evaluation

The equipment sizing and economic evaluation methodology is applied for heating duties of both 1 MW and 10 MW to evaluate the feasibility and economic performance of the VCHP and RBHP at medium and large industrial scales. The thermodynamic simulations are performed for a heating duty of 1 MW, and it is assumed that the working-fluid mass flow and heat-transfer area scale linearly with heating duty.

3.5. Reference heat supply

A conventional pure-fluid subcritical VCHP is modeled and sized using the same methodology and assumptions as the other high-temperature heat pumps to compare performance, investment costs, and LCOH. Cyclopentane is used because it has a high critical temperature and an AIT of 320 °C. Because REFPROP property calculations consistently failed while estimating the heat transfer coefficient in the evaporator, an overall heat-transfer coefficient of 3000 $W/m^2 \cdot K$ was assumed for the evaporator.

4
Results

This chapter presents the results of the thermodynamic screening, working-fluid selection, equipment sizing, and economic evaluation. First, the chapter analyzes the thermodynamic performance of the VCHP and RBHP. The most promising working-fluid candidates are then selected using thermodynamic, environmental, safety, and practical criteria. Finally, the equipment requirements, investment costs, and LCOH for the selected working-fluid cycle combinations are evaluated.

4.1. Thermodynamic performance

This section analyzes the thermodynamic performance of the simulated working-fluid cycle combinations across the different heating scenarios. The results are first screened to identify trends and working fluids that optimally balance the primary performance indicators using Pareto-based multi-objective screening. The primary performance and cycle behavior of the VCHP and RBHP are then compared using high-COP working-fluid cycle combinations. Additionally, the primary performance of the VCHP and RBHP is compared against the ACHP and conventional VCHP. The performance of characteristic chemical families is compared to identify families with favorable performance properties. Next, the effect of zeotropic mixtures, transcritical or supercritical operation, and the use of natural working fluids on the COP and VHC are compared. Finally, the results are synthesized to select favorable working-fluid cycle combinations for the VCHP and RBHP for each heating scenario for further evaluation.

4.1.1. Fluid screening

The thermodynamic simulation results for the VCHP and RBHP are screened using a Pareto-based multi-objective method to identify working fluids that offer a favorable balance between COP, VHC, pressure ratio, and estimated heat transfer area.

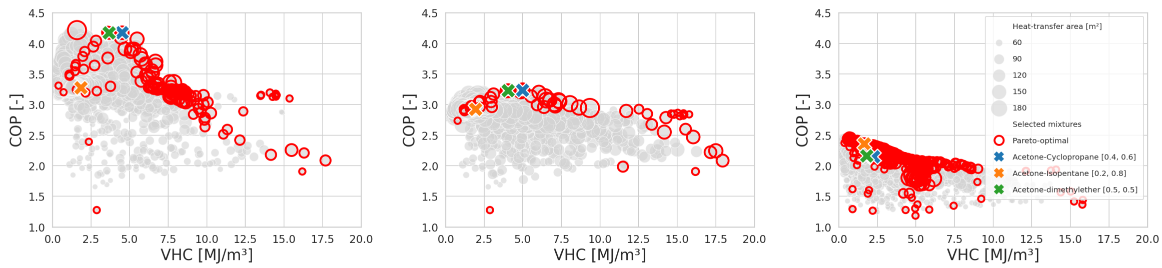

(a) (b) (c)

Figure 4.1: The coefficient of performance (COP) is compared against the volumetric heating capacity (VHC), along with the required heat transfer area derived from the simulation results of the vapor-compression heat pump for different heating scenarios: S1 (a), S2 (b), and S3 (c). Selected and Pareto-optimal mixtures, which maximize both COP and VHC while minimizing pressure ratio and required heat transfer area, are highlighted.

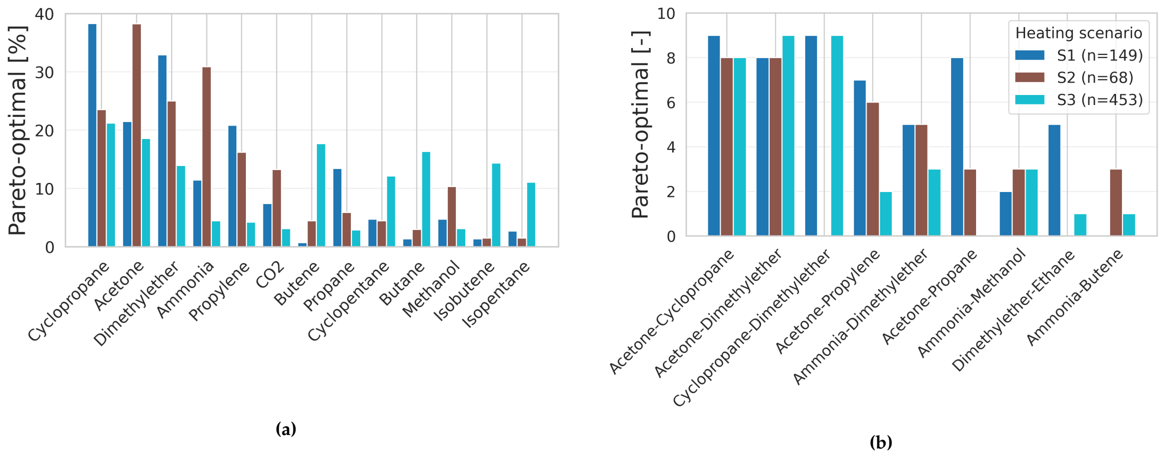

Figure 4.2: The relative occurrence of (a) individual fluids and (b) specific mixtures in the Pareto-optimal solutions of the vapor-compression heat pump simulation results is compared for different heating scenarios. The occurrence of an individual working fluid can be as a pure fluid or as part of a mixture, and the occurrence of a mixture can be any composition.

Figure 4.1 and Figure 4.3 compare the thermodynamic performance of the simulation results of the VCHP and RBHP, respectively, across the three heating scenarios by plotting the COP against the VHC, while also indicating the estimated heat transfer area. Each working-fluid simulation result is represented by a grey circle, whose size indicates the estimated heat-transfer area. The Pareto-optimal working fluids are highlighted with red circles, highlighting the trade-off between COP, VHC, and the estimated heat-transfer area. Additionally, three high-COP mixtures are highlighted with crosses to show how the performance of a selected working fluid can vary across the three heating scenarios.

Figure 4.2 and Figure 4.4 show the count of the most common individual working-fluid components and specific mixtures as Pareto-optimal solutions across the three different heating scenarios for the VCHP and RBHP, respectively. The occurrence of a working-fluid component (Figure 4.2a and Figure 4.4a and 4.4c) can be as a pure fluid or as part of a mixture and is displayed as a percentage of the total number of Pareto-optimal working fluids. The occurrence of a mixture (Figure 4.2b and Figure 4.4b and 4.4d)

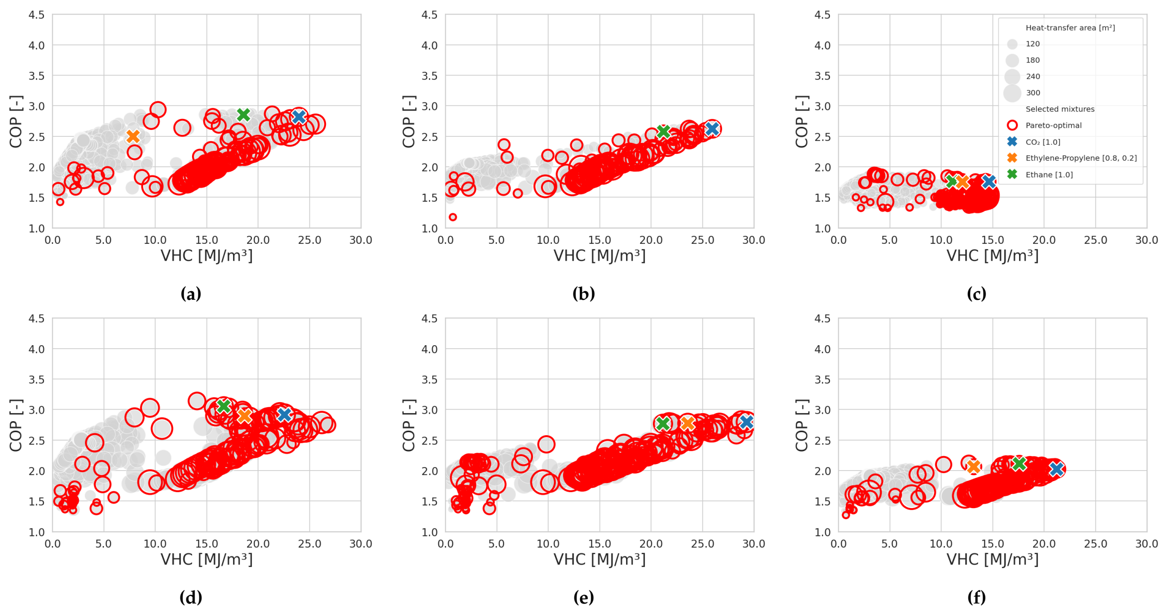

Figure 4.3: The coefficient of performance (COP) is compared against the volumetric heating capacity (VHC), along with the required heat transfer area derived from the simulation results of the reversed-Brayton heat pump without (a, b, c) and with an internal heat exchanger (d, e, f) for different heating scenarios: S1 (a & d), S2 (b & e), and S3 (c & f). Selected and Pareto-optimal mixtures, which maximize both COP and VHC while minimizing pressure ratio and required heat transfer area, are highlighted.

can be any composition and is displayed as the absolute number of occurrences. A mixture can occur at most nine times, as there are nine different compositions. All fluids and mixtures with a relative occurrence higher than 10% and 3%, respectively, are included in the figures. The legend shows the total count of Pareto-optimal working fluids.

Vapor-compression heat pump Figure 4.1 displays a clear trade-off between a high COP and a high VHC across all heating scenarios. Additionally, there is a trade-off between a small heat-transfer area and either a high COP or a high VHC. For heating scenario S1, the COP-VHC trade-off is large, while for S2 and S3, it is relatively small. Additionally, heating scenario S3 shows a different COP-VHC trade-off shape than S1 and S2. The selected mixtures show acetone-cyclopropane and acetone-dimethylether sitting atop the Pareto-optimal COP peak for both S1 and S2, but dropping significantly below and next to the peak in S3. Acetone-isopentane displays opposite behavior. Overall, the results also show a very large spread across the full set of simulation results.

Figure 4.2a shows that the Pareto-optimal solutions are dominated by a small group of working-fluid components, especially in heating scenarios S1 and S2, and consist solely of natural fluids. For heating scenario S3, the occurrence is more spread out across fluids, but S3 also has a very large number of Pareto-optimal working fluids. Heating scenario S2 has the fewest Pareto-optimal working fluids. Figure 4.2b shows that the most common Pareto-optimal mixtures occur with many compositions. This high occurrence count is usually not limited to one heating scenario; however, they usually occur less often in heating scenario S3.

Reversed-Brayton heat pump Figure 4.3 shows that a clear linear correlation exists between high COP and high VHC in heating scenario S2. For heating scenario S1, this correlation also exists, but an additional group of Pareto-optimal working fluids sits above the linear correlation group. For heating scenario S3, the linear correlation is less clear, and the Pareto-optimal working fluids are more grouped together. Overall, the results show less spread than the VCHP across the full set of simulation results. The selected mixtures also, with one exception, show little variance in their performance.

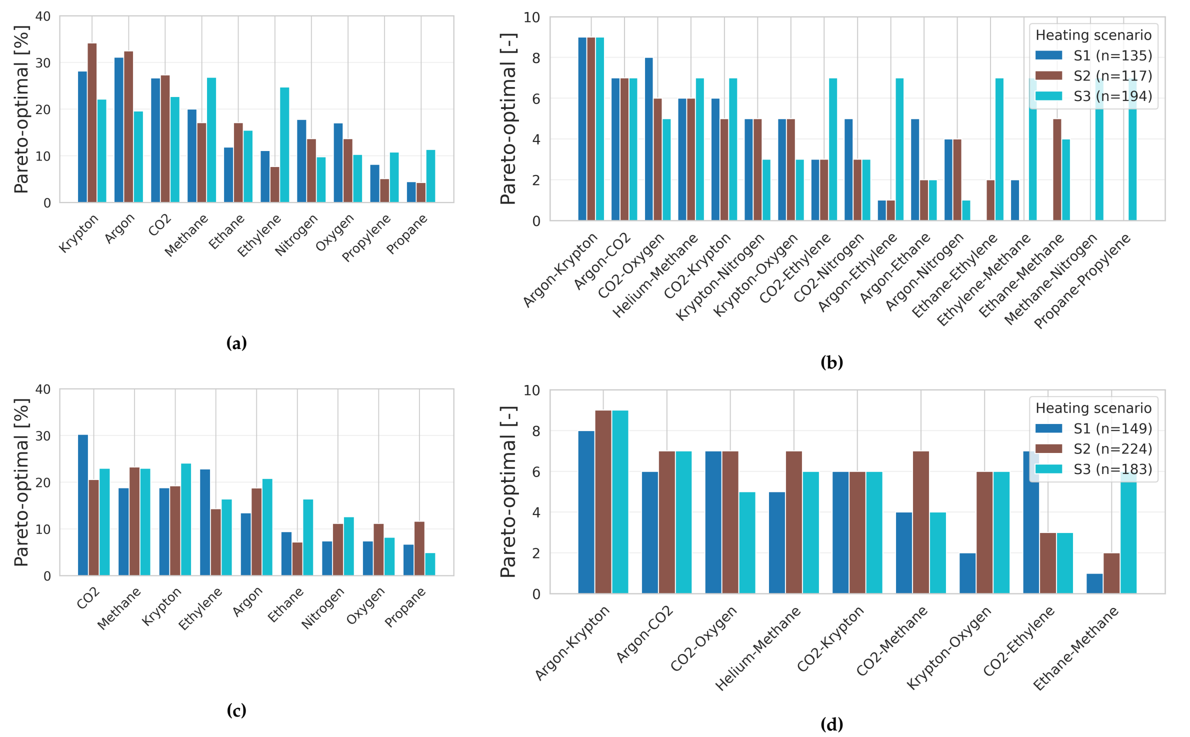

(a)

(b)

(c)

(d)

Figure 4.4: The relative occurrence of (a & c) individual fluids and (b & d) specific mixtures in the Pareto-optimal solutions of the reversed-Brayton heat pump simulation results (a & b) without and (c & d) with an internal heat exchanger is compared for different heating scenarios. The occurrence of an individual working fluid can be as a pure fluid or as part of a mixture, and the occurrence of a mixture can be any composition.

Figure 4.4a shows that the Pareto-optimal solutions for the RBHP without an IHX are slightly dominated by a small group of working-fluid components, which are somewhat evenly distributed across the three heating scenarios. The total number of Pareto-optimal working fluids is also somewhat equal across the heating scenarios. Figure 4.4b shows that the most common Pareto-optimal mixtures for the RBHP without IHX also show little variance across the heating scenarios, with less common mixtures showing mostly occurrence in heating scenario S3. Figure 4.4b and 4.4d show that the RBHP with an IHX shows an even more equal distribution of the most common Pareto-optimal working-fluid components and mixtures, also across the three heating scenarios.

4.1.2. Cycle comparison

High-COP working-fluid cycle combinations for the VCHP and RBHP are compared to the ACHP and a conventional VCHP. The thermodynamic and temperature-glide behavior of the VCHP and RBHP working-fluid cycle combinations are then evaluated individually. Figure 4.5 compares the primary performance indicators and the Lorenz efficiency of high-COP working fluid cycle combinations to the obtained ACHP vendor data and the modeled conventional VCHP.

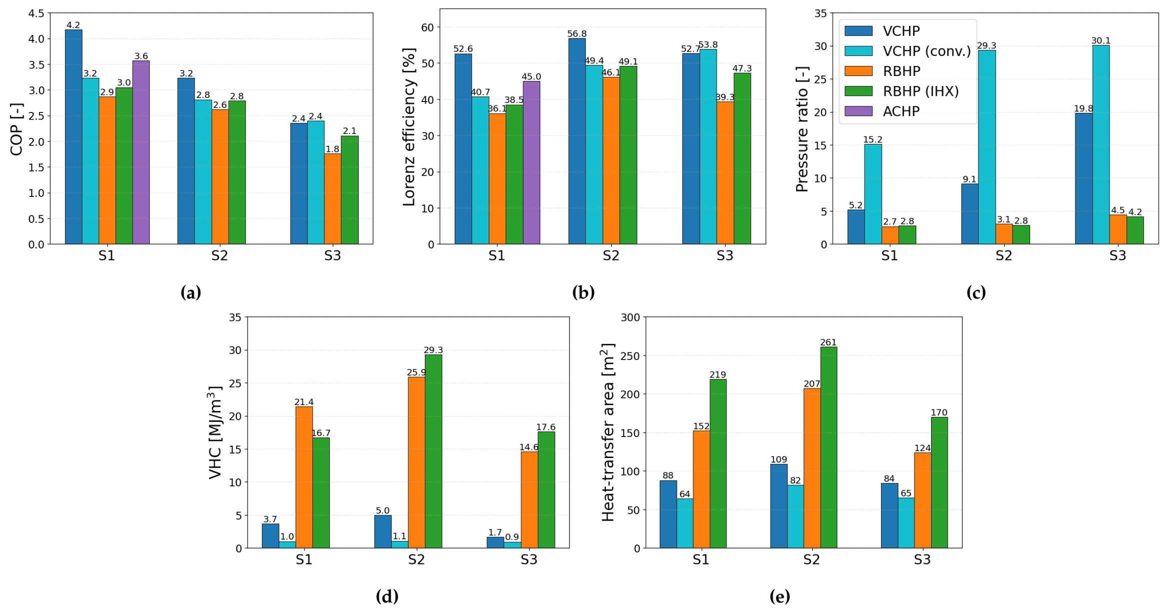

Figure 4.5: The coefficient of performance (COP), Lorenz efficiency, pressure ratio, volumetric heating capacity (VHC), and estimated heat-transfer area of selected high-COP working-fluid cycle combinations of the vapor-compression heat pump and the reversed-Brayton heat pump compared across the three heating scenarios to the obtained absorption-compression heat pump vendor performance data and the modeled conventional pure fluid subcritical vapor-compression heat pump.

The VCHP achieves a consistently high COP and Lorenz efficiency but requires a significantly higher pressure ratio for heating scenarios S2 and S3. The VCHP does require smaller pressure ratios than the conventional VCHP. The COP and Lorenz efficiency of the RBHP are much less consistent and lower than those of the VCHP, but the RBHP consistently requires a very small pressure ratio. The RBHP also achieves very high VHCs, but requires large heat-transfer areas. The RBHP with IHX consistently requires more heat-transfer area than the RBHP without IHX, but achieves a significant COP and efficiency advantage over the RBHP without IHX only in heating scenario S3.

In heating scenario S1, the ACHP performs better than the RBHP and the conventional VCHP, but not as well as the temperature-glide VCHP. In heating scenario S3, the performance advantage of the temperature-glide cycles decreases, and the conventional VCHP achieves a COP and efficiency similar to the temperature-glide VCHP and better than the RBHP. The conventional VCHP does consistently achieve smaller VHCs, but it also requires less heat-transfer area.

Vapor-compression heat pump Figure 4.6 shows the temperature-entropy and temperature-heat transfer diagrams for the selected high-COP mixtures of the VCHP for heating scenarios S1 (4.6a), S2 (4.6b), and S3 (4.6c). The results show that temperature glides can be achieved similarly to the heating scenarios. The phase-change temperature glide of acetone-dimethylether fits heating scenario S1 nearly perfectly. Heating scenario S2 shows that a smaller latent heat of condensation, resulting from higher heat sink temperatures, and a larger temperature glide require significant amounts of de-superheating and subcooling. For heating scenario S3, a transcritical cycle with a minimal phase-change temperature glide mixture is used; unlike the other scenarios, it requires a high IHX heat-transfer duty.

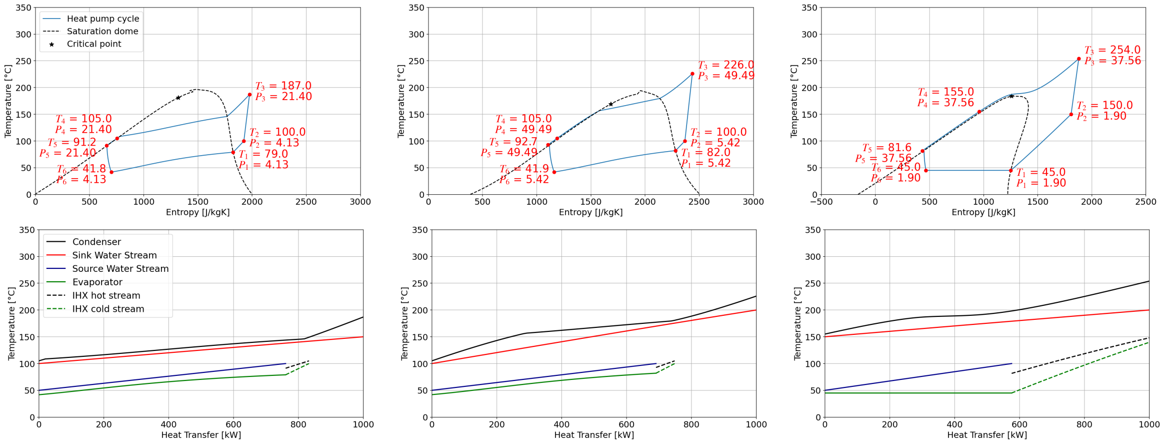

(a) (b) (c)

Figure 4.6: Temperature-entropy and temperature-heat transfer diagrams of selected high-coefficient-of-performance working fluids of the vapor-compression heat pump simulation results for heating scenarios (a) S1, (b) S2, and (c) S3.

Reversed-Brayton heat pump Figure 4.7 shows the temperature-entropy and temperature-heat transfer diagrams for the selected high-COP mixtures of the RBHP for heating scenarios S1 (4.7a), S2 (4.7b), and S3 (4.7c). Across all heating scenarios, the RBHP achieves an optimal COP when the turbine outlet is close to the critical point. Consequently, the optimal solutions all operate at high pressures, especially for the higher heat sink temperatures in heating scenarios S2 and S3. The temperature glide achieved by the RBHP in heating scenario S2, compared with the other scenarios, closely matches that of the heat sink. This indicates that the ratio of heat source temperature glide to heat sink temperature glide for S2 best fits the RBHP. Heating scenario S3 requires a high IHX heat-transfer duty, indicating that the required duty is most affected by the heat-source-to-heat-sink temperature gap.

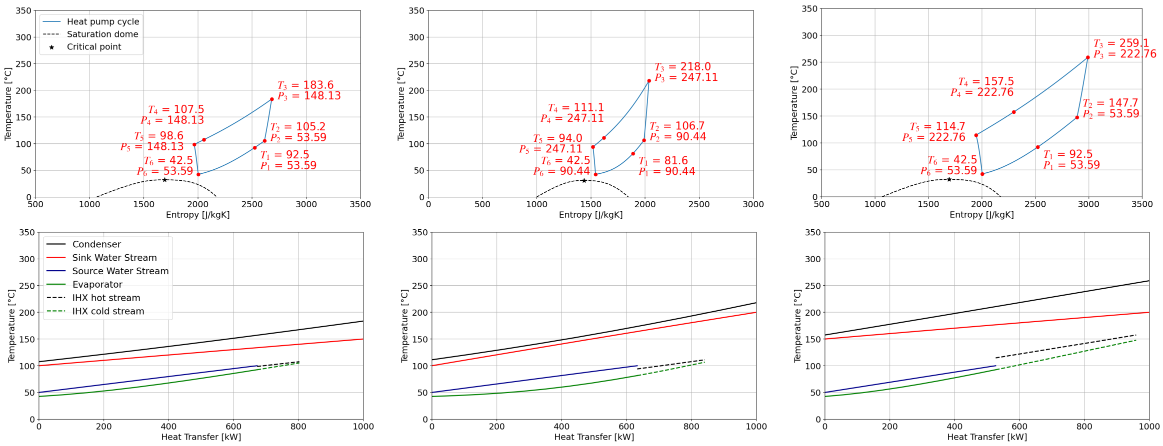

(a) (b) (c)

Figure 4.7: Temperature-entropy and temperature-heat transfer diagrams of selected high-coefficient-of-performance working fluids of the reversed-Brayton heat pump with an internal heat exchanger simulation results for heating scenarios (a) S1, (b) S2, and (c) S3.

4.1.3. Zeotropic mixtures

Figure 4.8 and Figure 4.9 assess the effect of zeotropic mixtures by comparing the thermodynamic performance of mixtures and pure fluids for the VCHP and RBHP, respectively, across the three heating scenarios by plotting the COP against the VHC.

Vapor-compression heat pump Figure 4.8 shows that the VCHP achieves large COP gains when using mixtures in heating scenario S1. For heating scenario S2, this effect is greatly reduced, and for S3, mixtures provide no COP gains.

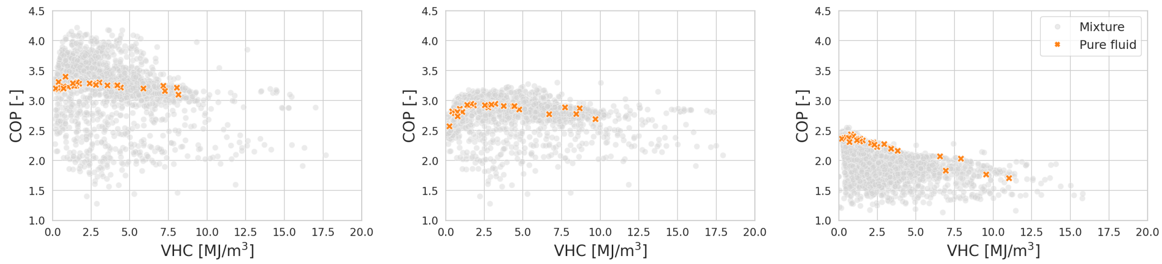

(a) (b) (c)

Figure 4.8: The coefficient of performance (COP) is compared against the volumetric heating capacity (VHC) of the vapor-compression heat pump simulation results for heating scenarios (a) S1, (b) S2, and (c) S3, with mixtures and pure fluids highlighted.

Reversed-Brayton heat pump Figure 4.9 shows three distinct clusters of pure fluids, with mixtures scattered around and between them, for the RBHP. It shows no systematic pattern indicating any performance gain for using mixtures or pure fluids. For heating scenarios S1 and S3, a small subset of mixtures shows a slight COP peak between two clusters of pure fluids.

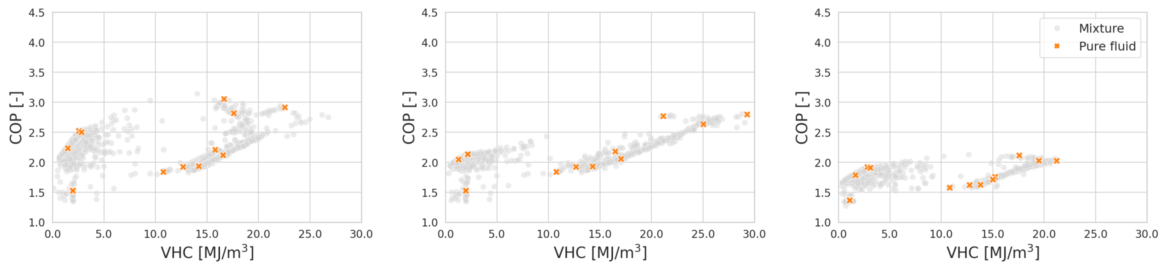

(a) (b) (c)

Figure 4.9: The coefficient of performance (COP) is compared against the volumetric heating capacity (VHC) of the reversed-Brayton heat pump simulation results for heating scenarios (a) S1, (b) S2, and (c) S3, with mixtures and pure fluids highlighted.

4.1.4. Transcritical operation

Figure 4.10 and Figure 4.11 assess the effect of subcritical, transcritical, and supercritical operation by comparing the thermodynamic performance of each operation type for the VCHP and RBHP, respectively, across the three heating scenarios by plotting the COP against the VHC.

Vapor-compression heat pump Figure 4.10 shows a clear COP advantage for subcritical cycles in heating scenario S1. For heating scenarios S2 and S3, subcritical cycles show approximately no COP advantage. Additionally, in heating scenario S1, most cycles are subcritical, whereas in S2 and S3 most cycles are transcritical. Also, across all heating scenarios, transcritical cycles achieve a higher VHC.

Reversed-Brayton heat pump Figure 4.11 shows trans- and supercritical cycles achieving the highest COP across all three heating scenarios. For heating scenario S2, supercritical cycles show a significant COP advantage over transcritical. Additionally, the number of sub-, trans-, and supercritical cycles

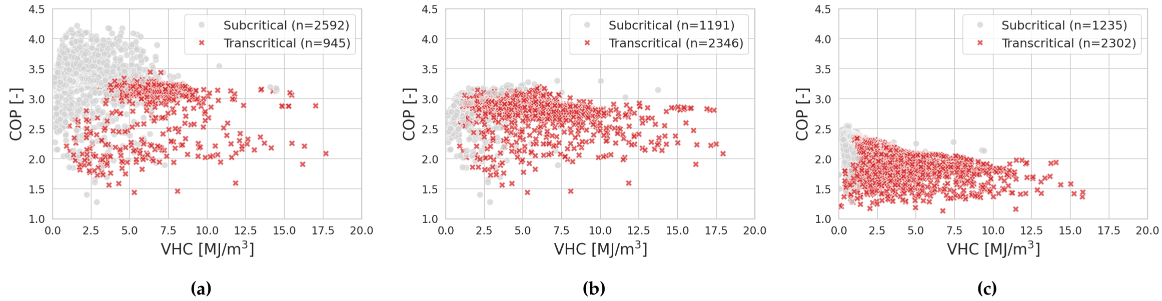

Figure 4.10: The coefficient of performance (COP) is compared against the volumetric heating capacity (VHC) of the vapor-compression heat pump simulation results for heating scenarios (a) S1, (b) S2, and (c) S3, with subcritical and transcritical cycles highlighted.

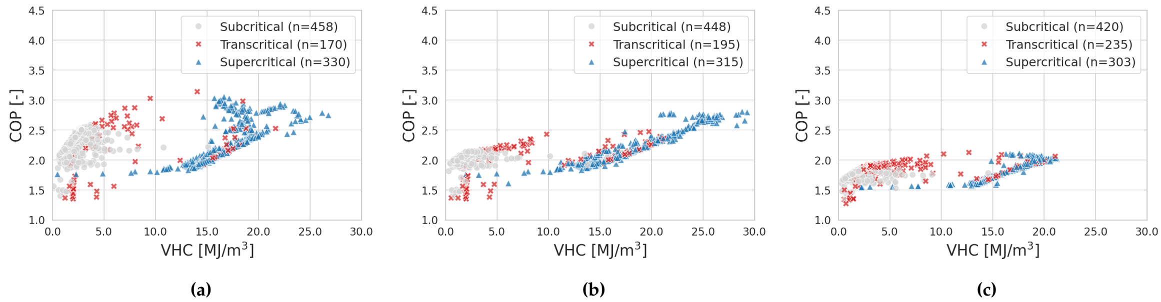

Figure 4.11: The coefficient of performance (COP) is compared against the volumetric heating capacity (VHC) of the reversed-Brayton heat pump simulation results with an internal heat exchanger for heating scenarios (a) S1, (b) S2, and (c) S3, with subcritical, transcritical, and supercritical cycles highlighted.

remains approximately equal across the three heating scenarios, and, as expected, supercritical cycles achieve a higher VHC than transcritical cycles, which achieve a higher VHC than subcritical cycles.

4.1.5. Natural working fluids

Figure 4.12 assesses the effect of natural and synthetic working fluids by comparing the thermodynamic performance of each fluid type for the VCHP across the three heating scenarios by plotting the COP against the VHC. A mixture is highlighted as a natural working fluid when it contains only natural fluids; a mixture is highlighted as a synthetic working fluid when it contains any fraction of synthetic fluid. Figure 4.12 shows no systematic COP or VHC advantage for either synthetic or natural fluids. They occupy roughly the same area on the plot across all three heating scenarios, with natural working fluids occupying a slightly larger area.

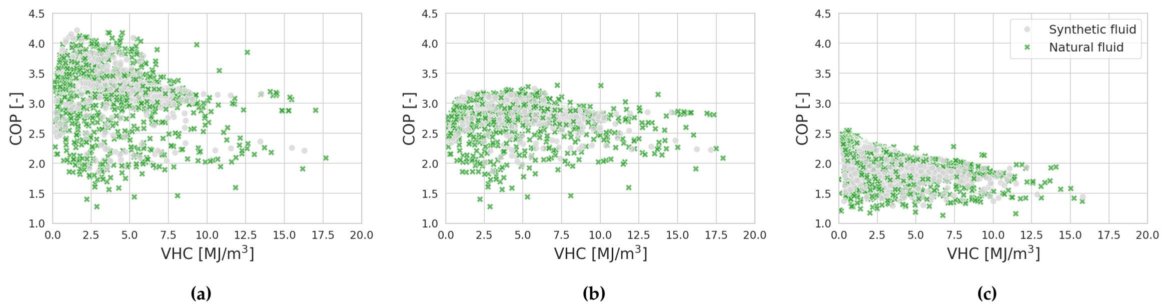

Figure 4.12: The coefficient of performance (COP) is compared against the volumetric heating capacity (VHC) of the vapor-compression heat pump simulation results for heating scenarios (a) S1, (b) S2, and (c) S3, with synthetic and natural working fluids highlighted. A mixture is highlighted as a natural working fluid when it contains only natural fluids.

4.1.6. Working-fluid family mean performance

To support working-fluid selection, individual working-fluid performance results are generalized to identify whether favorable performance is characteristic of a chemical family. The mean values of the defined performance indicators of the top-COP working fluids are compared for the VCHP and RBHP.

Vapor-compression heat pump Table 4.1 summarizes the main advantages and disadvantages that are identified from the VCHP working-fluid family mean performance analysis. The advantages and disadvantages are identified based on the full results per heating scenario listed in Table C.2

Table 4.1: Summary of the vapor-compression heat pump working-fluid family mean performance analysis.

Family	Best scenario(s)	Main advantage	Main disadvantage
Acetone	S1-S3	Highest COP	-
Alcohol	S1-S2	High COP	Low VHC and high S3 discharge temperature
Ammonia	S1-S2	High COP and high VHC	High discharge pressure and temperature
Ether	S1-S3	High COP	-
CO_2	-	High VHC	Low COP and high discharge pressure
C1 hydrocarbon	-	-	Low COP and high discharge pressure
C2 hydrocarbon	-	-	Low COP and high discharge pressure
C3 hydrocarbon	S1-S2	Good COP and VHC balance	-
C4 hydrocarbon	S1-S3	Good COP across all scenarios	-
C5 hydrocarbon	S3	High COP for S3	Low VHC
C6 hydrocarbon	S1-S3	Good COP	Low VHC
C7 hydrocarbon	S1 and S3	High COP for S3	Low COP for S2 and low VHC
Synthetic	S1-S3	Good COP across all scenarios	Low VHC
Water	S1-S3	Good COP for S1 and S2 and highest COP for S3	Very low VHC, large pressure ratio, and high discharge temperature

The results show that almost all working-fluid families can achieve a competitive COP in at least one heating scenario. Only the CO_2-, C1-hydrocarbon-, and C2-hydrocarbon-families consistently achieve significantly lower COPs. Acetone, the ether-family, and the C4-hydrocarbon-family achieve high COPs across all heating scenarios and show no thermodynamic disadvantages compared to the other families. Additionally, the C3-hydrocarbon-family also shows no thermodynamic disadvantage compared to the other families, but its COP falls for heating scenario S3.

Reversed-Brayton heat pump This paragraph summarizes advantages and disadvantages of the best-performing working-fluid families identified from the RBHP working-fluid family mean performance analysis. Table C.3 and Table C.4 list the full results of the working-fluid mean performance analysis for RBHP with and without IHX, respectively, for each heating scenario.

The results show that the gas-, C2-hydrocarbon-, and noble-gas-family, all with low critical temperatures, achieve the highest COPs across all scenarios, both with and without an IHX. The high COP comes paired with a low pressure ratio, high discharge pressure, and high VHC. The key difference between the families is that the gas-family consistently achieves the highest VHC and the noble gas-family consistently requires a significantly larger heat-transfer area. Other families with lower discharge pressures consistently achieve low COPs.

4.1.7. Thermodynamic screening synthesis

The thermodynamic screening shows that the benefit of temperature-glide matching depends on both the heat pump cycle and the heating scenario. The VCHP generally achieves the highest COP and an approximately constant Lorenz efficiency across the heating scenarios, but its advantage over the conventional VCHP decreases for heating scenario S2 and is insignificant for S3. This indicates that higher heat sink temperatures and a larger mean temperature difference between the heat source and heat sink reduce the benefit of temperature-glide matching in a VCHP. The Lorenz efficiency of the RBHP fluctuates more across the heating scenarios but peaks in S2, where its COP is comparable to the conventional VCHP. The ACHP (S1) achieves a higher COP than the conventional VCHP, but not as high as a temperature-glide-matched VCHP.

Zeotropic mixtures operated subcritically show the largest COP advantage for the VCHP in heating scenario S1, a smaller advantage in S2, and no systematic COP improvement in S3. Simultaneously, the number of transcritical cycles increases significantly from heating scenario S1 to S2 and S3 and shows no systematic COP advantage over subcritical cycles. This indicates that the advantage of zeotropic mixtures is only significant for heating scenarios where transcritical cycles are not optimal. Additionally, the high-COP temperature-glide VCHP mixtures show a systematically lower pressure ratio and higher VHC than a conventional VCHP, but also require a larger heat-transfer area. The working-fluid family analysis shows many working fluids capable of achieving high COPs, and supports the individual Pareto-based fluid screening by identifying acetone, ethers, and several hydrocarbons as consistently thermodynamically favorable VCHP working fluids. The working-fluid family analysis also identifies possible working-fluid family disadvantages to consider when selecting a working fluid.

In contrast, mixtures do not provide systematic performance advantages for the RBHP. Performance is primarily governed by the heating scenario. While mixtures provide a very small benefit in heating scenarios S1 and S3, it is insignificant compared to the Lorenz efficiency achieved in S2 using a pure working fluid. This indicates that performance is not dominated by heat-transfer losses, and that the heat-source-to-heat-sink temperature glide ratio in S2 is most compatible with its sensible heat-transfer profile.

4.2. Fluid selection

The thermodynamic screening results are combined with environmental, safety, and practical data to select working-fluid cycle combinations for the further evaluation of equipment requirements and economic performance. The working fluid parameters defined in subsection 2.3.4 are used and are listed in Table C.1. The data are compiled only for working-fluid components relevant to the selection and are gathered from literature and other publicly available sources to the greatest extent and accuracy known to the author.

Vapor-compression heat pump Based on the thermodynamic screening results and the environmental, safety, and practical criteria, a selection of suitable working-fluid families was made. Families identified as having a low COP are not included, as are ethers due to their very low AIT and C6- and C7-hydrocarbons due to their very low LFL and AIT. The main thermodynamic and secondary considerations are compiled in Table 4.2 along with their best applicability range and an overall interpretation of the applicability and feasibility of the selected working-fluid families as components of a high-temperature VCHP working fluid.

Table 4.2: Combined thermodynamic, environmental, safety, and practical assessment of the most favorable vapor-compression heat pump working-fluid families.

Family	Best scenario(s)	Main thermodynamic advantage	Main practical advantage	Main drawback	Overall interpretation
Acetone	S1-S3	Highest COP	Very high AIT	Strong solvent, material compatibility concerns	Best COP-focused family
Alcohol	S1-S2	High COP	Slightly less flammable and acceptable AIT possible with methanol	Toxicity and S3 high discharge temperatures	Good (slightly) less flammable alternative if toxicity is manageable
Ammonia	S1-S2	High COP and high VHC	Less flammable and technically well-known	Toxicity and high discharge temperatures and pressures	Best for compact design, and good less flammable alternative if toxicity is manageable
C3 hydrocarbon	S1-S2	Good COP and VHC balance	High AIT and low discharge temperatures	Flammability	Good for lower heat sink temperatures
C4 hydrocarbon	S1-S3	Good COP across all scenarios	High AIT possible and low discharge temperature	More flammability and lower AIT than C3	Good across all temperatures
C5 hydrocarbon	S3	High COP for S3	Acceptable AIT possible with Isopentane	More flammability and lower AIT than C5	Good for high temperatures if flammability is manageable
Synthetic	S1-S3	Good COP across all scenarios	Less flammable	PFAs/TFA concerns	Good safety-focused alternative

No working-fluid family is favorable across all thermodynamic and secondary criteria. Acetone and several hydrocarbon families offer strong thermodynamic performance across all three heating scenarios, but their downside is flammability, and acetone also has restricted material compatibility. Ammonia offers a favorable combination of high COP and VHC with lower flammability than hydrocarbons, but it introduces toxicity and compressor discharge temperature concerns. Synthetic refrigerants also offer good COP across all heating scenarios with lower flammability, but their environmental persistence and degradation products are important to consider.

For further evaluation, hydrocarbon working-fluid mixtures are selected for the VCHP for heating scenarios S1 and S2 to minimize environmental impact and toxicity, as flammability is assumed to be manageable. Additionally, no oil or material concerns are known for these working-fluid components. For heating scenario S3, a less flammable working fluid is selected to avoid flammability issues due to the higher compressor discharge temperature associated with S3. The exact mixture compositions and performance data of the selected mixtures are listed in Table 4.3.

Reversed-Brayton heat pump The thermodynamic screening identified three working-fluid families with the most favorable thermodynamic performance. Of these families, the gas-family and noble-gas-family are environmentally friendly, non-flammable, and non-toxic. For further evaluation, pure CO_2 is selected for both the RBHP without and with IHX for all heating scenarios. High-pressure CO_2 is well known and is estimated to require a smaller heat-transfer area than noble gases. The performance data of the CO_2 RBHPs is listed in Table 4.3.

Table 4.3: Performance data of the selected working fluids for further evaluation of the vapor-compression heat pump and the reversed-Brayton heat pump per heating scenario.

Scenario	Type	Working fluid	Safety class	COP [-]	η_{Lorenz} [%]	VHC $[MJ/m^3]$	$\dot{m}$ $[kg/s]$	Pressure ratio [-]	$p_{discharge}$ $[bar]$	$T_{discharge}$ [°C]	$A*$ $[m^2]$
S1	VCHP	Cyclopropane-cyclopentane [0.6, 0.4]	A3	4.02	50.6	4.4	2.29	4.8	26.1	178	100
	RBHP	CO_2 [1.0]	A1	2.82	35.5	24.0	6.38	2.7	220.8	199	218
	RBHP (IHX)	CO_2 [1.0]	A1	2.91	36.7	22.6	6.36	2.4	199.4	202	280
S2	VCHP	Propylene-cyclopentane [0.8, 0,2]	A3	3.01	53.0	8.1	2.42	6.9	77.3	213	123
	RBHP	CO_2 [1.0]	A1	2.62	46.1	25.9	5.80	3.1	250.0	215	207
	RBHP (IHX)	CO_2 [1.0]	A1	2.79	49.1	29.3	5.26	2.8	250.0	223	261
S3	VCHP	R1233zd(E)-Neopentane [0.8, 0.2]	A2(L)	2.27	50.8	2.2	4.62	14.0	40.5	253	100
	RBHP	CO_2 [1.0]	A1	1.76	39.3	14.6	6.49	4.5	250.0	263	124
	RBHP (IHX)	CO_2 [1.0]	A1	2.02	45.3	21.2	5.47	3.1	250.0	285	196

4.3. Equipment sizing

The equipment for the selected working-fluid cycle combinations is sized, and their feasibility is assessed. The centrifugal compressor sizing results are used to assess the feasibility using the stage count, rotational speed, and efficiency, as well as to assess the feasibility of a radial turbine. The heat exchanger sizing results are used to choose an appropriate heat exchanger type. The resulting equipment is then used for the economic evaluation.

4.3.1. Centrifugal compressor

Table 4.4 shows the results of the centrifugal compressor sizing and evaluation using the one-dimensional loss-correlation-based model for the VCHP and RBHP for all three heating scenarios and a 1 MW and 10 MW heating duty. It lists the number of stages, the rotational speed of the impeller and driving axis of the compressor, and the overall isentropic efficiency. Table C.5 and Table C.6 list the power consumption and impeller diameter per compression stage, as well as the effect of the calculated isentropic efficiency on the COP.

The centrifugal compressor sizing results show better overall feasibility for the 10 MW heating duty for both the VCHP and RBHP, with lower rotational speeds (and larger impeller diameters) and significantly higher isentropic efficiencies. In particular, the RBHP requires very small, fast-spinning centrifugal compressors that achieve low overall isentropic efficiencies at a 1 MW heating duty. For a heating duty of 10 MW, the RBHP requires impeller diameters of around 15 cm and consistently achieves an overall isentropic efficiency higher than 80%, significantly higher than assumed in the model.

The VCHP requires impeller diameters around 10 cm for the 1 MW heating duty and consistently achieves an overall isentropic efficiency of around 76%. For a 10 MW heating duty, the VCHP requires impeller diameters ranging from 20 to 45 cm and achieves an overall isentropic efficiency of around 80%. This indicates that a centrifugal compressor is feasible for the VCHP across a wider range than the RBHP, but it does not always achieve a very high isentropic efficiency. Notably, propylene-cyclopentane in heating scenario S2 requires a smaller impeller diameter and achieves a lower overall isentropic efficiency than the other working fluids and heating scenarios.

Table 4.4: The required stage count and rotational speed, as well as the resulting overall isentropic efficiency, of the centrifugal compressor sizing and efficiency estimation for the vapor-compression heat pump and reversed-Brayton heat pump for the three heating scenarios for a 1 MW and 10 MW heating duty.

Scenario	Heating duty	Type	Number of stages [-]	Rotational speed [$krpm$]	Isentropic efficiency [%]
S1	1 MW	VCHP	2	52.1	78.1
		RBHP	1	130.8	73.0
		RBHP (IHX)	1	118.8	74.6
	10 MW	VCHP	2	16.1	82.2
		RBHP	1	41.9	81.8
		RBHP (IHX)	1	38.1	82.5
S2	1 MW	VCHP	2	88.8	74.0
		RBHP	1	165.7	70.1
		RBHP (IHX)	1	167.7	70.5
	10 MW	VCHP	2	31.2	77.9
		RBHP	1	50.4	80.6
		RBHP (IHX)	1	51.6	80.8
S3	1 MW	VCHP	3	32.6	76.6
		RBHP	2	107.9	72.6
		RBHP (IHX)	1	175.0	71.0
	10 MW	VCHP	3	9.5	80.8
		RBHP	2	33.0	80.6
		RBHP (IHX)	1	54.6	80.7

Overall, the preliminary centrifugal compressor design is feasible for a heating duty of 10 MW. For a heating duty of 1 MW, the preliminary centrifugal designs are less feasible, and a reciprocating or rotary screw compressor could enable a more feasible design; however, as listed in Table 4.3, the compressor discharge temperatures of both the VCHP and the RBHP selected working fluids are well above the limit of reciprocating compressors in heating scenarios S2 and S3. In heating scenario S1, the compressor discharge temperatures of both the VCHP and RBHP are roughly below the operating limit of reciprocating and rotary screw compressors. Table 4.5 lists the estimated compressor technologies most feasible for the VCHP and RBHP.

Table 4.5: Estimated most feasible compressor technologies for the vapor-compression heat pump and reversed-Brayton heat pump for the three heating scenarios and a 1 MW and 10 MW heating duty.

Scenario	Heating duty	VCHP	RBHP	RBHP (IHX)
S1	1 MW	Screw	Reciprocating	Reciprocating
	10 MW	Centrifugal	Centrifugal	Centrifugal
S2	1 MW	Reciprocating*	Reciprocating*	Reciprocating*
	10 MW	Centrifugal	Centrifugal	Centrifugal
S3	1 MW	Centrifugal	Reciprocating*	Reciprocating*
	10 MW	Centrifugal	Centrifugal	Centrifugal

*Requires compressor discharge temperature reduction

As the RBHP requires high discharge pressures, rotary screw compressors are not feasible. For the VCHP, the rotary screw compressor is feasible for heating scenarios S1 and S3; however, for S3, the centrifugal design is feasible because it has three stages, which increases the dimensions. Otherwise, reciprocating compressors are solely used for heating scenarios S2 and S3 for a heating duty of 1 MW, but they require a reduction in compressor discharge temperature. For the economic evaluation, reciprocating compressors will be considered without adding extra costs to mitigate the high compressor discharge temperature.

4.3.2. Radial turbines

Radial turbines are estimated to be less feasible for a heating duty of 1 MW. The centrifugal compressor sizing results show that fast-spinning and small turbomachinery is required for the small volumetric flows of CO_2. For the heating duty of 10 MW, turbomachinery is more feasible, but detailed design is required to fully assess the effect of the volumetric flows and the design on a common driving axis. For the economic evaluation, radial turbines will be considered, as the cost of other expanders or more complex designs is not readily available, and the effect of turbine cost is estimated to be small.

4.3.3. Heat exchanger

Multiple-pipe and shell-and-tube heat exchangers are the most feasible options based on the applicability and cost assumptions. Table C.7 lists the heat exchanger type and design specifications along with the estimated required heat-transfer area.

Because temperature-glide applications require large estimated heat-transfer areas, shell-and-tube heat exchangers are most commonly used. Multiple-pipe heat exchangers are most commonly used for smaller required heat-transfer areas, and plate heat exchangers are used only when the differential pressure is limited and the estimated plate heat exchanger heat-transfer area is moderate (100– 200 m^2).

4.3.4. Equipment overview

The equipment assessment shows greater uncertainty on the feasibility for a 1 MW heating duty, especially for the RBHP. The RBHP requires large, bulky heat exchangers, and the feasibility and the effect on compressor and turbine performance are uncertain. For a 10 MW heating duty, turbomachinery feasibility is more certain for both the VCHP and RBHP and potentially allows the RBHP to achieve higher COPs than estimated.

The VCHP shows some compressor feasibility uncertainty for the 1 MW heating duty, as the estimated centrifugal designs are on the faster and smaller side and show lower overall isentropic efficiencies than originally estimated. The higher discharge temperature requirement for heating scenario S2 and S3 also complicates the use of reciprocating and rotary screw compressors; however, means to lower the compressor discharge temperature are common and feasible, as there is liquid available in the cycle to absorb part of the heat of compression. Additionally, working fluids with lower VHC and higher required pressure ratios could also increase the feasibility of centrifugal compressors. For the 10 MW heating duty, the estimated centrifugal compressor designs are feasible for the VCHP. For heat exchangers, the VCHP shows no feasibility issues except that both the 1 MW and 10 MW heating-duty heat exchangers had lower heat-transfer coefficients and larger volume-to-heat-transfer-area ratios, causing them to occupy a large footprint. In contrast, welded plate heat exchangers are also feasible and could be implemented, though potentially at higher cost.

Because the RBHP operates with much lower volumetric flows than the VCHP, the estimated turbomachinery designs are also faster and smaller than those for VCHPs. For the 1 MW heating duty, the RBHP would require micro-scale centrifugal compressors and radial turbines, making the design very complex. Additionally, there are no alternatives to a radial turbine, and both compressor and turbine efficiency strongly affect the already lower RBHP COP. For the 10 MW heating duty, the estimated turbomachinery designs are feasible but still on the faster and smaller side; however, the estimated centrifugal compressor efficiencies increased significantly over the originally estimated efficiency, which could outweigh the complexity of the smaller turbomachinery design. The RBHP also requires large volume heat exchangers in addition to already requiring very large heat-transfer surfaces. This significantly affects the applicability of the RBHP, and more compact plate heat exchangers are mostly not applicable due to the high pressure differences.

4.4. Economic performance

The equipment sizing results for the selected working-fluid cycle combinations are translated into investment costs and LCOH. The differences in investment cost and the effect of the operating costs, electricity consumption, and scale are compared.

4.4.1. Investment costs

Table 4.6 lists the capital investment costs of the VCHP and RBHP for the three heating scenarios for both 1 MW and 10 MW, along with the total capital investment costs for the conventional VCHP and the ACHP for heating scenario S1 for a heating duty of 1 MW. The total capital investment costs of the VCHP and RBHP consist of the capital investment costs for the compressor, turbine, electric drive, and heat exchangers and include direct and indirect costs associated with a process plant. The capital investment cost for the electric drive is included in the compressor, and, if applicable, the cost of the centrifugal compressor was calculated using the power consumption estimated in subsection 4.3.1.

Table 4.6: Total, specific, and per-component capital investment costs for the vapor-compression heat pump and reversed-Brayton heat pump as a result of the equipment sizing and cost estimation, compared to a conventional vapor-compression heat pump and an absorption-compression heat pump.

Heating duty	Scenario	Type	Compressor [Mio. €]	Turbine [Mio. €]	HEXs [Mio. €]	TCI [Mio. €]	tci [€/kW]	Difference [%]
1 MW	S1	VCHP	1.4	-	0.8	2.3	2261	-
		VCHP (conv.)	1.3	-	0.5	1.8	1795	-20.6
		ACHP				2.2	2190	-3.1
		RBHP	1.3	0.1	1.0	2.4	2381	+5.3
		RBHP (IHX)	1.2	0.1	1.5	2.8	2820	+24.7
	S2	VCHP	0.9	-	1.1	2.0	1989	-
		VCHP (conv.)	1.1	-	0.6	1.8	1793	-9.8
		RBHP	1.4	0.1	1.1	2.6	2616	+31.5
		RBHP (IHX)	1.2	0.1	1.5	2.9	2862	+43.9
	S3	VCHP	1.0	-	0.7	1.7	1733	-
		VCHP (conv.)	1.4	-	0.5	1.9	1929	+11.3
		RBHP	2.0	0.2	1.3	3.4	3442	+98.6
		RBHP (IHX)	1.6	0.1	1.2	2.9	2882	+66.3
10 MW	S1	VCHP	3.6	-	2.2	5.9	585	-
		VCHP (conv.)	5.3	-	1.7	7.0	705	+20.5
		RBHP	5.5	0.5	5.5	11.4	1144	+95.6
		RBHP (IHX)	5.1	0.4	6.6	12.1	1209	+106.7
	S2	VCHP	4.6	-	3.1	7.7	772	-
		VCHP (conv.)	6.5	-	2.1	8.6	856	+11.0
		RBHP	5.9	0.5	5.2	11.6	1161	+50.4
		RBHP (IHX)	5.2	0.4	6.2	11.8	1177	+52.5
	S3	VCHP	6.2	-	1.9	8.1	808	-
		VCHP (conv.)	7.6	-	1.9	9.4	942	+16.6
		RBHP	9.9	1.0	3.2	14.0	1404	+73.8
		RBHP (IHX)	7.1	0.5	4.6	12.2	1219	+50.9

The total capital investment costs of the conventional VCHP are calculated using equipment selected in a similar manner to that done for the VCHP and RBHP, and no corrected centrifugal compressor power consumption is used. The total capital investment costs of the ACHP are the vendor-reported delivered and commissioned system costs and include factory prefabrication, transport and delivery, crane placement, initial charging, and commissioning. The specific total capital investment cost tci is also listed, along with a relative difference compared to the VCHP in each case.

Across all three heating scenarios and for both heating duties, the RBHP has a higher total capital investment cost than the VCHP. In almost all cases, the relative differences to the VCHP are significant and can even be double that of the VCHP. The total capital investment costs of the conventional VCHP varies around 20% both cheaper and more expensive compared to the temperature-glide VCHP. The total capital investment cost of the ACHP for heating scenario S1, for a heating duty of 1 MW, is similar to that of the VCHP. Additionally, the specific total capital investment costs of the temperature-glide and the conventional VCHP generally decrease more with increasing heating duty than those of the RBHP.

4.4.2. LCOH

Figure 4.13 shows the specific LCOH for the VCHP and RBHP for the three heating scenarios and a heating duty of 1 MW based on the thermodynamic simulation, equipment sizing, efficiency and cost estimation, and operating assumptions, along with the LCOH for the ACHP based on operating assumptions and the vendor-reported COP and delivered and commissioned system costs. The figure also includes the LCOH for a gas-driven and an electric boiler, based on the same fuel prices. Both gas and electricity prices have a 20% uncertainty, as indicated by the error bars.

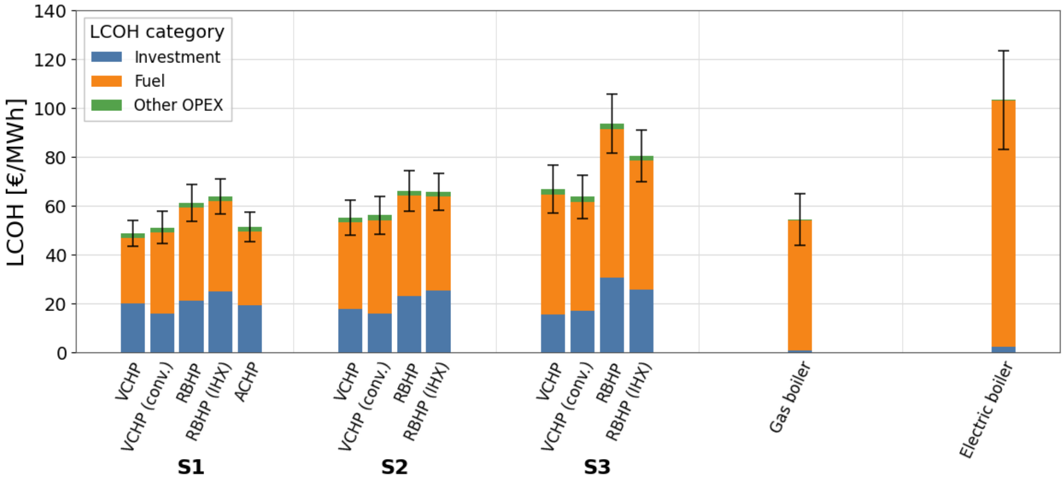

Figure 4.13: Specific levelized cost of heat (LCOH) for the vapor-compression heat pump and the reversed-Brayton heat pump for the three heating scenarios with a heating duty of 1 MW, compared to a conventional vapor-compression heat pump and an absorption-compression heat pump, as well as a gas-driven and electric boiler.

Both the temperature-glide and the conventional VCHP have an LCOH comparable to a gas-driven boiler for heating scenarios S1 and S2; however, the COP advantage of a temperature-glide VCHP over a conventional VCHP is offset by higher investment costs, resulting in similar levelized costs of heat. In heating scenario S3, the conventional VCHP even has a lower LCOH than the temperature-glide VCHP, but it's still higher than the gas-driven boiler. The ACHP achieves an LCOH similar to the conventional VCHP in heating scenario S1.

The RBHP has an LCOH about 10 $€/MWh$ higher than the temperature-glide and conventional VCHP, as well as the gas-driven boiler, in heating scenarios S1 and S2. In heating scenario S3, the differences become bigger, and the RBHP without an IHX becomes relatively more expensive. The RBHP does always achieves a significantly lower LCOH than the electric boiler.

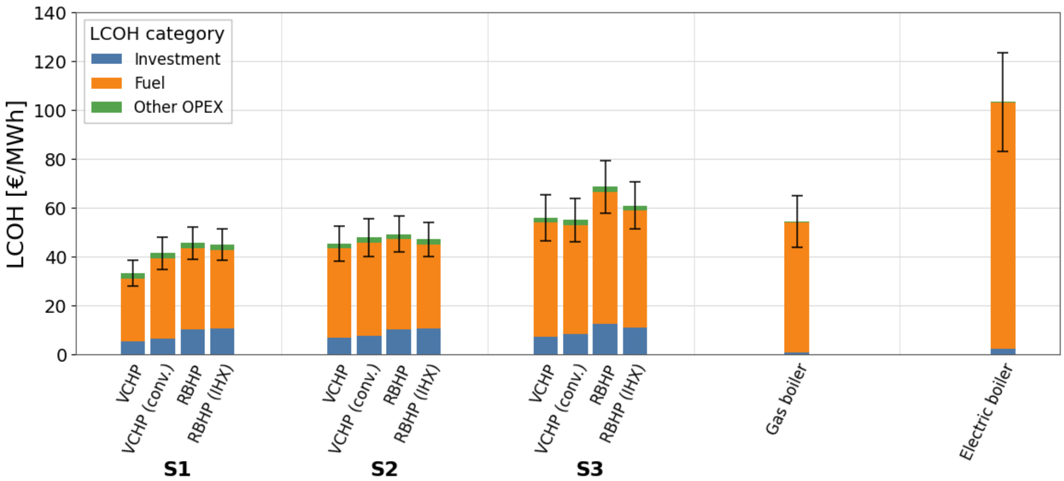

Figure 4.14: Specific levelized cost of heat (LCOH) for the vapor-compression heat pump and the reversed-Brayton heat pump for the three heating scenarios with a heating duty of 10 MW, compared to a conventional vapor-compression heat pump and a gas-driven and electric boiler.

4.4.3. Effect of scale

Figure 4.13 shows the specific LCOH for the VCHP and RBHP for the three heating scenarios and a heating duty of 10 MW. The figure also includes the LCOH for a gas-driven and an electric boiler, based on the same fuel prices. Both gas and electricity prices have a 20% uncertainty, as indicated by the error bars.

Compared with a heating duty of 1 MW, the absolute LCOH decreases significantly for all heat pump technologies, and the relative differences among them become smaller. All heat pump technologies achieve a lower LCOH than the gas-driven boiler in heating scenarios S1 and S2, with the temperature-glide VCHP in S1 being significantly cheaper. The RBHP with IHX achieves roughly the same LCOH as the temperature-glide VCHP in heating scenario S2 because of increased compressor efficiency. In heating scenario S3, both the temperature-glide and conventional VCHP achieve an LCOH similar to the gas-driven boiler.

5 Conclusions, discussion, and recommendations

This chapter presents the conclusions of the thermodynamic and techno-economic evaluation of high-temperature heat pumps and working fluids for industrial sensible heat upgrading with substantial temperature glides at both the heat source and heat sink, discusses the study's uncertainties and limitations, and offers recommendations for industrial decision-makers and future research.

5.1. Conclusions

High-temperature heat pumps that absorb and reject heat over a substantial temperature glide can provide thermodynamic and economic advantages for industrial sensible heat upgrading. Still, the benefit is strongly dependent on cycle architecture, heat source and heat sink temperature profiles, operating temperature, and scale. Of the evaluated high-temperature heat pump technologies, the temperature-glide VCHP provides the most consistently favorable balance between COP, equipment feasibility, capital cost, and LCOH. Its largest advantage over a conventional VCHP occurs when a subcritical zeotropic mixture can closely match the heat source and heat sink temperature profiles, as in heating scenario S1. This advantage decreases at higher heat sink temperatures and temperature lifts, where transcritical and low-temperature-glide cycles become more competitive. The RBHP offers broad high-temperature and temperature-lift applicability with favorable pressure ratios. Still, its lower COP, high-pressure heat exchangers, and high-pressure and low-volumetric-flow compressors and expanders generally prevent it from outperforming the VCHP under the investigated conditions. Larger heating duty improves the technical and economic feasibility of both cycles, especially the RBHP.

The VCHP's highest-COP working fluids achieve an almost constant Lorenz efficiency across all heating scenarios. Still, zeotropic mixtures show little to no COP benefit in heating scenarios S2 and S3. The higher heat sink temperature and larger heat sink temperature glide in heating scenario S2 make transcritical cycles more efficient, reducing the COP advantage of the subcritical cycle using a zeotropic mixture. In heating scenario S3, with the largest mean temperature difference, pure fluids achieve COPs similar to mixtures. Together, this indicates that as the mean temperature difference between the heat source and heat sink increases, the advantage of lowering the heat pump's mean temperature lift decreases, and compression and expansion losses dominate heat-transfer temperature-profile mismatch losses. While working fluid (mixtures) in the RBHP with a better temperature-profile match achieve a slightly higher COP than pure working fluids in heating scenarios S1 and S3, its Lorenz efficiency is highest for (nearly) pure working fluids in S2. This indicates that compression and expansion losses dominate temperature-profile mismatch losses across most heating conditions. Additionally, the RBHP IHX showed a significant COP advantage only in heating scenario S3, due to the heat-source-to-heat-sink temperature gap, which allowed a larger heat duty to be transferred in the IHX.

The working-fluid screening and selection show that many VCHP working fluids can achieve a high COP, even at higher heat-sink temperatures and larger heat-source-to-heat-sink mean temperature differences in heating scenarios S2 and S3; however, no individual working fluid or working-fluid family satisfied all environmental, safety, and practical criteria. Each non-flammable working fluid had its own disadvantage, and the number of flammable working fluids with a reasonable margin between the compressor discharge temperature and the AIT at higher heat sink temperatures was limited. The RBHP working-fluid screening and selection shows only working fluids with low critical temperatures to achieve high COPs. Additionally, high-COP flammable working fluids showed no advantage over high-COP non-flammable working fluids, and both operated at high pressures.

The economic evaluation shows that electricity consumption dominates the LCOH, particularly for larger heating duties. The differences in LCOH due to investment costs among the heat pump technologies are small at a heating duty of 1 MW and become irrelevant at 10 MW. At the smaller heating duty, VCHPs and ACHPs can achieve an LCOH comparable to the gas-driven boiler. At the larger heating duty, in addition to the VCHPs, the RBHPs also become competitive except for heating scenario S3. Only the temperature-glide VCHP achieves a significantly lower LCOH than the conventional VCHP, specifically, in heating scenario S1 for the larger heating duty.

Temperature-glide matching should therefore not be treated as a technological objective by itself. It is valuable when the improved mean temperature lift and temperature-profile match produce sufficient electricity savings in VCHPs without requiring disproportionate equipment, safety, or capital-cost penalties. Additionally, high-temperature sensible heat sources and sinks are valuable when they allow transcritical VCHPs and/or RBHPs to operate efficiently when subcritical VCHPs are unfeasible, expanding the operational capabilities of high-temperature heat pumps.

5.2. Discussion and limitations

The results provide a comparative thermodynamic, technical, and economic screening of high-temperature heat pumps for three sensible heat-upgrading scenarios. The thermodynamic models, working-fluid screening, preliminary equipment selection and sizing, and cost calculations identify key trade-offs among the VCHP, RBHP, ACHP, and reference heating technologies. However, the study does not include detailed equipment design, process-safety assessment, equipment vendor quotation, or detailed cost assessment of individual designs. The conclusions should therefore be interpreted as indicating promising combinations of working fluids, cycles, and operating regimes. The broad working-fluid-family and cycle-level trends are considered more reliable than the exact thermodynamic, environmental, safety, and practical performance of individual mixtures, calculated component dimensions, and absolute investment costs.

The VCHP and RBHP were modeled and optimized using assumptions, while the ACHP was represented by technical vendor data for a single operating case. The gas-driven and electric boiler were represented by literature-based, non-scenario-specific performance and cost assumptions. The comparison combines information from different approaches with different levels of maturity and detail, adding uncertainty when comparing the VCHP or RBHP with the ACHP or the gas-driven or electric boiler.

The results of the thermodynamic model and optimization of the VCHP and RBHP are based on fixed component efficiencies, neglected pressure and heat losses, steady-state operation, equations-of-state approximations, and assumptions for optimization and discretization. The fixed compressor and turbine efficiencies do not distinguish between fluid, scale, flow, pressure ratio, and geometry effects. The assumptions add uncertainty to the thermodynamic performance results of individual working-fluid cycle combinations. An attempt was made to estimate the effect of these factors using the centrifugal compressor estimation. The estimation identified greater uncertainty for all VCHP and RBHP working-fluid cycle combinations at a heating duty of 1 MW and indicates that the assumed efficiencies overestimate performance at this scale. The heat exchanger assumptions may lead to less feasible designs, requiring larger temperature differences and reducing performance. Neglected pressure and heat losses, as well as the assumed steady-state operation, also overestimate performance in real-world operation. Combined, the thermodynamic performance is likely overestimated compared to real-world operation; however, these do not necessarily alter cycle-level trends. Additionally, the equations-of-state approximations and optimization and discretization assumptions add uncertainty to individual results, but, as with the modeling assumptions, there is no indication of a systematic effect on the working-fluid-family or cycle-level trends.

The working-fluid family analysis is based on unequally represented generic chemical categories. It uses only the highest-COP working fluids, which can contain up to 50 $mol\%$ of a different working-fluid family. These results do not represent chemical-family trends across other working fluids and apply only to high-COP mixtures that contain working fluids evaluated in this study. However, because the thermodynamic screening combines a large set of performance data using Pareto-based screening and working-fluid family analysis, general performance trends are less affected by individual outliers.

The environmental and safety assessment is largely based on generalizations and data from various information sources. The results do not represent a full process-safety assessment, and the outcome of one potentially draws different conclusions. However, it highlights the complexity and importance of assessing these factors.

Equipment sizing and economic cost estimates are based on compressor-loss and heat-transfer coefficient correlations, as well as assumptions, generalized cost correlations, and bare-module factors. These estimations and assumptions introduce large uncertainty to individual sizing and cost results. Additionally, detailed component design might reveal trade-offs relevant to thermodynamic performance or to environmental, safety, and practical assessment. As a result, the absolute values of the individual levelized cost of heat cases are also uncertain. Still, the observed scaling and investment-to-electricity cost trends are likely more certain, as they are visible across all evaluated cases.

5.3. Recommendations

This study explored the operating regimes, working fluids, and equipment of different high-temperature heat pump technologies to evaluate the potential of industrial sensible-heat upgrading. From these explorations, several recommendations are made to further enhance the potential of high-temperature heat pumps and their key role in decarbonizing industrial process heat. These recommendations are split into recommendations for industrial decision-makers and the scientific research community.

5.3.1. Industrial decision-makers

This study shows that the considered high-temperature heat pump technologies can provide technically promising and economically competitive solutions for industrial sensible-heat upgrading when the cycle architecture, working fluid, temperature profiles, and heating duty are selected together. Not every combination of these parameters produces favorable performance, so high-temperature heat pumps should not be selected solely based on the required maximum heat sink temperature. Industrial decision-makers should instead consider the complete source and sink temperature profiles and select, or where possible design, the heat-recovery and heat-delivery systems to match the operating characteristics of the most suitable heat pump technology.

Under the conditions investigated and among previous studies, subcritical VCHPs are particularly suitable for heat delivery up to approximately 150 °C, with zeotropic mixtures offering additional flexibility to match sensible heat source and heat sink temperature profiles. At higher heat sink temperatures, transcritical VCHPs become increasingly relevant because they inherently reject sensible heat and are not explicitly constrained in their maximum heat sink temperature. For applications with a large temperature lift or heat-source-to-heat-sink temperature gap, the RBHP may provide an alternative when the temperature profiles are compatible with the sensible temperature profile of the working fluid, such as CO_2.

The principal recommendation is therefore to treat high-temperature heat pump selection as a process-integration problem: the cycle, working fluid, heat source and heat sink profile, and heating scale should be optimized together rather than selecting a heat pump only after the process temperatures have been fixed. This approach is particularly attractive at larger heating duties, where efficient turbomachinery becomes more practical, and capital costs are distributed over a greater heat output, potentially enabling high-temperature heat pumps to compete with fossil-fuel heating and substantially reduce direct industrial CO_2 emissions.

5.3.2. Scientific research

This study highlights the complexity and added value of evaluating the industrial feasibility alongside the thermodynamic performance of high-temperature heat pumps. Because studies often overlook the complexity of industrial feasibility, future research should further integrate thermodynamic screening with industrial feasibility assessment. Despite the added modeling complexity, combining environmental, safety, and practical working-fluid properties with cycle performance, equipment dimensions, operating limits, and cost provides considerably greater decision value than thermodynamic optimization alone. A more comprehensive and automated methodology could ultimately serve as a screening tool for selecting a suitable working-fluid high-temperature heat pump combination for a given heating scenario and heating duty.

Because compressor and turbine feasibility is crucial to thermodynamic performance and is more uncertain, a complete screening tool requires improved models or correlations to estimate compressor type, efficiency, staging, dimensions, rotational speed, and discharge conditions. This is particularly true for small-scale reciprocating, screw, and centrifugal compressors, as well as radial turbines, which remain difficult to assess rapidly using existing screening methods.

The VCHP's high-temperature operating range is governed mainly by working-fluid constraints and compressor pressure and temperature limits. Its applicability at smaller scales and higher temperatures could therefore expand through reciprocating compressors capable of higher discharge temperatures; screw compressors capable of higher discharge pressures and temperatures; more feasible (certainty) of small centrifugal compressors; and experimental validation of promising working fluids such as acetone and less well-known hydrocarbons, including their thermal stability and material and lubricant compatibility.

Finally, a broader and more systematic comparison of heating conditions such as: temperature lift; heat source and heat sink temperature glide; heat-source-to-heat-sink temperature glide ratio; heat-source-to-heat-sink temperature gap; absolute temperature level; and heating duty is recommended for both the VCHP and RBHP. These results could provide essential insights into the optimal operating and working-fluid regime of the high-temperature heat pump technologies supporting their selection and process integration at an industrial level. Ideally, a high-temperature heat pump scenario map would give industrial decision-makers a quick overview of their options under their specific boundary conditions.

References

[1] Keri-Marie Adamson et al. "High-temperature and transcritical heat pump cycles and advancements: A review". In: *Renewable and Sustainable Energy Reviews* 167 (Oct. 2022), p. 112798. ISSN: 1364-0321. DOI: 10.1016/j.rser.2022.112798. URL: https://www.sciencedirect.com/science/article/pii/S1364032122006827.

[2] Fuhaid Alshammari, Muhammad Usman, and Apostolos Pesyridis. "Expanders for Organic Rankine Cycle Technology". en. In: *Organic Rankine Cycle Technology for Heat Recovery*. IntechOpen, Nov. 2018. ISBN: 978-1-78984-348-4 978-1-78984-347-7 978-1-83881-773-2. DOI: 10.5772/intechopen.78720. URL: https://www.intechopen.com/chapters/62026 (visited on 07/06/2026).

[3] Anthony L. Andrady et al. *Environmental Effects of Stratospheric Ozone Depletion, UV Radiation, and interactions with Climate Change: 2022 Assessment Report*. en. report. United Nations Environment Programme Ozone Secretariat, Mar. 2023. URL: https://ro.uow.edu.au/articles/report/Environmental_Effects_of_Stratospheric_Ozone_Depletion_UV_Radiation_and_interactions_with_Climate_Change_2022_Assessment_Report/27845382/1.

[4] G Angelino and C Invernizzi. "Prospects for real-gas reversed Brayton cycle heat pumps". In: *International Journal of Refrigeration* 18.4 (May 1995), pp. 272–280. ISSN: 0140-7007. DOI: 10.1016/0140-7007(95)00005-V. URL: https://www.sciencedirect.com/science/article/pii/014070079500005V.

[5] Hans Peter H. Arp et al. "The Global Threat from the Irreversible Accumulation of Trifluoroacetic Acid (TFA)". In: *Environmental Science & Technology* 58.45 (Nov. 2024), pp. 19925–19935. ISSN: 0013-936X. DOI: 10.1021/acs.est.4c06189. URL: https://doi.org/10.1021/acs.est.4c06189.

[6] Cordin Arpagaus et al. "High temperature heat pumps: Market overview, state of the art, research status, refrigerants, and application potentials". In: *Energy* 152 (June 2018), pp. 985–1010. ISSN: 0360-5442. DOI: 10.1016/j.energy.2018.03.166. URL: https://www.sciencedirect.com/science/article/pii/S0360544218305759.

[7] ASHRAE. *2021 ASHRAE Handbook: Fundamentals*. ASHRAE, 2021. ISBN: 1947192892; 9781947192898. URL: libgen.li/file.php?md5=f14c6f815b6b634a106f8449baea85dc.

[8] Gas Processors Association. *Gas Processors Suppliers Association - GPSA Engineering Data Book*. 12th Ed. URL: libgen.li/file.php?md5=8b22d2dcd6015a594c4d920fa6323b81.

[9] Ronald H. Aungier. *Turbine Aerodynamics: Axial-Flow and Radial-Flow Turbine Design and Analysis*. en. ASME Press, Jan. 2006. ISBN: 978-0-7918-0241-0. DOI: 10.1115/1.802418. URL: https://asmedigitalcollection.asme.org/ebooks/book/100/Turbine-Aerodynamics-Axial-Flow-and-Radial-Flow (visited on 06/23/2026).

[10] Dereje S. Ayou, Wei Wu, and Alberto Coronas. "Absorption-based heat pumps for decarbonization of industrial process heating: performance, current status, and new developments". In: *Thermal Science and Engineering Progress* 62 (June 2025), p. 103679. ISSN: 2451-9049. DOI: 10.1016/j.tsep.2025.103679. URL: https://www.sciencedirect.com/science/article/pii/S245190492500469X.

[11] Opeyemi Bamigbetan et al. "Review of vapour compression heat pumps for high temperature heating using natural working fluids". In: *International Journal of Refrigeration* 80 (Aug. 2017), pp. 197–211. ISSN: 0140-7007. DOI: 10.1016/j.ijrefrig.2017.04.021. URL: https://www.sciencedirect.com/science/article/pii/S0140700717301780.

[12] Abdollah Bayati. *Interview on heat exchanger feasibility*. Personal communication. Senior Principal Mechanical Engineer; interview conducted by Jurre Stok. Aug. 2026.

[13] David Behringer et al. *Persistent Degradation Products of Halogenated Refrigerants and Blowing Agents in the Environment: Type, Environmental Concentrations, and Fate with Particular Regard to New Halogenated Substitutes with Low Global Warming Potential*. Research Report FKZ 3717 41 305 0. Volume: 73/2021. Dessau-Roßlau, Germany: Umweltbundesamt (German Environment Agency), May 2021. URL: https://www.umweltbundesamt.de/en/publikationen/persistent-degradation-products-of-halogenated.

[14] Ian H. Bell et al. *CoolProp: Open-source thermophysical property library, Version 7.2*. Accessed: 2026-02-27. 2023. URL: http://www.coolprop.org.

[15] Ian H. Bell et al. "Pure and Pseudo-Pure Fluid Thermophysical Property Evaluation and the Open-Source Thermophysical Property Library CoolProp". In: *Industrial & Engineering Chemistry Research* 53.6 (2014), pp. 2498–2508. DOI: 10.1021/ie4033999.

[16] Matteo Benvenuti, Guido Francesco Frate, and Lorenzo Ferrari. "Evaluating Brayton Heat Pump Potential for Industrial Decarbonisation". en. In: *Journal of Physics: Conference Series* 2893.1 (Nov. 2024), p. 012117. ISSN: 1742-6596. DOI: 10.1088/1742-6596/2893/1/012117. URL: https://doi.org/10.1088/1742-6596/2893/1/012117.

[17] Heinz P. Bloch and Claire Soares. *Turboexpanders and Process Applications*. 1st ed. Gulf Professional Publishing, 2001. ISBN: 0-88415-509-9. URL: https://books.google.com/books/about/Turboexpanders_and_Process_Applications.html?id=Z-RY1Emx4JwC.

[18] Leon P. M. Brendel et al. "Experimental Performance Comparison of High-Glide Hydrocarbon and Synthetic Refrigerant Mixtures in a High-Temperature Heat Pump". en. In: *Energies* 17.8 (Jan. 2024), p. 1981. ISSN: 1996-1073. DOI: 10.3390/en17081981. URL: https://www.mdpi.com/1996-1073/17/8/1981 (visited on 06/17/2026).

[19] Klaus Brun and Rainer Kurz, eds. *Compression Machinery for Oil and Gas*. 1st ed. Gulf Professional Publishing, 2018. ISBN: 0-12-814683-4. URL: https://shop.elsevier.com/books/compression-machinery-for-oil-and-gas/brun/978-0-12-814683-5.

[20] James Burkholder et al. *SUMMARY OF ABUNDANCES, LIFETIMES, ODPs, REs, GWPs, GTPs*. en. Feb. 2023. URL: https://tsapps.nist.gov/publication/get_pdf.cfm?pub_id=936562.

[21] In Ho Chung et al. "A study on the cycle variations of reversed Brayton cycle heat pumps for high-temperature heat supply to improve performance". In: *Case Studies in Thermal Engineering* 74 (Oct. 2025), p. 106954. ISSN: 2214-157X. DOI: 10.1016/j.csite.2025.106954. URL: https://www.sciencedirect.com/science/article/pii/S2214157X25012146 (visited on 04/21/2026).

[22] J. E. Coppage and Frederick D. Dallenbach. "STUDY OF SUPERSONIC RADIAL COMPRESSORS FOR REFRIGERATION AND PRESSURIZATION SYSTEMS". In: 1956. URL: https://api.semanticscholar.org/CorpusID:106861473.

[23] J. W. Daily and R. E. Nece. "Chamber Dimension Effects on Induced Flow and Frictional Resistance of Enclosed Rotating Disks". In: *Journal of Basic Engineering* 82.1 (Mar. 1960), pp. 217–230. ISSN: 0021-9223. DOI: 10.1115/1.3662532. URL: https://doi.org/10.1115/1.3662532 (visited on 08/30/2026).

[24] Dehon Service SAS. *HFO 1336mzz-Z: Safety Data Sheet*. Safety Data Sheet. Edition: Version 3.3. Vincennes Cedex, France: Dehon Service SAS, June 2025. URL: https://www.climalife.com.

[25] Brett Dewar et al. "CFD Modelling of a Centrifugal Compressor with Experimental Validation through Radial Diffuser Static Pressure Measurement". en. In: *International Journal of Rotating Machinery* 2019.1 (2019), p. 7415263. ISSN: 1542-3034. DOI: 10.1155/2019/7415263. URL: https://onlinelibrary.wiley.com/doi/abs/10.1155/2019/7415263 (visited on 08/22/2026).

[26] Frederick William Dittus and Llewellyn Michael Kraus Boelter. *Heat transfer in automobile radiators of the tubular type*. English. California, United States: Berkeley, Calif. University of California press, 1930. URL: https://searchworks.stanford.edu/view/1416803.

[27] Tala El Samad et al. "A review of compressors for high temperature heat pumps". In: *Thermal Science and Engineering Progress* 51 (June 2024), p. 102603. ISSN: 2451-9049. DOI: 10.1016/j.tsep.2024.102603. URL: https://www.sciencedirect.com/science/article/pii/S245190492400221X (visited on 07/02/2026).

[28] *EN 378:2016 — Refrigerating systems and heat pumps: Safety and environmental requirements (Parts 1–4)*. en. European Standard EN 378:2016. Brussels: European Committee for Standardization (CEN), 2016. URL: https://standards.cencenelec.eu.

[29] Eurostat. *Electricity prices for non-household consumers - bi-annual data (from 2007 onwards)*. Accessed: 2026-09-04. European Commission, 2023. DOI: 10.2908/NRG_PC_205. URL: https://doi.org/10.2908/NRG_PC_205.

[30] Eurostat. *Gas prices for non-household consumers - bi-annual data (from 2007 onwards)*. Accessed: 2026-09-04. European Commission, 2023. DOI: 10.2908/NRG_PC_203. URL: https://doi.org/10.2908/NRG_PC_203.

[31] Xiao-Wei Fan et al. "Theoretical study of heat pump system using CO2/dimethylether as refrigerant". In: *Thermal Science* 17.5 (2013), pp. 1261–1268. URL: https://doiserbia.nb.rs/Article.aspx?ID=0354-98361305261F (visited on 07/22/2026).

[32] Xiande Fang et al. "Saturated flow boiling heat transfer: review and assessment of prediction methods". en. In: *Heat and Mass Transfer* 55.1 (Jan. 2019), pp. 197–222. ISSN: 1432-1181. DOI: 10.1007/s00231-018-2432-1. URL: https://doi.org/10.1007/s00231-018-2432-1 (visited on 07/08/2026).

[33] *Gas cylinders — Gases and gas mixtures — Determination of fire potential and oxidizing ability for the selection of cylinder valve outlets*. Geneva, Switzerland: International Organization for Standardization, July 2017.

[34] Tony Giampaolo. "Compressor Handbook - Principles and Practice (2nd Edition)". In: (). ISSN: 978-87-7022-737-7. URL: https://app.knovel.com/hotlink/toc/id:kpCHPPE001/compressor-handbook-principles/compressor-handbook-principles.

[35] Bartosz Gil and Jacek Kasperski. "Efficiency analysis of alternative refrigerants for ejector cooling cycles". In: *Energy Conversion and Management* 94 (Apr. 2015), pp. 12–18. ISSN: 0196-8904. DOI: 10.1016/j.enconman.2015.01.056. URL: https://www.sciencedirect.com/science/article/pii/S0196890415000680 (visited on 07/22/2026).

[36] V. Gnielinski. "New equations for heat and mass transfer in the turbulent flow in pipes and channels". In: *NASA STI/Recon Technical Report A* 41 (Jan. 1975). ADS Bibcode: 1975STIA...7522028G, pp. 8–16. URL: https://ui.adsabs.harvard.edu/abs/1975STIA...7522028G (visited on 07/08/2026).

[37] J. Gómez-Hernández et al. "Carbon dioxide and acetone mixtures as refrigerants for industry heat pumps to supply temperature in the range 150–220 C". In: *Energy* 269 (Apr. 2023), p. 126821. ISSN: 0360-5442. DOI: 10.1016/j.energy.2023.126821. URL: https://www.sciencedirect.com/science/article/pii/S0360544223002153 (visited on 07/22/2026).

[38] R Grosse et al. *Long term (2050) projections of techno-economic performance of large-scale heating and cooling in the EU*. Anticipation and foresight, Technical guidance KJ-NA-28859-EN-N. Luxembourg (Luxembourg): Publications Office of the European Union, 2017. DOI: 10.2760/24422.

[39] Khalid Hamid et al. "Potential evaluation of integrated high temperature heat pumps: A review of recent advances". In: *Applied Thermal Engineering* 230 (July 2023), p. 120720. ISSN: 1359-4311. DOI: 10.1016/j.applthermaleng.2023.120720. URL: https://www.sciencedirect.com/science/article/pii/S1359431123007494.

[40] Zian Hao et al. "Comprehensive assessment of high-temperature heat pumps using novel low-GWP refrigerant mixtures as working fluids: Energy, exergy, thermal properties, and safety". In: *Thermal Science and Engineering Progress* 64 (Aug. 2025), p. 103786. ISSN: 2451-9049. DOI: 10.1016/j.tsep.2025.103786. URL: https://www.sciencedirect.com/science/article/pii/S2451904925005761.

[41] K. Harby. "Hydrocarbons and their mixtures as alternatives to environmental unfriendly halogenated refrigerants: An updated overview". In: *Renewable and Sustainable Energy Reviews* 73 (June 2017), pp. 1247–1264. ISSN: 1364-0321. DOI: 10.1016/j.rser.2017.02.039. URL: https://www.sciencedirect.com/science/article/pii/S1364032117302551 (visited on 06/16/2026).

[42] Honeywell International Inc. *Solstice® yf Refrigerant (R-1234yf): Safety Data Sheet*. Safety Data Sheet. Edition: Version 3.4. Morris Plains, NJ, USA: Honeywell International Inc., Mar. 2024. URL: https://www.honeywell.com.

[43] Honeywell International Inc. *Solstice® ZE Refrigerant (HFO-1234ze): Ultra-Low GWP Hydrofluoroolefins (HFO) Alternative to Hydrofluorocarbons*. Product Brochure. Heverlee, Belgium: Honeywell International Inc., July 2022. URL: https://www.honeywell-refrigerants.com.

[44] International Energy Agency. *Net Zero by 2050: A Roadmap for the Global Energy Sector*. English. Tech. rep. Paris: International Energy Agency, May 2021. URL: https://www.iea.org/reports/net-zero-by-2050.

[45] International Energy Agency. *Renewables 2020: Analysis and forecast to 2025*. English. Tech. rep. Paris: International Energy Agency, Nov. 2020. URL: https://www.iea.org/reports/renewables-2020.

[46] International Energy Agency. *Renewables 2025: Analysis and Forecasts to 2030*. English. Tech. rep. Paris: International Energy Agency, Oct. 2025. URL: https://www.iea.org/reports/renewables-2025.

[47] Costante Mario Invernizzi and Gioele Di Marcoberardino. "An Overview of Real Gas Brayton Power Cycles: Working Fluids Selection and Thermodynamic Implications". en. In: *Energies* 16.10 (Jan. 2023), p. 3989. ISSN: 1996-1073. DOI: 10.3390/en16103989. URL: https://www.mdpi.com/1996-1073/16/10/3989.

[48] *ISO 817:2024 — Refrigerants: Designation and safety classification*. en. International Standard ISO 817:2024. Geneva: International Organization for Standardization (ISO), 2024. URL: https://www.iso.org/standard/83452.html.

[49] W Jansen. "A method for calculating the flow in a centrifugal compressor when entropy gradient are present". In: *Royal society conference on internal aerodynamics*. 1967, pp. 133–46.

[50] David Japikse. "Advanced diffusion levels in turbocharger compressors and component matching". In: (1982).

[51] David Japikse. *Centrifugal compressor design and performance*. Concepts ETI, 1996. URL: https://cir.nii.ac.jp/crid/1970867909884153621.

[52] Alireza Javanshir, Nenad Sarunac, and Zahra Razzaghpanah. "Thermodynamic analysis of simple and regenerative Brayton cycles for the concentrated solar power applications". In: *Energy Conversion and Management* 163 (May 2018), pp. 428–443. ISSN: 0196-8904. DOI: 10.1016/j.enconman.2018.02.079. URL: https://www.sciencedirect.com/science/article/pii/S0196890418301961.

[53] Jonas K. Jensen et al. "On the development of high temperature ammonia–water hybrid absorption–compression heat pumps". In: *International Journal of Refrigeration* 58 (Oct. 2015), pp. 79–89. ISSN: 0140-7007. DOI: 10.1016/j.ijrefrig.2015.06.006. URL: https://www.sciencedirect.com/science/article/pii/S0140700715001735.

[54] Jiatong Jiang et al. "A review and perspective on industry high-temperature heat pumps". In: *Renewable and Sustainable Energy Reviews* 161 (June 2022), p. 112106. ISSN: 1364-0321. DOI: 10.1016/j.rser.2022.112106. URL: https://www.sciencedirect.com/science/article/pii/S1364032122000351.

[55] J. P. Johnston and R. C. Dean Jr. "Losses in Vaneless Diffusers of Centrifugal Compressors and Pumps: Analysis, Experiment, and Design". In: *Journal of Engineering for Power* 88.1 (Jan. 1966), pp. 49–60. ISSN: 0022-0825. DOI: 10.1115/1.3678477. URL: https://doi.org/10.1115/1.3678477 (visited on 08/30/2026).

[56] Nancy Kabat et al. "Investigation on Process Architectures for High-Temperature Heat Pumps Based on a Reversed Brayton Cycle". en. In: American Society of Mechanical Engineers Digital Collection, Sept. 2023. DOI: 10.1115/GT2023-102497. URL: https://dx.doi.org/10.1115/GT2023-102497.

[57] D. Kraft. *A Software Package for Sequential Quadratic Programming*. Deutsche Forschungs- und Versuchsanstalt für Luft- und Raumfahrt Köln: Forschungsbericht. Wiss. Berichtswesen d. DFVLR, 1988. URL: https://books.google.nl/books?id=4rKaGwAACAAJ.

[58] Bartosz Kus and Petter Nekså. "Development of one-dimensional model for initial design and evaluation of oil-free Co2 turbo-compressor". In: *International Journal of Refrigeration* 36.8 (Dec. 2013), pp. 2079–2090. ISSN: 0140-7007. DOI: 10.1016/j.ijrefrig.2013.05.009. URL: https://www.sciencedirect.com/science/article/pii/S0140700713001217 (visited on 08/22/2026).

[59] J. H. Lammers. "Heat Pump Design for Industrial Drying: A Design Study into the Optimisation and Sizing of an Industrial Heat Pump Dryer with Evaporator Bypass and Recirculation for a Non-Isenthalpic Drying Process". PhD thesis. Delft, Netherlands: Delft University of Technology, Nov. 2025. URL: http://repository.tudelft.nl/.

[60] E. W. Lemmon et al. *NIST Standard Reference Database 23: Reference Fluid Thermodynamic and Transport Properties-REFPROP, Version 10.0, National Institute of Standards and Technology*. 2018. DOI: https://doi.org/10.18434/T4/1502528. URL: https://www.nist.gov/srd/refprop.

[61] S.M. Liao and T. Zhao. "Measurements of Heat Transfer Coefficients From Supercritical Carbon Dioxide Flowing in Horizontal Mini/Micro Channels". In: *Journal of Heat Transfer-transactions of The Asme - J HEAT TRANSFER* 124 (June 2002). DOI: 10.1115/1.1423906.

[62] Sajjad Mahmoudinezhad et al. "A comprehensive review on the current technologies and recent developments in high-temperature heat exchangers". In: *Renewable and Sustainable Energy Reviews* 183 (Sept. 2023), p. 113467. ISSN: 1364-0321. DOI: 10.1016/j.rser.2023.113467. URL: https://www.sciencedirect.com/science/article/pii/S1364032123003246 (visited on 06/23/2026).

[63] National Refrigerants Ltd. *Safety Data Sheet: Refrigerant R1234ze*. Safety Data Sheet. Edition: Revision 1. Hinckley, Leicestershire, United Kingdom: National Refrigerants Ltd, Jan. 2017.

[64] T Naukkarinen. "The aerodynamic design of a centrifugal compressor". PhD thesis. Master Thesis, Lappeenranta University of Technology (In Finnish), 2013.

[65] Hyoung-Woo Oh and. "Investigation on the design and performance analysis methods of centrifugal turbomachines". eng. In: (1999). Accepted: 2011-12-14T05:17:05Z. URL: https://koasas.kaist.ac.kr/handle/10203/42956 (visited on 08/30/2026).

[66] B.S. Petukhov. "Theoretical Calculation of Heat Exchange and Frictional Resistance in Turbulent Flow in Tubes of an Incompressible Fluid with Variable Physical Properties". In: *Teplofiz. Vysok. Temperatur (High Temperature Heat Physics)* 1 (1963). URL: https://cir.nii.ac.jp/crid/1571417124888528000.

[67] Physikalisch-Technische Bundesanstalt (PTB), Bundesanstalt fuer Materialforschung und -pruefung (BAM), and DECHEMA. *CHEMSAFE: Database for Safety Characteristics in Explosion Protection*. Accessed: 12-06-2026. 2026. URL: https://www.chemsafe.ptb.de/.

[68] *prEN 378 — Refrigerating systems and heat pumps: Safety and environmental requirements (Draft Standard)*. en. Draft European Standard prEN 378. Brussels: European Committee for Standardization (CEN), 2025.

[69] Energy Efficiency Best Practice Programme. *Compact heat exchangers : a training package for engineers*. Energy Efficiency Best Practice Programme, 2001. URL: libgen.li/file.php?md5=a55e344505efaf73bf05cb7aa878cb3c.

[70] Python Software Foundation. *Python*. Version 3.13.3. URL: https://www.python.org/.

[71] Amir Qatarani Nejad et al. "Comparative evaluation of COP and phase change impacts in reversed rankine and brayton cycles for high-temperature heat pump systems". In: *Energy Conversion and Management: X* 28 (Oct. 2025), p. 101393. ISSN: 2590-1745. DOI: 10.1016/j.ecmx.2025.101393. URL: https://www.sciencedirect.com/science/article/pii/S2590174525005252.

[72] *Regulation (EU) 2024/573*. en. Legislative Body: OP_DATPRO. Feb. 2024. URL: http://data.europa.eu/eli/reg/2024/573/2024-02-20.

[73] *Regulation (EU) 2024/590*. en. Legislative Body: EP, CONSIL. Feb. 2024. URL: http://data.europa.eu/eli/reg/2024/590/oj.

[74] Farhad Salek et al. "Energy and exergy analysis of a novel turbo-compounding system for supercharging and mild hybridization of a gasoline engine". In: *Journal of Thermal Analysis and Calorimetry* 145 (Sept. 2020), pp. 1–12. DOI: 10.1007/s10973-020-10178-z.

[75] Gabriel Salierno. "On the Chemical Pathways Influencing the Effective Global Warming Potential of Commercial Hydrofluoroolefin Gases". English. In: *ChemSusChem* 17.17 (2024). ISSN: 1864-5631. DOI: 10.1002/cssc.202400280.

[76] J. Schiffmann and D. Favrat. "Design, experimental investigation and multi-objective optimization of a small-scale radial compressor for heat pump applications". In: *Energy* 35.1 (Jan. 2010), pp. 436–450. ISSN: 0360-5442. DOI: 10.1016/j.energy.2009.10.010. URL: https://www.sciencedirect.com/science/article/pii/S0360544209004435 (visited on 08/22/2026).

[77] J. Schiffmann and D. Favrat. "Experimental investigation of a direct driven radial compressor for domestic heat pumps". In: *International Journal of Refrigeration* 32.8 (Dec. 2009), pp. 1918–1928. ISSN: 0140-7007. DOI: 10.1016/j.ijrefrig.2009.07.006. URL: https://www.sciencedirect.com/science/article/pii/S0140700709001686 (visited on 08/22/2026).

[78] Volkmar Schroeder. *Calculation of Flammability and Lower Flammability Limits of Gas Mixtures for Classification Purposes*. Tech. rep. Berlin: Bundesanstalt für Materialforschung und -prüfung (BAM), Sept. 2016. URL: https://opus4.kobv.de/opus4-bam/files/41830/Schroeder++Calculation+of+Flammability+Limits.pdf.

[79] M.M. Shah. "Chart correlation for saturated boiling heat transfer: equations and further study". English. In: *ASHRAE Trans.* Vol. 88. pt 1. Journal Abbreviation: ASHRAE Trans. ASHRAE, 1982, pp. 185–196.

[80] Mirza M. Shah. "An Evaluation of Correlations for Predicting the Heat Transfer Coefficient during the Condensation of Saturated and Superheated Vapors Inside Channels". en. In: *Thermo* 4.2 (June 2024), pp. 164–184. ISSN: 2673-7264. DOI: 10.3390/thermo4020010. URL: https://www.mdpi.com/2673-7264/4/2/10 (visited on 06/05/2026).

[81] Mirza M. Shah. "Improved correlation for heat transfer during condensation in conventional and mini/micro channels". In: *International Journal of Refrigeration* 98 (Feb. 2019), pp. 222–237. ISSN: 0140-7007. DOI: 10.1016/j.ijrefrig.2018.07.037. URL: https://www.sciencedirect.com/science/article/pii/S0140700718302871 (visited on 06/02/2026).

[82] Mirza M. Shah. "Improved General Correlation for Condensation in Channels". en. In: *Inventions* 7.4 (Dec. 2022), p. 114. ISSN: 2411-5134. DOI: 10.3390/inventions7040114. URL: https://www.mdpi.com/2411-5134/7/4/114 (visited on 07/08/2026).

[83] Robin Smith. *Chemical Process: Design and Integration*. John Wiley & Sons, 2005. ISBN: 0-471-48680-9. URL: https://books.google.com/books/about/Chemical_Process.html?id=cdyiWR0d1o8C.

[84] Solstice Advanced Materials Ireland Limited. *Solstice® ZD, Solstice® 1233zd (E): Safety Data Sheet*. Safety Data Sheet. Edition: Version 2.12. Dublin, Ireland: Solstice Advanced Materials Ireland Limited, July 2025.

[85] TEGA - Technische Gase und Gasetechnik GmbH. *Safety Data Sheet: R 1224yd*. English. Safety Data Sheet. Würzburg, Germany: TEGA - Technische Gase und Gasetechnik GmbH, Dec. 2023. URL: https://www.tega.de/fileadmin/user_upload/SDB_R_1224yd_DE_2023-12-01_eng_TEGA.pdf (visited on 07/22/2026).

[86] LLC The Chemours Company FC. *Opteon™ MZ Heat Transfer Fluid: Technical Information*. Technical Information Bulletin. The Chemours Company FC, LLC, Sept. 2018. URL: https://www.opteon.com.

[87] *The Kyoto Protocol | UNFCCC*. URL: https://www.unfccc.int/process-and-meetings/the-kyoto-protocol.

[88] *The Montreal Protocol on Substances that Deplete the Ozone Layer | Ozone Secretariat*. URL: https://ozone.unep.org/treaties/montreal-protocol.

[89] M. E. H. Tijani et al. "Selection of lubricant oils for high temperature heat pumps: A review and selection methodology guidelines". In: *Applied Thermal Engineering* 273 (Aug. 2025), p. 126483. ISSN: 1359-4311. DOI: 10.1016/j.applthermaleng.2025.126483. URL: https://www.sciencedirect.com/science/article/pii/S1359431125010750 (visited on 07/02/2026).

[90] Gavin Towler and Ray Sinnott. *Chemical Engineering Design: Principles, Practice and Economics of Plant and Process Design*. 3rd ed. Butterworth-Heinemann, 2021. ISBN: 0-12-821179-2. URL: https://shop.elsevier.com/books/chemical-engineering-design/towler/978-0-12-821179-3.

[91] Richard Turton et al. *Analysis, synthesis, and design of chemical processes*. English. Fourth edition, International edition. Prentice-Hall international series in the physical and chemical engineering sciences. Section: xxxv, 965 pages : illustrations (black and white) ; 26 cm + 1 CD-ROM. Upper Saddle River, NJ: Pearson Education International, 2013. ISBN: 978-0-13-294029-0 0-13-294029-9.

[92] Antti Uusitalo, Teemu Turunen-Saaresti, and Aki Grönman. "Design and loss analysis of radial turbines for supercritical CO2 Brayton cycles". In: *Energy* 230 (Sept. 2021), p. 120878. ISSN: 0360-5442. DOI: 10.1016/j.energy.2021.120878. URL: https://www.sciencedirect.com/science/article/pii/S0360544221011269 (visited on 08/01/2026).

[93] Antti Uusitalo et al. "Centrifugal compressor design and cycle analysis of large-scale high temperature heat pumps using hydrocarbons". In: *Applied Thermal Engineering* 247 (June 2024), p. 123035. ISSN: 1359-4311. DOI: 10.1016/j.applthermaleng.2024.123035. URL: https://www.sciencedirect.com/science/article/pii/S1359431124007038 (visited on 07/08/2026).

[94] Antti Uusitalo et al. "Numerical analysis of working fluids for large scale centrifugal compressor driven cascade heat pumps upgrading waste heat". In: *Applied Energy* 269 (July 2020), p. 115056. ISSN: 0306-2619. DOI: 10.1016/j.apenergy.2020.115056. URL: https://www.sciencedirect.com/science/article/pii/S0306261920305687 (visited on 07/29/2026).

[95] Elias Vieren et al. "The thermodynamic potential of high-temperature transcritical heat pump cycles for industrial processes with large temperature glides". In: *Applied Thermal Engineering* 234 (Nov. 2023), p. 121197. ISSN: 1359-4311. DOI: 10.1016/j.applthermaleng.2023.121197. URL: https://www.sciencedirect.com/science/article/pii/S1359431123012267.

[96] Pauli Virtanen et al. "SciPy 1.0: Fundamental Algorithms for Scientific Computing in Python". In: *Nature Methods* 17 (2020), pp. 261–272. DOI: 10.1038/s41592-019-0686-2.

[97] Qingyang Wang et al. "A Critical Review on Heat Transfer of Supercritical Fluids". In: *Heat Transfer Engineering* 44.21-22 (Dec. 2023), pp. 1969–1994. ISSN: 0145-7632. DOI: 10.1080/01457632.2022.2164684. URL: https://doi.org/10.1080/01457632.2022.2164684 (visited on 06/03/2026).

[98] Ruzhu Wang et al. "High temperature heat pumps for industrial heating processes using water as refrigerant". In: *Energy* 313 (Dec. 2024), p. 133847. ISSN: 0360-5442. DOI: 10.1016/j.energy.2024.133847. URL: https://www.sciencedirect.com/science/article/pii/S0360544224036259.

[99] Philip Widmaier et al. "One Mixture to Rule Them All: Enhancing Efficiency and Standardization of Industrial High-Temperature Heat Pumps". English. In: *ACS Engineering Au* 5.4 (2025), pp. 359–369. ISSN: 2694-2488. DOI: 10.1021/acsengineeringau.4c00060.

[100] Alireza Zendehboudi. "Thermo-economic evaluation of low-GWP CO2-based zeotropic mixtures in space heating heat pumps with and without internal heat exchanger". In: *International Journal of Refrigeration* 173 (May 2025), pp. 1–17. ISSN: 0140-7007. DOI: 10.1016/j.ijrefrig.2025.01.036. URL: https://www.sciencedirect.com/science/article/pii/S0140700725000507.

[101] Xinxin Zhang and Yingzhen Li. "A review of recent research on hydrofluoroolefin (HFO) and hydrochlorofluoroolefin (HCFO) refrigerants". In: *Energy* 311 (Dec. 2024), p. 133423. ISSN: 0360-5442. DOI: 10.1016/j.energy.2024.133423. URL: https://www.sciencedirect.com/science/article/pii/S0360544224031992 (visited on 06/16/2026).

[102] Bingguo Zhu et al. "The general supercritical heat transfer correlation for vertical up-flow tubes: *K* number correlation". In: *International Journal of Heat and Mass Transfer* 148 (Feb. 2020), p. 119080. ISSN: 0017-9310. DOI: 10.1016/j.ijheatmasstransfer.2019.119080. URL: https://www.sciencedirect.com/science/article/pii/S0017931019342073 (visited on 07/08/2026).

[103] B. Zühlsdorf et al. "Analysis of technologies and potentials for heat pump-based process heat supply above 150°C". In: *Energy Conversion and Management: X* 2 (Apr. 2019), p. 100011. ISSN: 2590-1745. DOI: 10.1016/j.ecmx.2019.100011. URL: https://www.sciencedirect.com/science/article/pii/S2590174519300091.

[104] Benjamin Zühlsdorf et al. "Analysis of temperature glide matching of heat pumps with zeotropic working fluid mixtures for different temperature glides". In: *Energy* 153 (June 2018), pp. 650–660. ISSN: 0360-5442. DOI: 10.1016/j.energy.2018.04.048. URL: https://www.sciencedirect.com/science/article/pii/S0360544218306522.

[105] Benjamin Zühlsdorf et al. *Annex 58: High-Temperature Heat Pumps: Task 1 – Technologies, Task Report*. Report 978-91-89821-34-7. Borås, Sweden: Heat Pump Centre / RISE Research Institutes of Sweden, Aug. 2023. URL: https://heatpumpingtechnologies.org/annex58/wp-content/uploads/sites/70/2023/09/annex-58-task-1-technologies-task-report.pdf.

A

Working fluids

Table A.1: Selected high-temperature heat pump working fluids and their critical selection criteria [105][7][104][20].

Class	Name	Critical temperature (°C)	Critical pressure (bar)	ODP (-)	GWP (-)	Safety classification
HFC	R134a	101.1	40.6	0	1300	A1
	R245fa	153.9	36.5	0	858	B1
	R365mfc	186.9	32.7	0	804	A2
HFO	R1234yf	94.7	33.8	0	<1	A2L
	R1234ze(E)	109.4	36.3	0	<1	A2L
	R1336mzz(E)	130.4	27.8	0	18	A1
	R1234ze(Z)	150.1	35.3	0	<1	A2L
	R1336mzz(Z)	171.3	29	0	2	A1
HCFO	R1224yd(Z)	155.5	33.3	0.00012	<1	A1
	R1233zd(E)	166.5	36.2	0.00034	1	A1
Natural	CO_2	31	73.8	0	1	A1
	Propylene	91.1	45.5	0	8	A3
	Dimethyl ether	127.2	53.4	0	1	A3
	Ammonia	132.4	113.6	0	0	B2L
	Diethyl ether	194.7	37.2	0	4	A3
	Acetone	235	46.9	0	0.5	
	Methanol	240.2	82.2		2.8	
	Ethanol	241.6	62.7	0	<1	
	Water	373.9	220.6	0	0	A1
	Methane	-82.6	46	0	25	A3
	Ethylene	9.2	50.4	0	6.8	A3
	Ethane	32.2	48.7	0	2.9	A3
	Propylene	91.1	45.5	0	1	A3
	Propane	96.7	42.5	0	3	A3
	Cyclopropane	125.5	56.1			
	Isobutane	134.7	36.3	0	3	A3
	Isobutene	144.9	40.2	0	<1	
	Butene	146.1	40.1			
	Butane	152	38	0	4	A3
	Neopentane	160.6	32			
	Isopentane	187.2	33.8	0	4	A3
	Pentane	196.5	33.7	0	5	A3
	Isohexane	224.6	30.4			
	Hexane	234.7	30.4			
	Cyclopentane	238.6	45.8	0	<1	
	Heptane	268.1	27.7			
	Cyclohexane	280.5	40.8			
	Helium	-268	2.3			A1
	Argon	-122.5	48.6			A1
	Krypton	-63.7	55.3			

B
Equipment sizing

Table B.1: Centrifugal compressor one-dimensional loss correlations.

Disk friction $\Delta h_{df} = 0.5 f(\rho_1 + \rho_2) D_1^2 \frac{U_2^3}{16\dot{m}}$ $f = \frac{0.0622}{Re_2^2}$ $Re_2 = \rho_2 U_2 \frac{D_2}{2\mu_2}$	Daily and Nece [23]
Tip clearance $\Delta h_{tc} = 0.6 C_{u2} \frac{t}{b_2} \sqrt{2 C_{u2} C_{r1} \frac{\pi}{Z b_2} \frac{D_{1,tip}^2 - D_{1,hub}^2}{(D_2 - D_{1,tip})(1+\rho_1/\rho_2)}}$	Jansen [49]
Skin friction $\Delta h_{sf} = 2 f \frac{L_b}{D_h} \overline{W}^2$ $f = 0.006$ $L_b = \frac{D_{1,tip}}{2} + D_2 - D_{1,hub}$ $D_h = \pi \frac{D_{1,tip}^2 - D_{1,hub}^2}{\pi D_{1,tip} + 2Z(D_{1,tip} - D_{1,hub})}$ $\overline{W} = \frac{2W_2 + W_{1,tip} + W_1,hub}{4}$	Jansen [49]
Blade loading $\Delta h_{bl} = 0.05 D_f^2 U_2^2$ $D_f = 1 - \frac{W_2}{W_{1,tip}}(1 + \frac{0.75(U_2 C_{u2} - U_1 C_{u1})/U_2^2}{Z/\pi(1 - D_{1,tip}/D_2) + 2D_{1,tip}/D_2})$	Coppage and Dallenbach [22]
Recirculation $\Delta h_{rec} = 8e^{-5} \sinh(3.5\alpha_2^3) D_f^2 U_2^2$	Oh and [65]
Mixing $\Delta h_{mix} = \frac{1}{1+tan^2(\alpha_2)} \frac{C_2^2}{2} (\frac{1-e-b^*}{1-e})^2$	Johnston and Dean [55]
Diffuser $\Delta h_{diff} = 2 f \frac{L_{diff}}{D_{h,diff}} C_{avg}^2$ $f = 0.015(\frac{1.8e^5}{Re_{diff}})^{0.2}$ $Re_{diff} = \frac{\rho C_{r,avg} D_{h,diff}}{\mu_2}$ $C_{r,avg} = C_{r2} \frac{D_2}{2L_{diff}} ln(\frac{D_3}{D_2}) \frac{\rho_2}{0.5(\rho_2 + \rho_3)}$ $L_{diff} = \frac{D_3 - D_2}{2}$ $D_{h,diff} = 2 b_2 b^*$ $C_{avg} = \frac{C_2 + C_3}{2}$	Japikse [50]

Table B.2: Input parameters for the centrifugal compressor one-dimensional loss-correlation model literature comparison.

Parameter	Unit	Compressor 1 [64, 25]	Compressor 2 [58]	Compressor 3 [77, 76, 93]
$\dot{m}$	kg/s	1.79	6.3	0.04
p_{in}	bar	0.96	120	1.77
T_{in}	K	300	320	266.15
Π	-	2.36	1.6	3.3
$D_{1,hub}/D_{1,tip}$	-	0.3	0.267	0.357
D_3/D_2	-	2	1.87	1.65
x	mm	2	0.76	0.2
t	mm	0.5	0.25	0.1
C_{u2}/U_2	-	0.67	0.66	0.64
N	$krpm$	27.66	75.0	210

Table B.3: Heat-transfer coefficient correlations.

Single phase heating/cooling	
For $2300 < Re < 10^6$ and $0.6 < Pr < 10^5$	
$\alpha = \frac{(f/8)(Re-1000)Pr}{1+12.7\sqrt{f/8}(Pr^{2/3}-1)}\frac{k}{D_h}$	Gnielinski [36]
$f = (0.79\ln(Re) - 1.64)^{-2}$	Petukhov [66]
Supercritical heating	
$\alpha = 0.0012Re^{0.9484}Pr_{ave}^{0.718}K^{-0.0313}\frac{k}{D_h}$	Zhu et al. [102]
$K = (\frac{q}{Gh_{wall}})^2\frac{\rho}{\rho_{wall}}$	
Supercritical cooling	
$\alpha = 0.128Re_{wall}^{0.8}Pr_{wall}^{0.3}(\frac{\rho}{\rho_{wall}})^{0.437}(\frac{c_{p,ave}}{c_{p,wall}})^{0.411}(\frac{Gr}{Re^2})^{0.205}\frac{k_{wall}}{D_h}$	Liao and Zhao [61]
Evaporation	
$\alpha = \Psi\alpha_l$	Shah [79]
For $Re > 4000$	
$\alpha_l = 0.023Re_l^{0.8}Pr_l^{0.4}\frac{k_l}{Dh}$	Dittus and Boelter [26]
$\Psi = max(\Psi_{cb}, \Psi_{nb}, \Psi_{bs})$	Shah [79]
$\Psi_{cb} = \frac{1.8}{N^{0.8}}$	
For $N > 1$	
$\Psi_{bs} = 0$	
For $Bo > 0.00003$	
$\Psi_{nb} = 230\sqrt{Bo}$	
For $Bo < 0.00003$	
$\Psi_{nb} = 1 + 46\sqrt{Bo}$	
For $0.1 < N < 1$	
$\Psi_{nb} = 0$	
$\Psi_{bs} = C\sqrt{Bo}\exp(2.74N^{-0.1})$	
For $N < 0.1$	
$\Psi_{nb} = 0$	
$\Psi_{bs} = C\sqrt{Bo}\exp(2.47N^{-0.15})$	
For $Bo > 0.0011$	
$C = 14.7$	
For $Bo < 0.0011$	
$C = 15.43$	
For $Fr_l > 0.04$	
$N = Co$	
For $Fr_l < 0.04$	

$N = 0.38 Fr_l^{-0.3} Co$	
Condensation	
For $J_g > 0.98(Z+0.263)^{-0.62}$:	Shah [81, 82]
$\alpha = \alpha_I$	
For $J_g < 0.95(1.254+2.27Z^{1.249})^{-1}$:	
$\alpha = \alpha_{Nu}$	
Else:	
$\alpha = \alpha_I + \alpha_{Nu}$	
$Z = (\frac{1}{x}-1)^{0.8} p_r^{0.4}$	
$\alpha_I = \alpha_l (1 + \frac{3.8}{Z^{0.95}})(\frac{\mu_l}{14\mu_g})^{(0.0058+0.557p_r)}$	
For $Re > 4000$	
$\alpha_l = 0.023 Re_l^{0.8} Pr_l^{0.4} \frac{k_l}{Dh}$	Dittus and Boelter [26]
$\alpha_{Nu} = 1.32 Re_l^{-0.333} (\frac{\rho_l(\rho_l-\rho_g) g k_l^3}{\mu_l^2})^{0.333}$	Shah [81, 82]
Parameters	
$Re = \frac{GD_h}{\mu}$	
$Re_{wall} = \frac{GD_h}{\mu_{wall}}$	
$Re_l = \frac{G(1-x)D_h}{\mu_l}$	
$Pr = \frac{c_p \mu}{k}$	
$Pr_{ave} = \frac{c_{p,ave}\mu}{k}$	
$c_{p,ave} = \frac{h_{wall}-h}{T_{wall}-T}$	
$Pr_{wall} = \frac{c_{p,wall}\mu_{wall}}{k_{wall}}$	
$Pr_l = \frac{c_{p,l}\mu_l}{k_l}$	
$Gr = \frac{g\beta\lvert T_{wall}-T\rvert D_h^3}{\nu^2}$	
$Bo = \frac{q}{Gh_{fg}}$	
$h_{fg} = h_g - h_l$	
$Co = (\frac{1}{x}-1)^{0.8}\sqrt{\frac{\rho_g}{\rho_l}}$	
$Fr_l = \frac{G^2}{\rho_l^2 g D_h}$	
$p_r = \frac{p}{p_c rit}$	

C

Results

Table C.1: Environmental, safety, and practical parameters for working-fluid selection of the individual working-fluid components of the vapor-compression heat pump and the reversed-Brayton heat pump [24, 86, 43, 42, 84, 85, 63, 3, 13].

Fluid	ODP	GWP	PFAS	TFA	OEL $[mg/m^3]$	ISO	LFL $[\%mol]$	AIT [°C]
Acetone	0	1	no	-	1210		2.4	528
Ammonia	0	0	no	-	14	B2L	14	630
Butane			no	-	1000		1.2	392
Butene			no	-	1530		1.5	360
CO2	0	1	no	-	9000	A1	n/a	n/a
Cyclohexane			no	-	700	A3	1.0	246
Cyclopentane	0	11	no	-	600	A3	1.4	320
Cyclopropane		1.8	no	-		A3	2.4	495
Diethylether			no	-	308		1.7	175
Dimethylether	0	1	no	-	950	A3	2.8	240
Ethane	0	2.9	no	-	1000	A3	2.4	515
Ethanol	0	1	no	-	260		3.3	260
Ethylene			no	-	330		2.4	440
Heptane			no	-	1200		0.8	220
Hexane			no	-	72		0.9	230
Isobutane	0	3	no	-	1000	A3	1.5	460
Isobutene			no	-	1530		1.6	465
Isohexane			no	-	1800		1.2	300
Isopentane	0	4	no	-	1800	A3	1.3	420
Methane			no	-	1000		4.3	595
Methanol	0	2.8	no	-	133	n/a	6.0	450
Neopentane			no	-			1.3	450
Pentane			no	-	1800		1.1	260
Propane	0	3	no	-	1800	A3	1.7	459
Propylene	0	2	no	-	900	A3	2.0	485
R1224yd(Z)	0	1	yes	high	1260	A1	16	543
R1233zd(E)		4.5	yes	low	1779			380
R1234yf		4	yes	high			6.2	405
R1234ze(E)	0	1	yes	low	3902	A2L	7.0	368
R1234ze(Z)	0	1	yes		3902	A2L	7.0	368
R1236mzz(E)			yes	low				
R1236mzz(Z)	0	2	yes	low	3354			492

Table C.2: Mean performance indicators of the best-performing vapor-compression heat pump working fluids of distinct working-fluid families.

Scenario	Fluid family	COP [-]	VHC $[MJ/m^3]$	Pressure ratio [-]	$p_{discharge}$ $[bar]$	$T_{discharge}$ $[°C]$	A $[m^2]$
S1	Maximum	3.92	8.5	18.2	114	279	144
	Minimum	1.79	0.6	5.2	5.8	159	46
	Acetone	3.90	2.8	6.4	19.3	187	86
	Alcohol	3.85	2.6	8.9	19.1	228	
	Ammonia	3.84	8.0	6.1	46.9	279	
	Ether	3.83	3.9	6.3	26.0	184	103
	CO2	2.38	8.5	8.4	96.8	234	67
	C1-hydrocarbon	1.79	4.4	18.2	114.0	241	46
	C2-hydrocarbon	2.62	6.8	5.8	66.6	191	75
	C3-hydrocarbon	3.79	4.7	5.2	30.5	179	103
	C4-hydrocarbon	3.82	2.4	6.9	18.1	173	115
	C5-hydrocarbon	3.63	2.0	8.4	16.8	176	104
	C6-hydrocarbon	3.80	1.5	8.5	12.3	168	113
	C7-hydrocarbon	3.92	0.8	10.7	6.9	159	144
	Synthetic	3.71	2.4	7.7	19.0	172	132
	Water	3.77	0.6	15.7	5.8	251	
S2	Maximum	3.23	9.3	52.7	110.6	477	176
	Minimum	1.80	0.5	7.7	14.6	207	68
	Acetone	3.11	3.2	12.9	39.5	227	100
	Alcohol	3.11	2.7	19.4	36.5	288	
	Ammonia	3.23	5.9	11.2	52.9	324	
	Ether	3.10	4.5	11.5	51.6	223	122
	CO2	2.46	9.3	9.0	107.7	238	88
	C1-hydrocarbon	1.80	4.4	17.3	110.6	238	68
	C2-hydrocarbon	2.55	8.9	7.7	101.8	213	114
	C3-hydrocarbon	3.08	5.3	9.6	57.0	215	120
	C4-hydrocarbon	3.06	2.8	14.8	41.9	211	147
	C5-hydrocarbon	2.98	2.5	17.1	39.8	210	146
	C6-hydrocarbon	3.06	1.7	20.5	30.7	207	176
	C7-hydrocarbon	2.74	0.5	52.7	18.2	209	133
	Synthetic	3.03	2.7	16.4	42.1	211	164
	Water	3.03	1.0	26.0	14.6	477	
S3	Maximum	2.47	5.5	112.9	201.4	484	96
	Minimum	1.43	0.3	12.2	12.3	238	38
	Acetone	2.44	0.8	31.7	21.6	299	68
	Alcohol	2.38	0.6	63.8	24.5	359	38
	Ammonia	2.21	5.5	22.1	90.4	460	
	Ether	2.38	1.1	27.9	29.6	262	86
	CO2	1.61	5.5	44.6	196.9	372	45
	C1-hydrocarbon	1.43	2.1	112.9	201.4	359	42
	C2-hydrocarbon	1.67	3.9	63.5	153.6	338	50
	C3-hydrocarbon	2.09	4.2	12.2	72.2	271	63
	C4-hydrocarbon	2.27	1.9	17.9	38.8	254	77
	C5-hydrocarbon	2.41	0.9	30.5	24.7	266	81
	C6-hydrocarbon	2.44	0.6	34.3	17.3	257	85
	C7-hydrocarbon	2.45	0.3	51.2	12.3	245	91
	Synthetic	2.32	1.6	21.0	35.5	265	96
	Water	2.47	0.6	52.0	16.8	484	

Table C.3: Mean performance indicators of the best-performing reversed-Brayton heat pump without internal heat exchanger working fluids of distinct working-fluid families.

Scenario	Fluid family	COP [-]	VHC MJ/m^3	Pressure ratio [-]	$p_{discharge}$ bar	$T_{discharge}$ $°C$	A m^2
S1	Maximum	2.86	21.2	12.3	233.2	196	332
	Minimum	1.91	0.5	2.5	15.8	168	128
	Ammonia	2.40	4.3	3.2	60.1	175	147
	Ether	2.29	2.3	4.2	36.2	174	162
	Gas	2.77	21.2	2.7	207.2	192	199
	C1-hydrocarbon	2.32	16.4	3.0	212.7	187	139
	C2-hydrocarbon	2.86	15.6	3.1	156.0	181	165
	C3-hydrocarbon	2.51	4.1	3.4	56.0	168	170
	C4-hydrocarbon	2.11	1.4	6.1	28.5	179	143
	C5-hydrocarbon	1.91	0.5	12.3	15.8	190	128
	Noble gasses	2.38	19.3	2.5	233.2	196	332
S2	Maximum	2.56	23.9	16.6	245.9	214	281
	Minimum	1.84	0.6	2.9	21.8	207	117
	Ammonia	1.98	2.7	4.6	48.0	209	127
	Ether	2.22	9.1	7.0	109.2	209	142
	Gas	2.54	23.9	3.3	243.2	214	175
	C1-hydrocarbon	2.13	17.3	3.6	240.5	210	122
	C2-hydrocarbon	2.56	22.4	4.4	245.9	211	150
	C3-hydrocarbon	2.11	3.5	6.8	64.1	209	117
	C4-hydrocarbon	1.94	1.2	10.6	30.9	209	133
	C5-hydrocarbon	1.84	0.6	16.6	21.8	207	153
	Noble gasses	2.27	20.1	2.9	242.7	213	281
S3	Maximum	1.87	12.8	39.7	234.8	268	147
	Minimum	1.60	0.5	5.1	42.1	220	87
	Ammonia	1.79	5.7	6.8	128.8	235	106
	Ether	1.79	2.8	9.5	79.1	224	124
	Gas	1.76	12.8	5.1	234.8	255	121
	C1-hydrocarbon	1.61	7.9	9.4	208.7	254	87
	C2-hydrocarbon	1.83	8.8	7.7	199.6	235	110
	C3-hydrocarbon	1.87	3.6	9.2	96.9	220	126
	C4-hydrocarbon	1.72	1.6	15.6	63.7	228	113
	C5-hydrocarbon	1.60	0.5	39.7	42.1	240	99
	Noble gasses	1.60	10.8	5.1	217.3	268	147

Table C.4: Mean performance indicators of the best-performing reversed-Brayton heat pump with internal heat exchanger working fluids of distinct working-fluid families.

Scenario	Fluid family	COP [-]	VHC $[MJ/m^3]$	Pressure ratio [-]	$p_{discharge}$ $[bar]$	$T_{discharge}$ $[°C]$	A $[m^2]$
S1	Maximum	3.03	21.2	7.3	206.5	196	494
	Minimum	2.01	0.7	2.3	16.5	172	187
	Ammonia	2.49	4.0	2.7	52.0	177	187
	Ether	2.57	7.6	3.3	76.2	181	218
	Gas	2.89	21.2	2.5	194.3	196	270
	C1-hydrocarbon	2.59	17.6	2.6	199.1	185	210
	C2-hydrocarbon	3.03	15.3	2.6	138.9	181	219
	C3-hydrocarbon	2.57	3.8	3.0	47.8	172	218
	C4-hydrocarbon	2.20	1.4	4.6	23.9	180	203
	C5-hydrocarbon	2.01	0.7	7.3	16.5	187	189
	Noble gasses	2.62	19	2.3	206.5	192	494
S2	Maximum	2.76	27.3	9.3	248	215	470
	Minimum	1.88	0.7	2.6	18.4	207	168
	Ammonia	2.16	4.2	3.1	59.7	207	168
	Ether	2.32	8.5	4.8	89.5	208	195
	Gas	2.75	27.3	2.8	245.6	215	270
	C1-hydrocarbon	2.39	21.6	3.3	248.0	208	184
	C2-hydrocarbon	2.76	23.3	3.5	219.4	209	230
	C3-hydrocarbon	2.29	8.2	3.7	94.7	208	220
	C4-hydrocarbon	2.01	1.2	7.4	25.1	208	179
	C5-hydrocarbon	1.88	0.7	9.3	18.4	208	204
	Noble gasses	2.50	22.6	2.6	241.9	210	470
S3	Maximum	2.10	20.3	11.3	249.4	275	374
	Minimum	1.68	0.7	2.8	22.7	236	144
	Ammonia	1.89	4.5	3.7	70.4	245	164
	Ether	1.93	8.2	4.7	111.5	251	170
	Gas	2.03	20.3	3.3	246.7	275	208
	C1-hydrocarbon	1.93	17.8	3.3	249.3	254	164
	C2-hydrocarbon	2.10	15.6	3.8	198.2	254	167
	C3-hydrocarbon	1.94	4.3	4.1	67.7	236	180
	C4-hydrocarbon	1.78	1.5	6.9	32.9	242	153
	C5-hydrocarbon	1.68	0.7	11.3	22.7	249	144
	Noble gasses	1.93	18.8	2.8	249.4	270	374

Table C.5: Centrifugal compressor dimensions and efficiency estimation results for the vapor-compression heat pump for the three heating scenarios for a heating duty of 1 MW and 10 MW.

	VCHP					
Heating scenario	S1		S2		S3	
Heating duty	1 MW	10 MW	1 MW	10 MW	1 MW	10 MW
Discharge pressure [bar]	26.1		77.3		40.5	
Inlet volume flow [m^3/s]	0.23	2.30	0.12	1.24	0.46	4.57
Number of stages	2		2		3	
Pressure ratio per stage	2.20		2.62		2.41	
Rotational speed [$krpm$]	52.1	16.1	88.8	31.2	32.6	9.5
Power [MW]	0.12	1.19	0.18	1.70	0.15	1.46
Diameter [cm]	10.6	33.6	7.2	20.1	13.3	44.3
Isentropic efficiency	80.2	83.6	75.4	79.4	76.8	81.1
Power [MW]	0.13	1.23	0.18	1.70	0.15	1.41
Diameter [cm]	10.8	34.3	7.3	20.1	13.0	43.7
Isentropic efficiency	77.7	82.3	75.8	79.3	82.9	85.7
Power [MW]	-	-	-	-	0.16	1.50
Diameter [cm]	-	-	-	-	13.5	44.7
Isentropic efficiency	-	-	-	-	75.0	79.4
Isentropic efficiency	78.1	82.2	74.0	77.9	76.6	80.8
Difference	-1.9	+2.2	-6.0	-2.1	-3.4	+0.8
Adjusted COP	3.92	4.13	2.79	2.94	2.17	2.29

Table C.6: Centrifugal compressor dimensions and efficiency estimation results for the reversed-Brayton heat pump without and with internal heat exchanger for the three heating scenarios for a heating duty of 1 MW and 10 MW.

	RBHP						RBHP (IHX)					
Heating scenario	S1		S2		S3		S1		S2		S3	
Heating duty	1 MW	10 MW	1 MW	10 MW	1 MW	10 MW	1 MW	10 MW	1 MW	10 MW	1 MW	10 MW
Discharge pressure [bar]	220.8		250.0		250.0		199.4		250.0		250.0	
Inlet volume flow [m^3/s]	0.04	0.42	0.04	0.39	0.07	0.68	0.04	0.44	0.03	0.34	0.05	0.47
Number of stages	1		1		2		1		1		1	
Pressure ratio per stage	2.69		3.08		2.11		2.40		2.83		3.08	
Rotational speed [$krpm$]	130.8	41.9	165.7	50.4	107.9	33.0	118.8	38.1	167.7	51.6	175.0	54.6
Power [MW]	0.53	4.76	0.59	5.13	0.41	3.78	0.49	4.39	0.52	4.50	0.70	6.16
Diameter [cm]	5.2	15.5	4.5	14.0	5.5	17.4	5.5	16.4	4.4	13.5	4.8	14.6
Isentropic efficiency	73.0	81.8	70.1	80.6	75.3	82.3	74.6	82.5	70.5	80.8	71.0	80.7
Power [MW]	-	-	-	-	0.54	4.78	-	-	-	-	-	-
Diameter [cm]	-	-	-	-	6.3	19.5	-	-	-	-	-	-
Isentropic efficiency	-	-	-	-	73.9	81.6	-	-	-	-	-	-
Isentropic efficiency	73.0	81.8	70.1	80.6	72.6	80.6	74.6	82.5	70.5	80.8	71.0	80.7
Difference	-2.0	+6.8	-4.9	+5.6	-2.4	+5.6	-0.4	+7.5	-4.5	+5.8	-4.0	+0.7
Adjusted COP	2.71	3.21	2.38	2.91	1.67	1.98	2.89	3.34	2.58	3.10	1.88	2.23

Table C.7: The required type and resulting heat transfer area requirement of the heat exchanger sizing for the vapor-compression heat pump and reversed-Brayton heat pump for the three heating scenarios.

Scenario	Type	Source			Sink			IHX		
		Type	Design	Area [m^2]	Type	Design	Area [m^2]	Type	Design	Area [m^2]
S1	VCHP	Multiple pipe	s/s tubes, <50 bar	133	Multiple pipe	s/s tubes, <50 bar	118	Multiple pipe	c/s tubes, <50 bar	48
	RBHP	Shell-and-tube	s/s tubes, 50-100 bar	562	Multiple pipe	s/s tubes, >150 bar	93	-	-	-
	RBHP (IHX)	Shell-and-tube	s/s tubes, 50-100 bar	566	Multiple pipe	s/s tubes, >150 bar	93	Multiple pipe	c/s tubes, >150 bar	180
	VCHP	Shell-and-tube	s/s tubes, <50 bar	1333	Shell-and-tube	s/s, low <50 bar	1180	Plate	c/s, <50 bar	160
	RBHP	Shell-and-tube	s/s tubes, 50-100 bar	5620	Shell-and-tube	s/s tubes, >150 bar	931	-	-	-
	RBHP (IHX)	Shell-and-tube	s/s tubes, 50-100 bar	5656	Shell-and-tube	s/s tubes, >150 bar	931	Shell-and-tube	c/s tubes, >150 bar	1803
S2	VCHP	Multiple pipe	s/s tubes, <50 bar	142	Multiple pipe	s/s tubes, 50-100 bar	191	Multiple pipe	c/s tubes, 50-100 bar	36
	RBHP	Shell-and-tube	s/s tubes, 50-100 bar	477	Multiple pipe	s/s tubes, >150 bar	145	-	-	-
	RBHP (IHX)	Shell-and-tube	s/s tubes, 50-100 bar	494	Multiple pipe	s/s tubes, >150 bar	129	Multiple pipe	c/s tubes, >150 bar	159
	VCHP	Shell-and-tube	s/s tubes, <50 bar	1417	Shell-and-tube	s/s tubes, 50-100 bar	1908	Plate	c/s, >50 bar	120
	RBHP	Shell-and-tube	s/s tubes, 50-100 bar	4766	Shell-and-tube	s/s tubes, >150 bar	1452	-	-	-
	RBHP (IHX)	Shell-and-tube	s/s tubes, 50-100 bar	4943	Shell-and-tube	s/s tubes, >150 bar	1289	Shell-and-tube	c/s tubes, >150 bar	1587
S3	VCHP	Multiple pipe	s/s tubes, <50 bar	67	Multiple pipe	s/s tubes, <50 bar	88	Multiple pipe	c/s tubes, <50 bar	144
	RBHP	Multiple pipe	s/s tubes, 50-100 bar	288	Multiple pipe	s/s tubes, >150 bar	85	-	-	-
	RBHP (IHX)	Shell-and-tube	s/s tubes, 50-100 bar	348	Multiple pipe	s/s tubes, >150 bar	71	Multiple pipe	c/s tubes, >150 bar	168
	VCHP	Shell-and-tube	s/s tubes, <50 bar	673	Shell-and-tube	s/s tubes, <50 bar	881	Shell-and-tube	c/s tubes, <50 bar	1440
	RBHP	Shell-and-tube	s/s tubes, 50-100 bar	2883	Shell-and-tube	s/s tubes, >150 bar	847	-	-	-
	RBHP (IHX)	Shell-and-tube	s/s tubes, 50-100 bar	3483	Shell-and-tube	s/s tubes, >150 bar	706	Shell-and-tube	c/s tubes, >150 bar	1676